THE UNIVERSITY
of EDINBURGH

Reconstituting the Spindle Assembly Checkpoint and the Signalling Roles of Mad1

Priya Amin

THE UNIVERSITY *of* EDINBURGH

Thesis presented for the degree of Doctor of Philosophy

Institute of Cell Biology
University of Edinburgh

2019

Declaration

I declare that this thesis was composed entirely by myself and that the work presented here is my own except where indicated otherwise. This work has not been submitted for any other degree or professional qualification.

Priya Amin
July 2019

Acknowledgements

Foremost, I would like to thank my supervisor Kevin for his guidance over the last few years. I felt our discussions, while grounding, inspired a sense of excitement and brought the subject alive. I couldn't have imagined a better mentor. Karen, for introducing me to fission yeast and patiently sharing her extensive expertise. You have been immensely helpful and your optimism brightened up the lab. Fellow lab members Ioanna and Sadhbh, for making the learning curve a groovy one, and to other friends for keeping me sane.

My thesis committee, Ken, JP, and Robin for their time and advice. A big thanks to Tay, Efty, Manu, Christos, Bethan and Rachael for various discussions. I would also like to thank other members of the Hardwick, Sawin, Marston, Allshire, Arulanandam and Tollervey labs. The friendly environment in the institute facilitated a collaborative work ethic and made this an enjoyable experience. Additional thanks to the Joglekar lab for hosting my summer visit. It was refreshing to gain a new perspective.

I would also like to express my sincere gratitude to my family. You have been kind and generous, and I would not have been able to do this without your support.

List of abbreviations

ABA	Abscisic acid
ABI	ABA insensitive 1
adh	Alcohol dehydrogenase (promoter)
APC/C	Anaphase Promoting Complex/Cyclosome
Bub	Budding uninhibited by benzimidazoles
CBZ	Carbendazim
CD1	Conserved Domain 1
Cdc	Cell division cycle
CDK	Cyclin-dependent kinase
CENP	Centromere protein
CID	Chemically induced dimerisation
DMSO	Dimethyl sulfoxide
DNA	Deoxyribonucleic acid
DTT	Dithiothreitol
g	Gram
GFP	Green Fluorescent Protein
GLEBS	Gle2-binding sequence
KMN	KNL1-Mis12-Ndc80 complex
L	Litre
M	Molar
m	Milli
Mad	Mitotic arrest deficient
MCC	Mitotic Checkpoint Complex
MIM	Mad2 Interaction Motif
min	Minute
NLS	Nuclear localisation sequence
nmt	No message in thiamine (promoter)
NPC	Nuclear Pore Complex
PCR	Polymerase chain reaction
PMG	Pombe minimal medium
PYL	Pyrabactin resistance 1-like
rTetR	Reverse tetracycline repressor
RZZ	Rod1-Zwilch-ZW10 complex
SAC	Spindle Assembly Checkpoint
SPB	Spindle pole body
TE	Tris(hydroxymethyl)aminomethane-EDTA
TetO	Tet operator
TPR	Tetratricopeptide repeat
WT	Wild type
YES	Yeast extract supplemented
µ	Micro

Lay summary

All living organisms are made of cells, the building blocks of life. Broadly, the process of cell division, where one cell becomes two, enables the growth of organisms in a process known as mitosis. During mitosis, a cell essentially increases its mass and duplicates its contents, including its DNA, and distributes it to two 'daughter' cells in a rather dramatic re-organisation of the cell. DNA acts as an instruction manual for a cell. Having the correct amount of DNA is crucial for maintaining healthy cells, as in most cases, incorrect amounts can cause cell death or contribute to cancer.

In this way, it is important that DNA is equally distributed to daughter cells during cell division. As a result, our cells have a mechanism of monitoring whether DNA, in the form of chromosomes, is going to distribute correctly. This mechanism is known as the spindle assembly checkpoint.

The checkpoint is able to delay cell division if chromosomes are not ready to divide correctly. By delaying cell division, chromosomes have time to re-position for correct distribution to daughter cells. The checkpoint is comprised of different members which come together to finally delay division. Although the members of the checkpoint pathway are known, how they interact to cause a delay is less clear.

This work provides insight into the functions of an integral member of the checkpoint pathway, Mad1. We have identified the additional components it interacts with to gain a greater understanding of how the checkpoint pathway works. Additionally, we have developed a minimalist method for switching the checkpoint on and off. This tool provides a novel method for studying how the individual members of the checkpoint pathway come together to delay division. Here, we use a microorganism called *S. pombe* which is a species of yeast commonly used in cell biology, to study the spindle assembly checkpoint as cell division in these cells is similar to that in human cells.

Abstract

Cell division allows the passage of genetic information to a new cell. During this process, maintaining chromosome transmission fidelity is important in preventing diseases such as cancer and Down's syndrome. To ensure accurate chromosome segregation, eukaryotes have developed a cell cycle control mechanism that monitors kinetochore-microtubule attachments, known as the spindle assembly checkpoint (SAC). The SAC is active in metaphase and is able to sense a lack of tension and incorrect attachments between kinetochores and microtubules. This leads to a metaphase arrest, allowing time for error correction to take place before anaphase onset.

The Mad and Bub proteins, along with Mps1 kinase are central to this signalling pathway which leads to the formation of the mitotic checkpoint complex (MCC) — the key inhibitor of the anaphase promoting complex/cyclosome (APC/C). APC/C inhibition prevents proteolytic degradation of Securin and Cyclin B, blocking cells in metaphase. Although we are familiar with the components of the SAC pathway, the mechanism by which they interact to form the MCC remains unclear.

It is well established that SAC signalling is initiated at kinetochores. These are complex structures that are involved in key mitotic functions such as microtubule attachment and bi-orientation of sister chromatids. To study the checkpoint without interfering with kinetochore function, we have devised a minimalist approach. This study describes an ectopic reconstitution of SAC activation and silencing in *S. pombe*. Using abscisic acid induced dimerisation, we are able to control the co-recruitment of the checkpoint proteins KNL1 and Mps1 to recapitulate robust SAC arrest and silencing. Additionally, we provide insight into how *S. pombe* and HeLa cells respond to a prolonged ectopic arrest.

It is widely accepted that Mad1 recruits Mad2 to unattached kinetochores, enabling MCC formation. However, recent findings point towards a more active role of Mad1 in checkpoint activation. This study shows that Mad1 interacts with Bub1 in *S. pombe* to form a scaffold complex that is essential for SAC function. We also investigate Mad1 C-terminal mutants to further dissect the roles of Mad1 and find that it forms a complex with the APC/C co-activator Cdc20. As a result, this study provides evidence in support of the hypothesis that the C-terminus of Mad1 has additional roles in SAC signalling aside from Mad2 kinetochore recruitment.

Table of contents

List of figures

CHAPTER 1

Introduction

1.1 Preamble: Cell theory

Cells are the fundamental structural unit of all living organisms, making up the immensely diverse bacterial, archaeal and eukaryotic species that occupy the evolutionary tree of life. The discovery of the microscope in the late 16th century greatly facilitated the study of cell biology (Wolpert, 1996). Observations of cells using early compound microscopes by Robert Hooke, Antoine van Leeuwenhoek, Nehemiah Grew and others in the mid-17th century led to the makings of cell theory. Hooke coined the term 'cellula', Latin for 'small room', to describe the compartments of dead cells in cork (Hooke, 1665). Van Leeuwenhoek is regarded as the father of microbiology, with bacteria being one of his most notable discoveries (Leeuwenhoek, 1682). Work by Grew detailed the anatomy of plant tissue (1682). Together, these works and others led to the idea that cells are the basic unit of many life forms.

In the 19th century, Schleiden and Schwann extended this to a unified principle that all organisms are composed of cells (Schleiden, 1838; Schwann, 1839). Although instrumental to the formation of cell theory, they based their observations on the assumption that cells are formed *de novo*, termed 'free cell formation'. In 1855, Rudolph Virchow dismissed free cell formation concluding classical cell theory with the axiom 'all cells come from pre-existing cells'. This is possible through the cell cycle.

1.2 The cell cycle

The mitotic cell cycle (Fig. **1.1**) is a process that enables the growth of an organism. It is an orchestrated series of events where cell mass increases and DNA duplicated and distributed to daughter cells. A typical eukaryotic cell cycle broadly comprises of interphase and mitosis. Interphase begins with G1 (**g**ap **1**), a growth phase where cell volume increases, organelles duplicate, and proteins required for DNA replication and packaging (such as histones) are produced. Cells in G1 can enter G0 (**g**ap **0**), a non-proliferation resting phase, before they commit to DNA replication. Nuclear DNA is replicated in S (**s**ynthesis) phase. This is followed by G2 (**g**ap **2**), during which there is additional growth and protein synthesis. G1, S

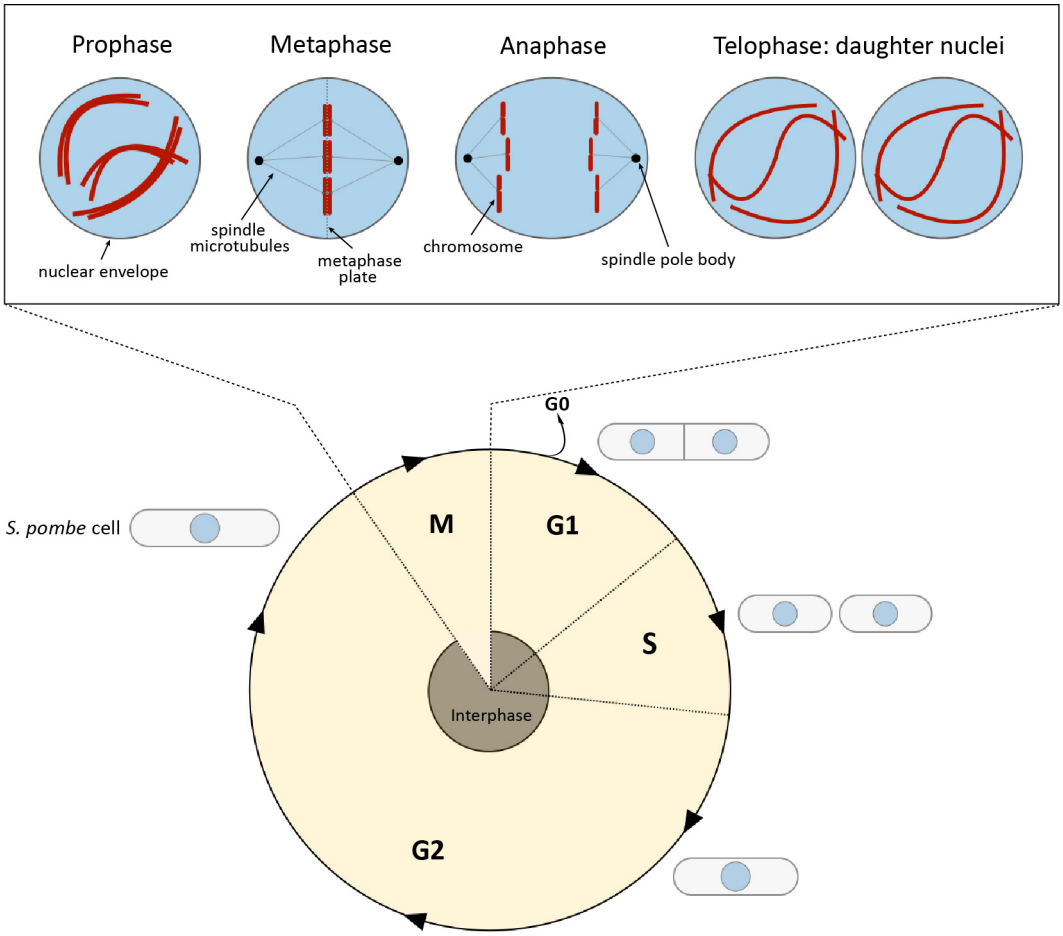

Figure 1.1: Overview of the cell cycle and mitosis. Schematic showing the cell cycle and *S. pombe* cell morphology. The cell cycle begins with a growth phase G1 where cells that have not committed to DNA replication can enter a resting phase G0. DNA replication takes place in S phase which is followed by an additional growth phase G2. These stages make up interphase. This is followed by mitosis where DNA is segregated to daughter nuclei. The cell forms a septum in a process known as cytokinesis (in *S. pombe*, the septum is cleaved in the following S phase). A cartoon (above) depicts the nucleus during mitosis. Duplicated DNA is compacted in prophase, the chromosomes align at the metaphase plate and kinetochore-microtubule attachements are formed. Chromosome segregation to opposite poles occurs in anaphase, with the nucleus dividing in telophase.

and G2 make up interphase, after which cells enter mitosis (**M**) (Fig. **1.1**) and undergo cytokinesis (reviewed in Schafer, 1998; McIntosh 2016).

Progression through the eukaryotic cell cycle is driven by **c**yclin-**d**ependent **k**inases (CDKs) — a conserved group of serine-threonine kinases whose enzymatic activity is dependent on association with cyclin subunits (reviewed in Hochegger et al., 2008; Harashima et al., 2013; Malumbres, 2014). CDK-cyclin complexes enable the switch-like initiation of key cell cycle transitions, particularly G1/S and G2/M, through the expression of the activating cyclin subunit. Lee Hartwell and Paul Nurse first isolated the CDK1 gene (from budding and fission yeast respectively) which, along with Tim Hunt's discovery of cyclin from sea urchin eggs, led to the characterisation of integral cell cycle regulators (Hartwell et al., 1974; Nurse et al., 1976; Evans et al., 1983). This paved the way to the study of cell cycle control.

The yeast cell cycle is controlled by CDK1 homologues, Cdc2 (**c**ell **d**ivision **c**ycle **2)** in *S. pombe* and Cdc28 in *S. cerevisiae* (Hadwiger et al., 1989). This mechanism of cell cycle control is well-conserved as a cdc2 mutant in *S. pombe* can be functionally complemented by human CDK1 (Lee and Nurse, 1987). Although Cdc2 can form a complex with different cyclins at various cell cycle stages, B-type cyclin Cdc13 (**c**ell **d**ivision **c**ycle **13**) is the only essential cyclin. It has been demonstrated that Cdc2-Cdc13 alone is able to control the cell cycle, suggesting that regulating the kinase activity of Cdc2 (through association with Cdc13) to reach certain thresholds is sufficient to drive the *S. pombe* cell cycle (Fisher and Nurse, 1996; Coudreuse and Nurse, 2010). Fission yeast mitotic entry is achieved by high levels of the Cdc2-Cdc13 (Stern and Nurse, 1996).

Mitosis results in the distribution of sister chromatids to daughter nuclei. Experimentation with aniline dyes allowed Walther Flemming to illustrate the segregation of chromosomes in impressive detail (1882). Flemming hugely influenced research into cell division through his pioneering work (Paweletz, 2001). Mitosis requires complex reorganisation of cellular architecture and is composed of 5 stages: prophase, prometaphase, metaphase, anaphase and telophase (reviewed in Schafer, 1998; McIntosh 2016). In prophase, duplicated DNA condenses to form tightly packed chromosomes (Martinez-Balbas et al., 1995), interphase microtubules disassemble and duplicated spindle pole bodies (centrosomes in higher eukaryotes) start to form spindle microtubules (Ding et al., 1997). Chromosomes are captured via kinetochore attachment to mitotic spindle in prometaphase. In metaphase, chromosomes are bi-oriented and aligned at the spindle equator. The position of the nucleus

determines the deposition of an actomyosin band which marks the future site of cytokinesis (Lee et al., 2012). Anaphase results in mitotic spindle-dependent segregation of sister chromatids to opposite spindle pole bodies as spindle microtubules lengthen (Watanabe, 2010). *S. pombe* have closed mitosis in which the nuclear envelope does not break down as in higher eukaryotes (McCully and Robinow, 1971). As a result, in telophase, the nucleus elongates and forms two nuclei. The actomyosin band forms a contractile ring, resulting in a septum (Krapp and Simanis, 2008; Stachowiak et al., 2014). Cytokinesis then occurs as the septum is degraded to form two individual, genetically identical cells.

1.3 Cell cycle checkpoints

In 1989, Leland Hartwell and Ted Weinert proposed that progression through the cell cycle is dependent on the completion of previous events. This linear progression is regulated through feedback loops, allowing the cycle to continue only after the successful completion of certain events. These feedback loops are known as cell cycle checkpoints. Checkpoints are pathways that identify errors and provide feedback through the initiation of a proliferative signal which blocks cell cycle progression, thus allowing time for errors to be completed. In this way, checkpoints act as surveillance mechanisms to ensure the fidelity of DNA replication and chromosome segregation (Weinert and Hartwell, 1988; Hartwell and Weinert, 1989). This prevents cell death and aneuploidy, which could contribute to cancer in higher eukaryotes (Holland and Cleveland, 2009). Checkpoint pathways ultimately affect CDK activity to control cell cycle progression. They monitor DNA replication fidelity, cell size and kinetochore-microtubule attachments at key transitions to licence cell cycle progression (reviewed in Elledge, 1996).

The **s**pindle **a**ssembly **c**heckpoint (SAC), also known as the spindle checkpoint or the mitotic checkpoint, monitors chromosome attachment to spindle microtubules at the metaphase/anaphase transition. How the SAC signalling pathway is activated and propagated to allow a metaphase delay, as well as 'silenced' to enable cell cycle progression in the fission yeast *S. pombe* will be the focus of this work and the remainder of this chapter.

1.4 Chapter layout

This chapter begins with an introduction to kinetochores as the sites of SAC initiation and describes how kinetochore bi-orientation can be achieved for correct chromosome segregation by monitoring the attachment status and tension at kinetochores. This is then

followed by an overview of the SAC and an outline of the contribution of Aurora B^{Ark1} and Mps1^{Mph1} kinase activity. SAC signalling is then detailed in chronological order, starting with the assembly of core KNL1-Bub and Mad1-Mad2 complexes which lead to the formation of the SAC effector and how it prevents anaphase, ending with an overview of how the checkpoint is silenced.

1.5 Kinetochores: sites of checkpoint initiation

Kinetochores are macromolecular structures present at the centromere of sister chromatids, consisting of over 80 proteins (Cheeseman and Desai, 2008; Santaguida and Musacchio, 2009). They provide a point of contact for microtubule interaction on a chromosome, thus enabling chromosome translocation during cell division (reviewed in Foley and Kapoor, 2013). The inner face of the kinetochore associates with the centromere, a region of heterochromatin distinguished by the histone H3 variant CENP-A (Palmer et al., 1987; Mellone and Allshire, 2003). The outer face of the kinetochore structure interacts with microtubules via the KMN network, comprising of KNL1/Mis12-complex /Ndc80-complex (**k**inetochore **n**u**l**l protein **1**/**mis**segregation **12**/**n**uclear **d**ivision **c**ycle **80** complex) (Cheeseman et al., 2006). This network is highly conserved between species, named the NMS network - Ndc80-Mis12-Spc7^{KNL1} in *S. pombe* (Jakopec et al., 2012).

Unlike yeast, vertebrates start assembling their kinetochores in S phase (Amor et al., 2004; Maiato et al., 2004). Upon mitotic entry in humans, the dispersed centromeres need to assemble. Although components such as CENP-A and Mis12 are constitutively associated with centromeres, the transient components do not usually associate until mitosis (Liu et al., 2005). CENP-A employs the constitutive centromere-associated network (CCAN) to assemble the KMN network, thus forming the outer kinetochore (Cheeseman and Desai, 2008). In *S. pombe* however, the 'basic' kinetochore structure is intact in interphase, as it remains bound to spindle pole bodies (Uzawa and Yanagida, 1992). Therefore, the NMS network is a constitutive feature at outer kinetochores (Liu et al., 2005).

In prophase, SAC proteins are recruited to the KMN/NMS network, KNL1^{Spc7} in particular, in a step-wise fashion (Desai et al., 2003; Vigneron et al., 2004; Liu et al., 2005; Shepperd et al., 2012; Yamagishi et al., 2012; London et al., 2012). Some of the proteins, such as Mad1 and Mad2, dissociate from kinetochores as stable chromosome-microtubule attachments form. Therefore, the KMN network links the kinetochore attachment information to SAC signalling pathway (Cheeseman et al., 2006; Varma and Salmon, 2012).

It is noteworthy that the potency of the checkpoint signal varies depending on the trigger and resulting impact on the state of kinetochore attachment (Weaver, 2003; Rieder and Maiato, 2004; Chen et al., 2019). The idea of the checkpoint being more akin to a 'rheostat', having a graded response where the severity of defect affects the SAC response, as opposed to a 'switch-like' activation, was first proposed in 2013 and is now favoured (Dick and Gerlich, 2013; Collin et al., 2013).

1.6 The attachment versus tension dichotomy

The SAC generates a 'wait anaphase' signal until all sister chromatids are correctly bi-oriented to achieve equal segregation of chromosomes to daughter cells. Bi-orientation is a state where sister chromatid kinetochores form stable, end-on attachments with microtubules emanating from opposite spindle pole bodies (reviewed in Foley and Kapoor, 2013). Organisms usually form multiple spindle attachments for each kinetochore, from 2-4 spindle microtubules binding fission yeast kinetochores to approximately 30 in mammalian cells (with the exception of budding yeast which binds 1) (Pidoux and Allshire, 2004; London and Biggins, 2014). Given that initial microtubule attachment to kinetochores occurs in a stochastic manner, kinetochore attachments tend to be error prone, and involve various rounds of attachment and destabilisation in early mitosis (Kitajima et al., 2011; Magidson et al., 2011). These errors need to be resolved to achieve biorientation and proper segregation. This can be done by stabilising correct attachments and destabilising incorrect attachments — allowing the opportunity to bi-orient correctly.

Bi-orientation is attained through bi-polar attachment and tension (Maresca and Salmon, 2010) which are controlled by the SAC and error correction pathways. Tension refers to the force generated at kinetochores when cohesion between sister chromatid pairs opposes the pulling force of bipolar mitotic spindle (Pinksy and Biggins, 2005). While it is widely accepted that the SAC proteins accumulate at unattached kinetochores (monotelic attachment), how a tensionless kinetochore which is attached to microtubules (syntelic and merotelic attachments) activates the 'wait anaphase' signal is more elusive (Fig. **1.2**) (London and Biggins, 2014; Nezi and Musacchio, 2009; Khodjakov and Pines, 2010; Maresca and Salmon, 2010). Elucidating a molecular mechanism for how different upstream pathways (triggered by tension and attachment) lead to checkpoint activation and a metaphase delay is important for understanding how the SAC ensures accurate segregation.

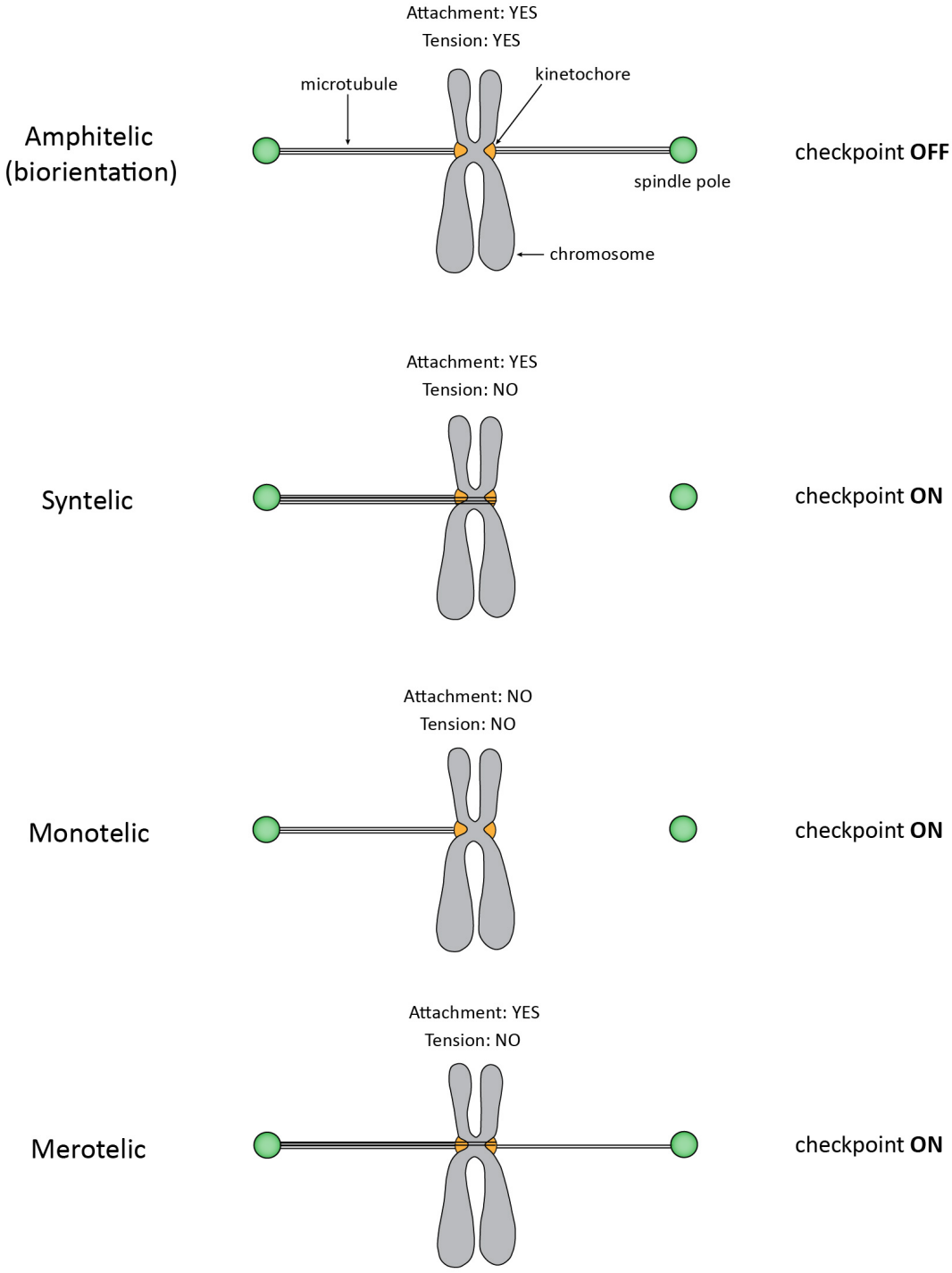

Figure 1.2: Types of kinetochore-microtubule attachments . Schematic depicting the different types of kinetochore-microtubule attachments. The resulting effect on the state of attachment and tension is indicated along with whether the SAC is activated.

A strong argument in support of the tension-sensing model is that syntelic attachments (where both sister chromatids bind microtubules from the same pole) activate the SAC (Watanabe, 2006). A study using grasshopper spermatocytes was the first to describe the role of tension in stabilising kinetochore-microtubule attachments and achieving bi-orientation. They demonstrated that artificially applying tension to an unpaired chromosome using a glass micro-needle enabled cell cycle progression. They also observed that improper attachments were destabilised, suggesting that cells are able to sense and correct errors (Nicklas and Koch, 1969). Further experiments were published in support of the tension hypothesis (Li and Nicklas, 1995; Jang et al., 1995; Stern and Murray 2001).

Early work by Rieder and colleagues used laser ablation to disrupt kinetochores and demonstrate that a single unattached kinetochore in mitotic rat Potoroo kidney cells can delay anaphase (Rieder et al., 1995). Subsequent ablation of an unattached kinetochore then allowed anaphase onset, suggesting that unattached kinetochores activate the SAC and delay anaphase. However, this unattached kinetochore also lacks tension. The difficulty in distinguishing the role of tension and attachment in SAC activation lies in the interconnectivity of unattached and tensionless states as they exist simultaneously. Microtubule attachments to kinetochores under reduced tension are destabilised to be corrected. This destabilisation results in a tensionless, unattached kinetochore state. Therefore, whether a tensionless kinetochore i) activates the SAC directly (by triggering SAC signalling), ii) indirectly (by producing an unattached kinetochore), or iii) delays anaphase via an independent mechanism, is unclear (Proudfoot et al., 2019).

It is possible that there is variation between organisms in the attachment versus tension signal that results in a metaphase delay. This could be a result of different kinetochore structures and or arrangements (London and Biggins, 2014). For instance, in mammalian cells where all kinetochores are unattached in prophase, attachment could be more important. Whereas yeast kinetochores are associated with SPBs throughout the cell cycle where unattached kinetochores may be less common and tension may need to play a greater role in signalling erroneous attachments. In addition, mammals which have several kinetochore microtubule attachments may be less sensitive to small changes in microtubule occupancy and tension. Whereas budding yeast, which have one microtubule attachment, may be more so (London and Biggins, 2014). Nevertheless, a molecular basis for how tension signals the

SAC is important for understanding the observations from studies based on mechanical disruption of kinetochores and/or microtubule attachments.

A molecular basis for tension sensing

A popular model for tension sensing is the Aurora B^{Ark1} kinase-mediated pathway (reviewed in Lampson and Cheeseman, 2011). It proposes that Aurora B is able to sense 'kinetochore stretch', a product of tension. Aurora B is part of the CPC, positioned at the inner centromere between sister chromatids. This model suggests that the tension sensing pathway is regulated spatially through Aurora B phosphorylation. Upon lack of bipolarity, 'kinetochore stretch' is low, positioning Aurora B closer its outer kinetochore substrates which include KNL1, Ndc80 and Dsn1. Phosphorylation of these proteins destabilises microtubule-binding at kinetochores, thus generating unattached kinetochores which can then activate the checkpoint (Welburn et al., 2010; Ciferri et al., 2008; Cheeseman et al., 2006; DeLuca et al., 2006). Protein phosphatase 1 (PP1), recruited to the outer kinetochore KNL1-RVSF motif is thought to oppose Aurora B (Liu et al., 2010). Aurora B-mediated phosphorylation of the KNL1-RVSF motif displaces PP1, in a positive feedback loop that destabilises kinetochore-microtubule attachments for error correction.

An alternate tension-sensing model put forward by the Desai lab argues that Aurora B, activated by Survivin-dependent centromeric chromatin clustering or Survivin-independent microtubule clustering, can differentiate between correct and incorrect attachments (Campbell and Desai, 2013). They speculate that this distinction is possible through substrate affinity, with attached kinetochores under tension being less sensitive to Aurora B activity.

1.7 Spindle assembly checkpoint: overview

The SAC is a conserved mechanism in eukaryotes that ensures chromosome transmission fidelity during mitosis and meiosis (Rieder et al., 1995; Li and Nicklas, 1995). It is able to respond to a lack of or incorrect attachment of kinetochores to spindle microtubules and prevent anaphase. Thus providing time for error correction to enable proper attachments prior to chromosome segregation. In order to satisfy the checkpoint and progress with anaphase, all of the kinetochores need to be attached to spindle fibres and correctly bi-oriented to opposite spindle poles (Rieder et al., 1995).

Kinetochores are multi-protein structures present at centromeres of sister chromatids. They form points of attachment for microtubules, and, an area for localisation of several

proteins (Cheeseman and Desai, 2008). The SAC signal is produced upon recruitment of proteins to the kinetochore. The SAC components required for the activation and potentiation of the signal in prometaphase are conserved and include the kinases Ark1$^{\text{Aurora B}}$ (**au**ro**r**a-B **k**inase) and Mph1$^{\text{Mps1}}$, the kinetochore protein Spc7$^{\text{KNL1}}$, and the Mad (**m**itotic **a**rrest **d**efective) and Bub (**b**udding **u**ninhibited by **b**enzimidazoles) proteins Mad1, Mad2, Mad3$^{\text{BubR1}}$, Bub1 and Bub3 (London and Biggins, 2014).

The SAC signalling pathway prevents anaphase by generating an effector complex named the MCC (**m**itotic **c**heckpoint **c**omplex). The MCC inhibits the APC/C (**a**naphase **p**romoting **c**omplex/**c**yclosome) (Hardwick et al., 2000; Fraschini et al., 2001; Sudakin et al., 2001), preventing ubiquitination and subsequent degradation of Securin$^{\text{Cut2}}$ and Cyclin B$^{\text{cdc13}}$ (Peters, 2006) (Fig. **1.3**). This prevents chromosome segregation and sustains CDK1-cyclin B activity, delaying metaphase exit until correct kinetochore-microtubule attachments form.

1.8 Kinase-dependent activation of the SAC

The balance between kinase and phosphatase activity plays a major role in regulating the cell cycle (Novak et al., 2010). In the same way, the activity of the serine/threonine protein kinase Aurora B$^{\text{Ark1}}$ and PP1$^{\text{Dis2}}$ (**p**rotein **p**hosphatase **1**) compete at the kinetochore. Aurora B, a subunit of the chromosomal passenger complex (CPC), phosphorylates CENP-A and the KMN network (KNL1$^{\text{Spc7}}$ in particular) (reviewed in Carmena et al., 2012), therefore decreasing microtubule-binding affinity at poorly attached kinetochores (Welburn et al., 2010), and delaying anaphase. This is an important point of control as it is the site of the 'tug of war' between the kinases and PP1$^{\text{Dis2}}$, which is responsible for silencing the checkpoint (Vanoosthuyse and Hardwick, 2009; Liu et al., 2010; Rosenberg et al., 2011).

A key role of Aurora B in the checkpoint is to help recruit Mps1$^{\text{Mph1}}$ (**m**ono**p**olar **s**pindle **1**) kinase to the kinetochore (Weiss and Winey, 1996; Vigneron et al., 2004; Heinrich et al., 2012). This is an important step in SAC activation because Mps1$^{\text{Mph1}}$ kinase has been found to phospho-regulate all downstream checkpoint substrates KNL1, Bub1, Bub3, Mad1, Mad2 and Mad3 (London et al., 2012; London and Biggins, 2014; Hardwick et al., 1996; Ji et al., 2017; Zich et al., 2012; Zich et al., 2016). Identified in all model organisms except *C. elegans*, Mps1 is a conserved kinase, essential for the checkpoint. Aside from its central checkpoint role, Mps1 has functions in spindle pole duplication and bi-orientation. Whereas its fission yeast homologue, Mph1 (**M**ps1 **p**ombe **h**omologue **1**), has an additional function in bi-orientation (Zich and Hardwick, 2010).

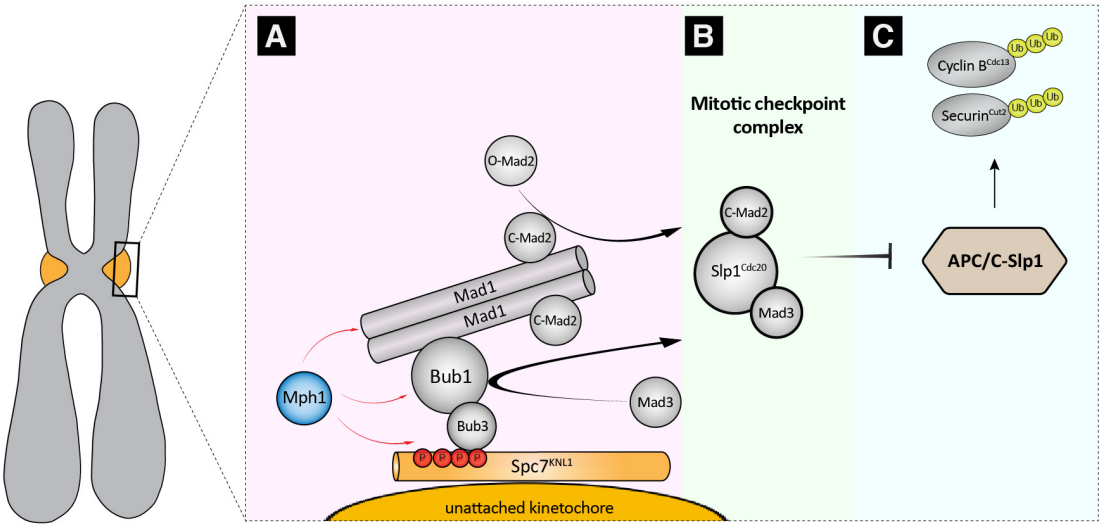

Figure 1.3: Spindle assembly checkpoint signalling in *S .pombe*. (A) Mph1^{Mps1} phosphorylation of Spc7^{KNL1} MELT motifs recruits Bub3-Bub1 and the Mad1-Mad2 tetramer to unattached kinetochores. **(B)** Bub and Mad scaffolds lead to the formation of MCC, comprising of C-Mad2, Slp1^{Cdc20} and Mad3^{BubR1} (this is phospho-dependent; and also includes Bub3 in other model systems). **(C)** MCC inhibits APC/C-Slp1, preventing the ubiquitination and subsequent proteolysis of Cyclin B^{Cdc13} and Securin^{Cut2}, causing a metaphase delay. Red arrows indicate phosphorylation.

Mps1 over-expression has been found to activate the checkpoint in the presence of intact kinetochore-microtubule attachments in a manner dependent on Mad and Bub proteins (Hardwick et al., 1996). Its persistence at the kinetochore delays checkpoint silencing and anaphase onset (Jelluma et al., 2010). Additionally, inhibiting Mps1 prevents the kinetochore localisation of all checkpoint proteins and impedes the checkpoint (Maciejowski et al., 2010; Sliedrecht et al., 2010; Vigneron et al., 2004).

Mps1 is responsible for the hierarchical recruitment of the Bub and Mad proteins to kinetochores (detailed in the following sections). To activate the SAC, it phosphorylates KNL1^{Spc7} on its MELT motifs, allowing Bub3-Bub1 recruitment (London et al., 2012; Shepperd et al., 2012; Yamagishi et al., 2012), subsequent Mad1-Mad2 recruitment, and MCC formation (London and Biggins, 2014). Despite the involvement of various kinases in checkpoint signalling, Mps1 kinase phosphorylates KNL1, Bub1 and Mad1, emphasising the importance of its role in MCC formation (Ji et al., 2017; discussed further in Chapters 3 and 5).

CDK1-cyclin B activity is required for mitotic entry and APC/C-mediated degradation of cyclin B leads to anaphase onset and mitotic exit (Oliveira et al., 2010). In addition, CDK1 has been found to phosphorylate the SAC components Bub1 and Cdc20 (**c**ell **di**vision **c**ycle **20**) (Ji et al., 2017; Miniowitz et al., 2012). Bub1 kinase has been found to play a role in biorientation through phosphorylation of histone H2A which enables Shugoshin-dependent loading of Aurora B to centromeres (Fernius and Hardwick, 2007; Kawashima et al., 2010). Data from our lab suggests that the kinase activity of Bub1 is required for an efficient metaphase delay in response to spindle perturbation caused by the anti-mitotic drug **c**ar**b**enda**z**im (CBZ), whereas this is less apparent in temperature sensitive β-tubulin mutant *nda3-KM311* (**n**uclear **di**vision **a**rrest **3**) arrests where spindle microtubules are completely inhibited (Onur Sen, unpublished). In addition, Bub1-mediated phosphorylation of Cdc20 in human cells has been found to contribute to checkpoint signalling (Jia et al., 2016; Tang et al., 2004; Faesen et al., 2017).

1.9 SAC signalling: assembly of the KNL1-Bub3-Bub1 scaffold

The discovery of BUB and MAD from genetic screens in budding yeast provided the first molecular evidence for SAC feedback control (Hoyt et al., 1991; Li and Murray, 1991). This opened a field of research into its regulation and mechanism of action. The following

sections describe how signalling at KNL1-Bub and Mad1-Mad2 scaffolds leads to the formation of an APC/C inhibitory complex.

It is widely accepted that checkpoint signalling initiates at the microtubule binding interface of the outer kinetochore, specifically at the KMN^{NMS} network, with $KNL1^{Spc7}$ being the principle receptor for the Bub proteins Bub1, Bub3, $BubR1^{Mad3}$ (**B**ub-**r**elated **k**inase **1**) (Ito et al., 2011; London et al., 2012; Shepperd et al., 2012; Yamagishi et al., 2012).

BubR1 is a Bub1 kinase paralogue and a pseudokinase in vertebrates which arose out of whole genome duplication events in yeast (Hardwick et al., 2000; Kellis et al., 2004; Vleugel et al., 2012). The kinase domain of BubR1 has been found to promote protein stability (Suijkerbuijk et al., 2012). Bub1 and BubR1 have kinase domain-dependent roles in kinetochore bi-orientation, although this is not required for their checkpoint role (Fernius and Hardwick, 2007; Suijkerbuijk et al., 2012; Kawashima et al., 2010). Consistently, the N-terminal Bub1 yeast paralogue Mad3 (also the result of whole genome duplication events) lacks the kinase domain is not implicated in bi-orientation (Vleugel et al., 2012).

The mechanism of Bub recruitment to $KNL1^{Spc7}$ surfaced in light of findings from our lab in collaboration with the Millar lab, and results from the Biggins and Watanabe groups (London et al., 2012; Shepperd et al., 2012; Yamagishi et al., 2012). These results demonstrated that $Mps1^{Mph1}$-dependent phosphorylation of threonine residues on the conserved MELT-like ([**M**/I/L/V]-[**E**/D]-[M/I/**L**/V]-**T**) motifs of $KNL1^{Spc7}$ (Spc105 in budding yeast) accommodates Bub3-Bub1 binding (see **Fig. 1.3**). This method of recruitment is conserved in fission yeast, budding yeast, as well as human cells, with non-phosphorylatable MELT mutants exhibiting defective checkpoint signalling. These studies also revealed that Bub1 recruitment to KNL1 occurs via Bub3, and that Bub1 stabilises the Bub3-KNL1 interaction (Krenn et al., 2012; Primorac et al., 2013).

Bub1 and BubR1 form stable, mutually exclusive, complexes with Bub3, both via the GLEBS domain (**Gle**2 **b**inding **s**equence) (Wang et al., 2001; Larsen et al., 2007). Perhaps surprisingly, it was found that BubR1 does not stabilise the Bub3-KNL1 interaction (Primorac et al., 2013; Krenn et al., 2014), suggesting an alternate kinetochore recruitment method. It was subsequently found that human BubR1 heterodimerises with Bub1 at kinetochores with an active SAC signal (Overlack et al., 2015). Although it has been suggested that this interaction is not required for checkpoint activation (Zhang et al., 2015). The recruitment of fission yeast Mad3 remains more elusive although recent findings point

towards a similar Bub1-dependent mechanism mediated by direct interactions between their TPR (**t**etratrico**p**eptide **r**epeat) domains (Ioanna Leontiou, unpublished). Bub1, BubR1 and Mad3 proteins all have a TPR domain (Vleugel et al., 2012). Data from our lab found that tethering Bub1 to telomeres recruited Mad3 (Rischitor et al., 2007). Furthermore, FRAP (**f**luorescence **r**ecovery **a**fter **p**hotobleaching) experiments confirmed the dynamic nature of Mad3 when at kinetochores compared to the stable association of Bub1. Interestingly, BubR1 and Mad3 also contain conserved degradation motifs - the D (**d**estruction) box (RxxLxxxx[EDNQ]) and KEN (Lys-Glu-Asn) boxes KEN1 and KEN2, which cause ubiquitin-mediated proteolysis (Tang et al., 2004). These signals are commonly recognised by APC/C-Cdc20.

The N-terminus of KNL1 contains multiple MELT motifs and the copy number of consensus sites varies amongst organisms. Human KNL1 has 19 putative MELT-like motifs, compared to 12 in *S. pombe* (Vleugel et al., 2013; Shepperd et al., 2012; Yamagishi et al., 2012). Recent data suggests that MELT motifs portray different signalling capacities as a result of Bub3-Bub1 binding affinity (Chen et al, 2019). This is indicative of Bub3-Bub1 MELT recruitment being an important modulator of SAC signalling output, able to rapidly initiate a signal which regulates cell cycle progression in the presence of varying inputs - a single, or several kinetochore-microtubule defects.

KNL1 has two N-terminal KI (lysine-isoleucine) motifs, conserved in a few vertebrates (Vleugel et al., 2012). They are implicated in Bub1 and BubR1 binding which, although found to be non-essential for SAC signalling in the past, may enhance localisation of Bub proteins to MELT motifs according to more recent data (Kiyomitsu et al., 2011; Krenn et al., 2012; Krenn et al., 2014).

1.10 Kinetochore recruitment of the Mad1-Mad2 scaffold

The Mad1-C-Mad2 (**c**losed-Mad2) heterotetramer (Chen et al., 1999) is an essential, conserved checkpoint complex which acts in concert with the KNL1-Bub1-Bub3 complex to generate MCC. Kinetochore localisation of Mad1-Mad2 in prometaphase marks an active checkpoint and studies have found that tethering Mad1 to kinetochores, using Mis12 as an anchor, activates the checkpoint (Maldonado and Kapoor, 2011; Kuijt et al., 2014; Heinrich et al., 2014).

In vivo yeast studies from our lab and others, *C. elegans* work, as well as *in vitro* work using human proteins have advanced our understanding regarding the long-standing question of the kinetochore receptor for Mad1 (detailed in Chapter 5). Mad1 is recruited to kinetochores by a direct interaction with Bub1 (Brady and Hardwick, 2000; London and Biggins, 2014; Moyle et al., 2014; Yuan et al., 2017; Zhang et al., 2017, Ji et al., 2017). The Mad1 RLK (arginine-leucine-lysine) motif binds Bub1-CD1 (**c**onserved **d**omain **1**) in a Mps1 kinase dependent manner in yeasts and humans (Brady and Hardwick, 2000; Klebig et al., 2007; Heinrich et al., 2014; Ballister et al., 2014; Yuan et al., 2017; Zhang et al., 2017, Ji et al., 2017).

Interestingly, Mad1 kinetochore localisation has functions beyond transporting Mad2 to the kinetochore as tethering Mad2 directly to kinetochores only triggers a checkpoint arrest in the presence of Mad1 (Kruse et al., 2014). In addition, targeting a C-terminal Mad1 mutant to the kinetochore in which Bub1, Mad2 and Mad1 localisation is intact, abrogates the checkpoint (Ballister et al., 2014; Heinrich et al., 2014; Kruse et al., 2014). This suggests that Mad1 has an additional, uncharacterised role in checkpoint activation which is the basis of Chapter 5.

While Bub1 is the only kinetochore receptor of Mad1 in fission yeast (Yuan et al., 2017), there is mounting evidence of an additional means of Mad1 kinetochore recruitment in humans as depleting Bub1 or mutating the RLK motif does not completely abolish Mad1 kinetochore localisation (Kim et al., 2012). The RZZ (Rod-ZW10-Zwilch) complex, primarily present in metazoans (Vleugel et al., 2012), is also required to recruit Mad1 in mammalian cells (Santaguida et al., 2010; Silio et al., 2015; Zhang et al., 2019; Rodriguez-Rodriguez et al., 2018). RZZ localises to the outer kinetochore soon after nuclear envelope breakdown through KNL1-Zwint (Kops et al., 2005; Varma et al., 2013).

Experiments carried out in diploid hTERT-RPE1 cells found that Bub1 is not required for checkpoint activation in response to unattached kinetochores (Currie et al., 2018). This is consistent with a study in human HAP1 cells (which are near-haploid) which found that neither receptor is essential for responding to unattached kinetochores (Raaijmakers et al., 2018). However it is important to note that studies (Currie et al., 2018, Raaijmakers et al., 2018) which rely on so-called CRISPR/Cas9 'knock-out' cells for complete Bub1 deletion should be treated with caution (Meraldi, 2019). It has been reported recently that low levels of Bub1 are expressed in clones constructed by short deletions and frame shifts of the first few exons of BUB1 as a result of alternatively spliced Bub1 mRNA (Rodriguez−Rodriguez

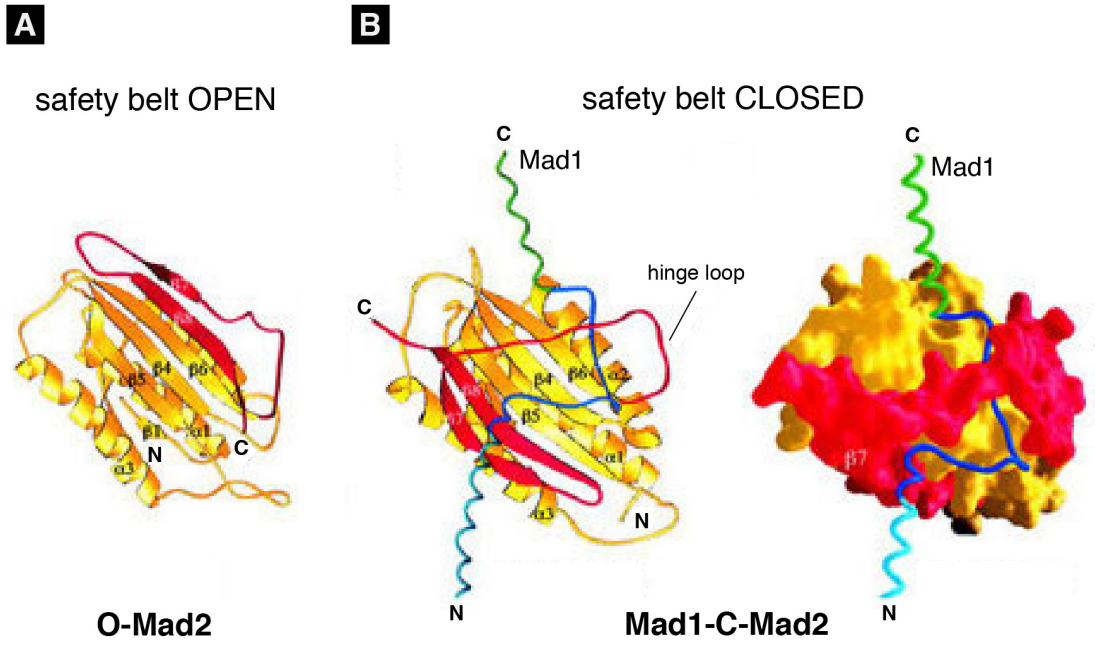

Figure 1.4: Structural rearrangement of Mad2 open and closed conformations. (A) Ribbon diagram representation of open-Mad2 monomer (yellow), showing the C-terminal tail in red. The flexible hinge loop region allows for the conformational change in the 'safety belt' **(B)** Left: Ribbon diagram representation of closed-Mad2 (yellow) with the C-terminal 'safety belt' rearranged (red) for stable Mad1 binding (worm representation of Mad1 residues 485-584 in blue/green). Mad1-C-Mad2 heterodimer (as opposed to tetramer) shown for clarity. Right: molecular surface of C-Mad2 (yellow/red) with worm representation of Mad1 (blue/green) (adapted from Sironi et al., 2002).

et al., 2018) which can be difficult to detect unless using sensitive mass spectrometry (Zhang et al., 2019).

More recent work in HeLa cells from the Nilsson lab suggests that the RZZ complex facilitates Mad1 binding to Bub1, with the two receptors acting synergistically to efficiently recruit Mad1 (Zhang et al., 2019). Using a combination of CRISPR-Cas9 and RNAi to deplete Rod and Bub1, they demonstrate that although RZZ improves Mad1 recruitment, it can be bypassed by tethering Mad1 to kinetochores or increasing the potency of Mad1-Bub1 binding. They find that the same does not apply to Bub1, which is necessary, suggesting that the fundamental Mad1 receptor mechanism is conserved.However, it is unclear in what way, if any, the Bub1 and RZZ receptors overlap to stimulate checkpoint signalling, and if this varies depending on the SAC trigger and/or cell type.

1.11 The Mad2 template model

The initial step in forming the SAC effector — the **m**itotic **c**heckpoint **c**omplex (MCC), consisting of C-Mad2-Mad3^{BubR1}-Bub3- Cdc20^{Slp1} (*S. pombe* MCC lacks Bub3) (Sudakin et al., 2001, Chao et al., 2012), is a conformational change in Mad2 resulting in Cdc20^{Slp1} binding. The 'Mad2 template model' (DeAntoni et al., 2005) is the favoured model for explaining the formation of the APC inhibitory C-Mad2-Cdc20^{Slp1} signal. It is known that all MCC components interact dynamically at or proximal to the outer kinetochore, rapidly cycling on and off (Kallio et al., 2002; Shah et al., 2004; Howell et al., 2004). FRAP experiments studying the dynamics of proteins at kinetochores and structural studies have been instrumental in capturing the unusual conversion behaviour of Mad2.

There are two distinct pools of Mad2, each assuming one of two conformations, a mobile, 'open' cytosolic conformation when unbound and a 'closed' conformation when bound to either of its ligands Mad1 or Cdc20^{Slp1} (Shah et al., 2004; Luo et al., 2004). When in the closed conformation, a C-terminal tail consisting of two mobile β-sheets comes across the face of C-Mad2 (**c**losed-Mad2), enclosing Mad1-MIM (**M**ad2 **i**nteracting **m**otif) in a molecular 'safety belt'-like mechanism (Sironi et al., 2002) (see Fig **1.4**). Mad1-C-Mad2, recruited to kinetochores in prometaphase, then assumes the role of receptor for the more transient O-Mad2 (**o**pen-Mad2) conformer. In accordance with this model, mutations perturbing the dimerisation of C-Mad2-O-Mad2 prevent kinetochore localisation of O-Mad2 and checkpoint signalling (DeAntoni et al., 2005; Mapelli et al., 2006; Nezi et al., 2006).

The Mad2 template model proposes that Mad1-C-Mad2 converts O-Mad2 to C-Mad2 to enable Cdc20^{Slp1} binding at the kinetochore (Luo et al., 2000; Luo et al., 2002; DeAntoni et al., 2005, Mariani et al., 2012). This binding interface resembles that of Mad1-C-Mad2 as the 123-137 amino acid segment of the Cdc20 N-terminus 'threads' through the C-terminal tail of Mad2 (Sironi et al., 2002). The template model is proposed to be a catalytically active process, facilitated by Mad1-C-Mad2, that results in a Cdc20^{Slp1}-C-Mad2 complex. It was found that Mps1 activity is necessary for Mad2 conversion as inhibiting Mps1 during mitosis prevents recruitment of O-Mad2 to Cdc20^{Slp1}-C-Mad2 present at kinetochores (Hewitt et al., 2010). A Mad2 mutant that is locked in the open conformation is unable to localise to kinetochores when Mps1 is inhibited. In comparison, kinetochore recruitment of a Mad2 mutant that is permanently bound to Mad1 was not hindered (Hewitt et al., 2010). In further support of this, a recent *in vitro* reconstitution study using FRET sensors to detect MCC formation has found that Mad1-C-Mad2 catalyses Mad2 conversion upon Mps1 phosphorylation (Faesen et al., 2017). Thus phosphorylated Mad1-C-Mad2 catalyses the formation of Cdc20^{Slp1}-C-Mad2, which is the rate-limiting step in MCC generation.

The template model results in prion-like (Lara-Gonzalez et al., 2012) expansion of the inhibitory signal with Mad1-C-Mad2 facilitating conversion of O-Mad2 to C-Mad2. Low levels of C-Mad2 during interphase, low Mps1 kinase activity, and the resulting slow O-Mad2 to C-Mad2 kinetics, can explain why Mad2 conversion is inefficient during interphase. How the Mad2 substrate formed upon dimerisation of O-Mad2 with Mad1-C-Mad2 is loaded onto Cdc20 is unknown and remains an interesting question. Whether C-Mad2 directly binds Cdc20 or forms an intermediate substrate is unclear.

1.12 MCC: The product of Bub and Mad signalling

The Cdc20^{Slp1}-C-Mad2 complex is not sufficient to inhibit APC/C. BubR1^{Mad3} has been found to associate with Cdc20^{Slp1} in a Mad2-dependent manner (Hardwick et al., 2000; Fang 2002; Davenport et al., 2006; Burton and Solomon, 2007). Integration with Cdc20^{Slp1}-C-Mad2 occurs through an N-terminal KEN box (KEN1) (King et al., 2007; Sczaniecka et al., 2008; Malureanu et al., 2009; Elowe et al., 2010). The crystal structure of *S. pombe* MCC depicts how the helix-turn-helix motif of the KEN box of BubR1^{Mad3} directly associates with both C-Mad2 and Cdc20^{Slp1} (Chao et al., 2012) (Fig. **1.5**). This structure also revealed a mutually exclusive binding pattern where BubR1^{Mad3} binds C-Mad2 at its O-Mad2

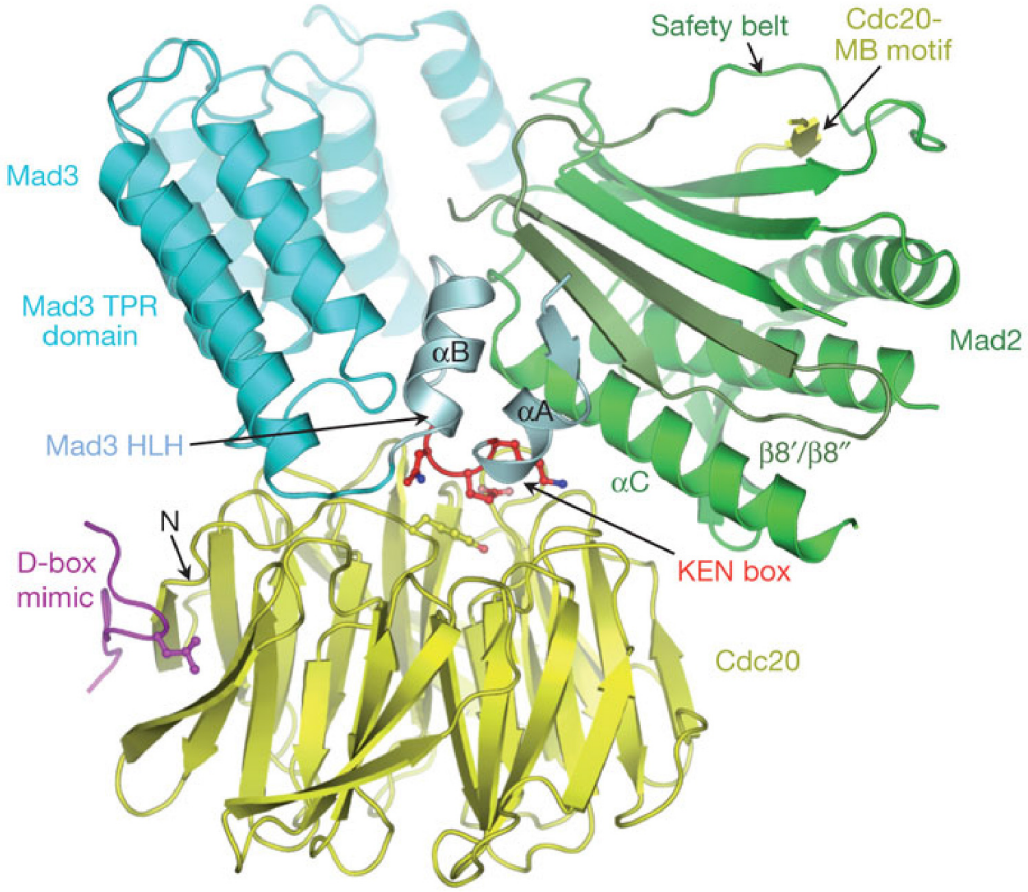

Figure 1.5: Structure of *S. pombe* mitotic checkpoint complex. Ribbon diagram representation of MCC trimer depicting C-Mad2 (green), Mad3^{BubR1} (cyan) and Cdc20^{Slp1} (yellow). KEN box shown in red. The Cdc20-bound C-terminal D-Box mimic is shown in magenta. The B8'/B8" hairpin forms the Mad2-Mad3^{BubR1} binding interface and is shown in dark green (adapted from Chao et al., 2012).

dimerisation region. This suggests that C-Mad2 can no longer convert O-Mad2 once MCC is formed. In addition, BubR1^{Mad3} TPR (**t**etratrico**p**eptide **r**epeat) domains have also been proposed to facilitate C-Mad2-Cdc20 binding (Lara-Gonzalez et al., 2011).

Whereas association of C-Mad2, Mad3^{BubR1} and Cdc20^{Slp1} is sufficient for MCC formation in *S. pombe* (Fig. **1.5**), Bub3 is a MCC component in other model organisms (Sudakin et al., 2001; Chao et al., 2012). Despite Bub3 not being required for BubR1^{Mad3} ligand binding, association of Bub3 with BubR1 is necessary for efficient APC/C inhibition, as mutating the Bub3 binding motif in BubR1 greatly reduces checkpoint efficiency despite retaining C-Mad2-Cdc20 and APC/C binding (Lara-Gonzalez et al., 2011; Elowe et al., 2010). Although *in vitro* studies indicate that Bub3 is not necessary for APC/C inhibition (Tang et al., 2001; Fang et al., 2002; Kulukian et al., 2009), it has been suggested that Bub3 may facilitate recruitment of BubR1 to SAC signalling kinetochores where MCC formation is accelerated (Lara-Gonzalez et al., 2011) since they are the major site of C-Mad2-Cdc20 production. Ultimately, the SAC effector — MCC, is formed.

1.13 APC/C inhibition

The APC/C is an E3 ubiquitin ligase that polyubiquitylates key mitotic substrates through KEN and/or D-box degron recognition, promoting anaphase entry (Clute and Pines 1999; Thornton and Tockzyski, 2003). This targets them for destruction by the 26s proteasome. The aim of SAC signalling is to inhibit the APC/C and prevent ubiquitin-mediated degradation of Securin and Cyclin B^{Cdc13}. Securin degradation promotes the cleavage of Cohesin, the ring-like structures which hold sister chromatids together, as it usually binds to and inhibits the protease Separase. The APC/C also targets Cyclin B, therefore depleting Cyclin B-CDK1mediated phosphorylation which promotes exit from mitosis (Peters, 2006).

The SAC signalling inhibits the APC/C by generating an effector complex named the MCC (**m**itotic **c**heckpoint **c**omplex) (Sudakin et al., 2001). The MCC incorporates the APC/C co-activator Cdc20^{Slp1}, which then binds to the APC/C, thereby preventing mitotic substrate binding (Mapelli and Musacchio, 2007). This occurs through the 'pseudo substrate model', confirmed by the crystal structure of MCC, which postulates that the KEN1 box of BubR1 acts as a pseudosubstrate inhibitor of Cdc20 (Burton and Solomon, 2007; Sczaneicka et al., 2008; Rahmani et al., 2009; Elowe et al., 2010; Chao et al., 2012). Recent findings from *in vivo* fission yeast studies demonstrate that a second molecule of Cdc20, already bound to activated APC/C 'Cdc20^{A}', is inhibited by the MCC through binding the C-

terminal KEN2 and ABBA motifs of Mad3 (May et al., 2017; Sewart and Hauf, 2017). This work supports *in vitro* reconstitution studieson human MCC-APC/C (Izawa and Pines, 2015; Alfieri et al., 2016; Yamaguchi et al., 2016).

1.14 Spindle assembly checkpoint silencing

Once stable kinetochore microtubule attachments are formed and the checkpoint is satisfied, SAC signalling needs to be rapidly inactivated to ensure timely segregation of chromosomes so that cells can progress to anaphase and resume the cell cycle. This inactivation of the checkpoint is termed 'silencing'. In order for the checkpoint to be silenced, the inhibitory signal targeting the APC/C needs to be lifted. This can occur by halting the production of new MCC as well as disassembing existing MCC from APC/C. The mechanisms and regulators of checkpoint silencing are less well characterised than checkpoint activation. This could be due to the difficulty in capturing cells undergoing SAC silencing in the cell cycle and requires further investigation.

PP1^{Dis2} (**p**rotein **p**hosphatase **1**; Dis2 in *S. pombe*; Glc7 in *S. cerevisiae*) is an important, well-conserved silencing factor in yeast and humans (Pinsky et al., 2009; Vanoosthuyse and Hardwick, 2009; Meadows et al., 2011). PP1 is recruited to kinetochores via KNL1^{Spc7} and the kinesins Klp5 and Klp6 (Liu et al., 2010; Meadows et al., 2011; Rosenberg et al., 2011). PP1 opposes Mps1^{Mph1} (Aravamudhan et al., 2015) and Aurora B activity (Liu et al., 2010) at KNL1^{Spc7} as stable end-on kinetochore attachments form. It is able to bind the conserved SILK and RVSF motifs (also referred to as the A and B motifs) present at the amino terminus of KNL1^{Spc7}. Mutating these motifs in both fission and budding yeast greatly abrogates silencing, causing a prolonged, lethal checkpoint arrest (Meadows et al., 2011; Rosenberg et al., 2011; Amin et al., 2018). Klp mutants have also been found to negatively impact silencing in yeast, albeit to a lesser extent (Meadows et al., 2011; Amin et al., 2018). Furthermore, studies have found that most of Mps1^{Mph1}, likely bound to Ndc80, is displaced upon stable end-on microtubule attachment (Aravamudhan et al., 2015; Hiruma et al., 2015; Ji et al., 2015). This release of Mps1 from kinetochores is essential for checkpoint silencing (Jelluma et al., 2010). The resulting reduction in kinase activity at kinetochores decreases Mad1-Mad2 localisation and helps 'tip the balance' in favour of increased dephosphorylation of Mps1^{Mph1} substrates and metaphase exit.

Another suggested mechanism for preventing kinetochore-associated MCC production is the 'stripping' of Mad1-Mad2 from kinetochores to spindle pole bodies (Howell et al., 2001;

Gassmann et al., 2008; Gassmann et al., 2010; Barisic et al., 2010). Upon satisfactory microtubule attachment, RZZ-associated Spindly enables binding to the minus-end directed microtubule motor dynein/dynactin for removal or 'stripping' of Mad1-Mad2 from the kinetochore. In *S. pombe*, movement to the spindle poles is driven by a Mad1-Cut7 Kinesin-5 motor (Eg5 homologue) (Akera et al., 2015), although its contribution to silencing, if any, is unclear.

There are two mechanisms in place to degrade cytosolic free and APC/C-bound MCC. The first is conserved APC/C-mediated ubiquitination and degradation of MCC associated $Cdc20^{Slp1}$ (Pan and Chen 2004; Reddy et al., 2007; Ge et al., 2009; Foe et al., 2011). The second, not found to occur in *S. pombe*, occurs via C-Mad2 inhibition in animal, plant and insect models. The HORMA domain protein $p31^{comet}$ and the AAA ATPase TRIP-13 inhibit C-Mad2, converting it to the unbound, open conformation (Habu et al., 2002; San-Segundo and Roeder, 1999; Vader, 2015; Ye et al., 2015). Therefore, in an ATP-dependent process, $p31^{comet}$ and TRIP-13 disassemble free MCC (Eytan et al., 2014). $p31^{comet}$ is also thought to bind to APC/C-bound MCC and 'extract' Mad2, eventually destabilising APC/C-bound MCC (Westhorpe et al., 2011). The links, if any, between the two MCC disassembly pathways are yet to be elucidated. An additional ATP-dependent factor that disassembles MCC by releasing Cdc20 has been identified as the chaperonin CCT/TRiC (**c**haperonin **c**ontaining **T**CP1 or **T**CP1–**Ri**ng **c**omplex) (Kaisari et al., 2017). This chaperone is conserved in yeast although it is unclear if it contributes to silencing as it is also necessary for activating Cdc20 (Camasses et al., 2003), making its roles difficult to distinguish.

1.15 Aims of this work

This work aims to:

I. Reconstitute checkpoint activation and silencing employing a novel chemically-induced dimerisation tool in *S. pombe*. Chapter 3 describes an assay to control checkpoint activation and silencing by regulating the formation of minimal Mph1 and Spc7 heterodimers. This method allows for ectopic control of the SAC, without impacting the structural and functional complexities associated with kinetochores. Chapter 4 follows on, studying the effects of prolonged checkpoint activation in *S. pombe* and HeLa cells.

II. Identify the kinetochore receptor of Mad1 in *S. pombe* and characterise the additional roles of the Mad1 C-terminus, aside from Mad2 recruitment to kinetochores, in

checkpoint activation. These questions are investigated in Chapter 5 using genetics and biochemistry where surprisingly stable interactions between the Mad1 C-terminus and $Cdc20^{Slp1}$ are detected.

CHAPTER 2

Materials and methods

2.1 DNA methods

2.1.1 Polymerase chain reaction

Q5® Hi-Fidelity 2X Master Mix (New England Biolabs) was used for cloning purposes in accordance with manufacturer's instructions.

To test the genotype of yeast clones, a colony PCR using Taq polymerase was used. A large yeast colony was transferred from a fresh plate to PCR tubes containing 10 µL of 0.02N NaOH. Cells are heated at 95°C for 5 minutes and then cooled on ice. The lysate is vortexted and 2 µL is added to 28 µL of the PCR reaction (in the table below) as a template. The steps for Colony PCR are also given below.

Colony PCR components:

Reagent	Volume (µL)
dH_2O	16.5
10X buffer	3.0
2mM dNTP	1.5
10µM forward primer	3.0
10µM reverse primer	3.0
Cell lysate	2.0
Taq polymerase	1.0

Colony PCR conditions:

Step	Temperature (°C)	Time
Initial boil	95	5 minutes
Denaturation	92	30 seconds
Annealing and Extension: 30 cycles	92	10 seconds
	50	5 seconds
	72	1 min/kb
Final extension	72	10 minutes
Hold	4-10	forever

2.1.2 Site-directed mutagenesis

Quikchange® Lightning or Quikchange® II site-directed mutagenesis kits were used (Agilent) in accordance with manufacturer's instructions with the exception that all volumes were scaled down by 5X to reach a final volume of 10 μL.

2.1.3 Gibson assembly

Individual DNA fragments to be assembled into a linearised vector backbone were obtained by PCR. The PCR fragments were treated with Dpn1 to degrade template DNA following heat inactivation of the enzyme. 5 μL of DNA fragments was added to 15 μL of homemade gibson master mix. It is important to use equimolar amounts of DNA for efficiency. Reaction is incubated at 50°C for 30 minutes. 2 μL of reaction was transformed into DH5α chemical competent E. coli using heat-shock transformation or 1 μL of reaction was transformed into NEB® 10-beta competent E. coli by electroporation. The optimal method of transformation was determined empirically.

2.1.4 Sequencing

Sanger sequencing was performed by Genepool (University of Edinburgh). Samples prepared using Big Dye® v3.1 Cycle Sequencing Kit (Applied Biosystems) according to the manufacturer's instructions.

2.1.5 Restriction endonuclease digestion

All restriction digests were carried out using enzymes and buffers supplied by New England Biolabs or Roche and used according to manufacturer's instructions.

2.1.6 De-phosphorylation

De-phosphorylation of linearised DNA was performed using Antarctic Phosphatase (New England Biolabs) according to manufacturer's instructions.

2.1.7 Ligation

Ligation was performed using T4 Quick DNA ligase (New England Biolabs) in accordance with manufacturer's instructions.

2.1.8 Bacterial transformation

While heat shock was more commonly used for bacterial transformation, electroporation was used in some instances following gibson assembly. The optimal method of transformation was determined empirically.

Heat shock

DNA was added to 50 µL of defrosted chemically competent DH5α E. coli cells in a pre-chilled tube, gently mixed, and incubated on ice for 30 minutes. Heat shock was performed at 42°C for 45 seconds, the mixture is then placed on ice for 2 minutes after which 250 µL of pre-warmed SOC medium is added. Cells recover at 37°C with shaking for 1 hour before plating on pre-warmed LB selection plates. Plates are incubated at 37°C overnight.

Electroporation

This was carried out with the help of Eftychia Kyriacou in the Heun lab. 1-10 pg DNA was added to 40 µL of thawed NEB® 10-beta competent E. coli (a kind gift from Patrick Heun's lab) in 0.5 mL pre-chilled microfuge tubes and kept on ice for 15-30 minutes. Gently transfer to pre-chilled electroporation cuvettes, tap the suspension to ensure it is at the bottom of the cuvette. Dry the moisture on the outside of the cuvette and electroporate at 25 µF capacitance, 2.5 kV, and 200 Ω resistance. As soon as the electrical pulse is delivered, remove the cuvette from the electroporation device and add 1 mL of SOC medium. Transfer the mixture to a 5 or 10 mL polypropylene tube and incubate at 37°C with gentle rotation (220 RPM) for 30 minutes. Plate onto LB selection plates and incubate at 37°C for 12-16 hours.

2.1.9 Ethanol precipitation of DNA

To isolate DNA from an aqueous solution, 1/10th volume of 3M sodium acetate and 3 volumes of ice-cold 96% ethanol was added and the mix is incubated at -20°C for 30 minutes. Samples were centrifuged at 4°C for 15 minutes at 12000-13000 RPM. The supernatant was removed and the pellet washed with 500 µL 70% ethanol. The samples were centrifuged at room temperature for 5 minutes at 13000 RPM. The supernatant was removed, the precipitated DNA pellet air-dried and re-suspended in 10 µL dH_2O.

2.2 List of plasmids used in this work

Plasmid	Source
pRAD41-P_{adh41}-$Mph1_{303-678}$-3xHA-ABI	this work
pLYS1U-P_{adh21}-NLS-$Spc7_{1-666}$-PYL	this work
pLYS1U-P_{adh21}-NLS-$Spc7_{1-666}$-12A-PYL	this work
pBluescript-hyg-$P_{endogenous}$-2xFLAG-mad1 (based on Karen May's pBluescript-hyg-$P_{endogenous}$-GFP-mad1. hyg-P_{endo}-GFP-mad1. Cassette amplified out for integration at the endogenous mad1 locus of a mad1Δ::ura strain)	this work
pBluescript-hyg-$P_{endogenous}$-2xFLAG-mad1ΔCC (based on Karen May's pBluescript-hyg-$P_{endogenous}$-GFP-mad1ΔCC (Yuan et al., 2017). Cassette amplified out for integration at the endogenous mad1 locus of a mad1Δ::ura strain)	this work
pRAD41-P_{adh41}-$Mph1_{303-678}$-GFP-ABI	this work
pLYS1U-P_{adh21}-NLS-$Spc7_{1-666}$-mCherry-2xFLAG-PYL	this work
pRAD41-P_{adh15}-GFP-ABI	this work
pLYS1U-P_{adh15}-NLS-rTetR-mCherry-2xFLAG-PYL	this work
pRAD41-P_{adh15}-GFP-GID	this work
pLYS1U-P_{adh15}-NLS-rTetR-mCherry-2xFLAG-GAI	this work

2.3 Plasmid construction

pRAD41-P_{adh41}-$Mph1_{303-678}$-3xHA-ABI

Mph1 (residues 303-678) was amplified from a pDONR 201 plasmid containing Mph1 (303-678) (Yuan et al., 2017). 3xHA was amplified from a plasmid from the Allshire laboratory (University of Edinburgh) containing codon-optimised PYL-3x-HA. ABI was amplified from a pMT_CID_ABI_VS_H vector from the Patrick Heun laboratory (University of Edinburgh). These PCR fragments were treated with Dpn1 and assembled into a Sma1-digested and antarctic phosphatase-treated gel-purified pRad41 yeast expression vector by Gibson assembly. A Blp1 digest linearlised the plasmid for yeast integration.

pLYS1U-P_{adh21}-$Spc7_{1-666}$-PYL

The yeast expression vector pLYS1U-P_{adh21}-NLS-rTetR-mCherry-2xFLAG-$spc7_{1-666}$ (Yuan et al., 2017, with a modified adh promoter TATA box: TAAATA for adh21) was digested with Nhe1 and Xho1 and gel purified to isolate the vector backbone. $Spc7_{1-666}$ was amplified from

pLYS1U-P_{adh21}-NLS-rTetR-mCherry-2xFLAG-$spc7_{1-666}$ (Yuan et al., 2017) containing wild type spc7. PYL was amplified from a bVNI-221 vector from the Heun laboratory. The fragments were then assembled into the digested vector backbone using Gibson Assembly. A Not1 digest linearlised the plasmid for yeast integration.

2.4 List of primers used in this work

No.	Name	Sequence (5'-3')	Purpose/Notes
22	Gibson pRAD GFP F	GAATTCATATGTCGACTCTAGAGGATCCCCATGGGTAAAGGAGAAGAACTTTTCACTGG	GFP-ABI construct
23	Gibson - GFP ABI R	GTGAAGCCGTACAGGGGCACTCCAGCTTTTTTGTACAAACTTGTGATATCTTTGTATAGTTCATCCATGC	GFP-ABI construct
24	Gibson - GFP ABI F	GCATGGATGAACTATACAAAGATATCACAAGTTTGTACAAAAAAGCTGGAGTGCCCCTGTACGGCTTCAC	GFP-ABI construct
25	Gibson ABI pRAD R	GGGAGACATTCCTTTTACCCAACTTTACGTTTTTTTTTAGGCTTCAGGTCCACCACCACC	reverse for ABI-pRAD term
26	Gibson - adh-$mph1_{303-678}$ F	TTCATATGTCGACTCTAGAGGATCCCCATGAAGCGTCAGCAGGACGTTGTTACTGTTGCC	mph1-GFP-ABI construct
27	Gibson mph1 - GFP R	GTTCTTCTCCTTTACCCATGTTAATTAACCCGGGGATCCGTTCTGGCATTTTTCGTAAAT	mph1-GFP-ABI construct
28	Gibson - GFP-mph1 F	ATTTACGAAAAATGCCAGAACGGATCCCCGGGTTAATTAACATGGGTAAAGGAGAAGAAC	mph1-GFP-ABI construct
30	$spc7_{1-666}$ + pac1 site R	ACCATGTTAATTAACCCGGGGATCCGATTCAAAGTTGAAATTGATTTT	spc7 to replace rTetR for spc7-mch-PYL construct
33	spc7 + nhe1-NLS F	AGAATTGCTAGCATGCCTAAGAAGAAGCGTAAAGTTATGCCAACATCGCCTCGTCG	spc7 to replace rTetR for spc7-mch-PYL construct
66	GA_mad1flag Pendogenous R	CATTTTGTCATCGTCGTCCTTGTAGTCCATGGGTTTATCGTCATCATCCTTATAATCCATGGATGTAGTCGCTTGATACA	P_{endo}-flag-mad1 construct. Template for mutants.
69	Gibson_spc7 (adh) F	CTTTTCTTTAAGCAAGAGAATTGCTAGCATGCCTAAGAAGAAGCGTAAAGTTATGCCAACATCGCCTCGTCGCAAT	gibson for spc7-PYL construct
70	Gibson_spc7 (PYL) R	TGAACTCGTCCTGGGTGGCCATGTTAATTAACCCGGGGATCCGATTCAAAGTTGAAATTGATTTT	gibson for spc7-PYL construct
71	Gibson_PYL (spc7) F	AAAATCAATTTCAACTTTGAATCGGATCCCCGGGTTAATTAACATGGCCACCCAGGACGAGTTCA	gibson for spc7-PYL construct
72	Gibson_PYL (term) R	CGCTTATTTAGAAGTGGCGCGCCCTCGAGTTAGTTCATGGCCTCGGTGATGGAGG	gibson for spc7-PYL construct
75	Gibson_ABI (term) R	CTGGCAAGGGAGACATTCCTTTTACCCCTTCAGGTCCACCACCACCACGCT	GA mph1-3xHA-ABI construct
76	GA_M1 3UTR-pBS F	CAATGCAAATGGTATAATCCACTATCGAATTCCTGCAGCCCGGG	P_{endo}-flag-Mad1 construct. Template for mutants.

No.	Name	Sequence (5'-3')	Purpose/Notes
78	GA_M1 3UTR-pBS R	CCCGGGCTGCAGGAATTCGATAGTGGATTATACCATTTGCATTG	amplify mad1 from genomic prep for P_{endo}-flag-Mad1 construct.
82	GA_mph1 (3XHA) R	ACATCGTATGGGTAGTTAATTAACCCGGGGATCCGTTCTGGCATTTTTCGTAAATTGCT	GA mph1-3xHA-ABI construct
83	GA_3XHA (mph1) F	GAAAAATGCCAGAACGGATCCCCGGGTTAATTAACTACCCATACGATGTTCCTGACTAT	GA mph1-3xHA-ABI construct
89	PYL F	ATGGCCACCCAGGACGAGTTCAC	PYL sequencing
90	PYL 280 F	CAACACCAGCAGAGAGAGACTGG	PYL sequencing
91	PYL 537 F	CCATCACCGAGGCCATGAAC	PYL sequencing
92	PYL R	GTGAACTCGTCCTGGGTGGCCAT	PYL sequencing
93	adh 724 F	GGGTGGTGGACAGGTGCCTTCG	sequencing
94	GA_3XHA (ABI) R	ATGCTGGTGAAGCCGTACAGGGGCACAGATCCACCAGATCCACCGCACTGAGCAGCGTAATCTGGAACGT	GA mph1-3xHA-ABI construct
95	GA_ABI (3XHA) F	ACGTTCCAGATTACGCTGCTCAGTGCGGTGGATCTGGTGGATCTGTGCCCCTGTACGGCTTCACCAGCAT	GA mph1-3xHA-ABI construct
98	GA_mad1flag FII	ATGGATTATAAGGATGATGACGATAAACCCATGGACTACAAGGACGACGATGACAAAATGGCGGATTCTCCTAGGGATCCGTTCC	amplify genomic mad1 adding N-term flag tag. For P_{endo}-flag-Mad1 construct.
99	Set1_1	AAAATCGAGCTTATATCCAAAAAGAGCAAAAACAGCTTCGCGAAATTCCAA	Mad1 mutagenesis S598A
100	Set1_2	CAGCTTCGCGAAATTCCAAAGCCTTTACTGAAAAAATCTCCTT	Mad1 mutagenesis introducing S589A to S598A construct
101	Set1_3	TTGGAATTTCGCGAAGCTGTTTTTGCTCTTTTTGGATATAAGCTCGATTTT	Mad1 mutagenesis S598A
102	Set1_4	AAGGAGATTTTTTCAGTAAAGGCTTTGGAATTTCGCGAAGCTG	Mad1 mutagenesis introducing S589A to S598A construct
103	Set2_1	CGAGAATATGTGGCTGTAACACGAACACTCCCATTAGGC	Mad1 mutagenesis S616A
104	Set2_2	GCCTAATGGGAGTGTTCGTGTTACAGCCACATATTCTCG	Mad1 mutagenesis S616A
105	Set3_1	GCCTGATGGATTACCAACCAATTTCATTGCGGCGGCTTCGCCATCAAATATAAAAGCGGTATTA	Mad1 mutagenesis S632A, S633A, T634A
106	Set3_2	TAATACCGCTTTTATATTTGATGGCGAAGCCGCCGCAATGAAATTGGTTGGTAATCCATCAGGC	Mad1 mutagenesis S632A, S633A, T634A
107	Set4_1	CAAGAAGCTCTAACGCTAGAGCCGCTAACATGCCT	Mad1 mutagenesis T668A
108	Set4_2	TGGTGTGATGAACGCAAAGCAATACCAGGCATGTTAG	Mad1 mutagenesis introducing T659A to T668A construct
109	Set4_3	CTAACATGCCTGGTATTGCTTTGCGTTCATCACACCA	Mad1 mutagenesis introducing T659A to T668A construct
110	Set4_4	AGGCATGTTAGCGGCTCTAGCGTTAGAGCTTCTTG	Mad1 mutagenesis T668A
113	spc7 1019 F	AATCACGATCAGTCGGAAAA	spc7 sequencing

No.	Name	Sequence (5'-3')	Purpose/Notes
114	spc7 1528 F	CAATTCTTCAAAGCCCATTC	spc7 sequencing
124	ABI 20 F	GTGCCCCTGTACGGCTTCACC	ABI sequencing
125	ABI 285 F	TGGAAAAGTGGAAGAAGGCC	ABI sequencing
126	ABI 602 F	TGAAGCCCAGCATCATCCC	ABI sequencing
137	M1 T659E F	TTTGGTGTGATGAACGCAAAGAAATACCAGGCATGTTAGCGG	Mad1 phosphomimetic mutant
138	M1 T659E R	CCGCTAACATGCCTGGTATTTCTTTGCGTTCATCACACCAAA	Mad1 phosphomimetic mutant
139	M1 T668E F	CAGGCATGTTAGCGGCTCTAGAGTTAGAGCTTCTTGACAAAA	Mad1 phosphomimetic mutant
140	M1 T668E R	TTTTGTCAAGAAGCTCTAACTCTAGAGCCGCTAACATGCCTG	Mad1 phosphomimetic mutant
KM 9	M1 3'UTR	AGCAGTTTTGACTAGTTTGTAATGG	from Karen May
KM 284	M1 5'UTR F1	ATGATAACTTGAATATGTA	from Karen May

2.5 Reaction kits

Product name	Manufacturer	Catalogue number
GeneJET Gel Extraction Kit	Thermo Scientific	K0691
	Promega	A9282
QiaQuick PCR Purification Kit	Qiagen	28104
Monarch® PCR and DNA Cleanup Kit	NEB	T1030S
GeneJET Plasmid Miniprep Kit	Thermo Scientific	K0503
Monarch® Plasmid Miniprep Kit	NEB	T1010L
Quikchange® Lightning	Agilent	210518
Quikchange® II	Agilent	200523

2.6 Protein methods

2.6.1 Yeast whole cell extracts: small-scale for SDS-PAGE

10 mL yeast cultures grown overnight in the appropriate liquid medium were harvested by centrifuging at 3000 RPM for 2 minutes, pellets were re-suspended in 1 mL ice-cold dH_2O and transferred to a screw-cap tubes. Tubes were centrifuged, the supernatant removed and

washed cell pellets were either lysed for immediate use or snap frozen on dry ice for later use.

Cells were lysed by adding 100 µL of lysis buffer (containing: 50 mM Hepes pH 7.6, 75 mM KCl, 1 mM MgCl2, 1 mM EGTA, 0.1% Triton X-100, 1 mM Na_3VO_4, 10 µg/mL CLAAPE (protease inhibitor mix containing chymostatin, leupeptin, aprotinin, antipain, pepstatin, E-64 dissolved in DMSO at a concentration of 10 mg/mL), 1 mM Pefabloc®, 0.01 mM Microcystin) per 0.3 g of cell pellet. An equal amount of zirconia/silica beads (BioSpec Products Inc.) were added to each sample and cells were broken by bead-beating for 2x 30 seconds (kept on ice for 30 seconds in between). 100 µL of 2XSDS sample buffer containing DTT per 0.3 g of cell pellet was added to each sample. The lysates were briefly vortexed and denatured at 95°C for 5 minutes. They were then centrifuged to remove pelleted cell debris 12000-13000 RPM for 5 minutes at 4°C. Clear lysates were then loaded on SDS-PAGE gels for size separation.

2.6.2 Yeast whole cell extracts: large-scale for Co-IP

1-2 L of overnight yeast cultures were harvested by centrifugation in a Beckman Coulter centrifuge at 3500 RPM for 10 minutes at room temperature. A small volume of dH2O (15-20% of pellet volume) was added to the cell pellet for a paste-like consistency. 1 mM Pefabloc was also added to the cell paste before freezing as cell droplets in liquid nitrogen.

Frozen cell droplets were ground to form cell powder using a mortar and pestle cooled over a bed of dry ice. Samples were ground for an equal duration of time. Powder was weighed and 1 mL of lysis buffer (50 mM Hepes pH 7.6, 75 mM KCl, 1 mM MgCl2, 1 mM EGTA, 10% Glycerol, 0.1% Triton X-100, 1 mM Na_3VO_4, 10 µg/mL CLAAPE (protease inhibitor mix containing chymostatin, leupeptin, aprotinin, antipain, pepstatin, E-64 dissolved in DMSO at a concentration of 10 mg/mL), 1 mM Pefabloc®, 0.01 mM Microcystin) was added per gram of powder. Samples were lysed by sonicating while on ice for 30 seconds (5 sec on, 5 sec off) at an amplitude of 25-30%. Lysates were then cleared by centrifugation at 14000 RPM for 10-20 minutes at 4°C to remove cell debris. The Co-IP protocol was then followed (2.2.3).

2.6.3 Co-immunoprecipitation

Antibody coupled Dynabeads were washed once with 1 mL 0.1% PBS-Tween 20 and twice with wash buffer (50 mM Hepes pH 7.6, 75 mM KCl, 1 mM $MgCl_2$, 1 mM EGTA, 10%

Glycerol, 0.02% Tween 20). The clear lysate was incubated with antibody-coupled Dynabeads for 15 minutes at 4°C. The beads were washed 4-5 times with wash buffer (changing eppendorf tubes twice). Proteins were either eluted from beads immediately for SDS-PAGE or beads stored at -80°C until needed. Proteins were eluted by adding 2X sample buffer containing DTT and standing at room temperature for 15 minutes, following this, they were then run on an SDS-PAGE gel (2.2.8).

2.6.4 Crosslinking using DSP

This protocol is from Adele Marston's lab. 1-2 L of overnight yeast cultures were harvested by centrifugation in a Beckman Coulter centrifuge at 3500 RPM for 10 minutes at room temperature and re-suspended in reaction buffer (20 mM Hepes pH 7.6, 100 mM KOAc). 20 mM DSP (in DMSO) was added to the cells and the cross-linking reaction was left to shake slowly for 30 minutes (or 2 hours at 4°C). To quench the reaction, cells were pelleted at room temperature 3000 RPM for 2 minutes, re-suspended in 100 mM Tris pH 7.5 and left to shake slowly for 15 minutes. Cells were pelleted at 4°C 3000 RPM for 2 minutes. A small volume of dH2O (15-20% of pellet volume) and 1 mM Pefabloc was added to the cell pellet before freezing yeast droplets in liquid nitrogen. The yeast droplets were then ground and lysed as described in 2.2.2 and the Co-IP protocol followed (2.2.3).

2.6.5 Cross-linking M2 FLAG antibody to Dynabeads®

This protocol was adapted from Robin Allshire's lab. For cross-linking anti-GFP antibody to Protein G Dynabeads® (10004D, Invitrogen), the same method was followed using approximately 1.5x more antibody (a 1:1 mix of anti-GFP sheep T and G was used).

500 µL Protein G Dynabeads®, first were washed 2 times in PBS containing 0.001% Triton X-100 in a screw cap tube and left in a final volume of 1 mL 0.001% PBS-Triton X-100. 150 µL of M2 antibody was added to the slurry and left to bind while rotating at room temperature for 30 minutes. Beads were washed with 1 mL PBS and 1 mL 1 M Borate buffer pH 9 (0.25 g boric acid, 1.53 g sodium tetraborate decahydrate, made up to 100 mL) and transferred to a 50 mL Falcon™ tube. Beads were isolated using a magnetic rack and resuspended in 15 mL cross-linking buffer made fresh just before use (room temperature 20 mM dimethyl pimelimitate (Thermo 21667) in Borate buffer pH 9). Slurry cross-linked for 30 minutes at room temperature while rotating. Beads washed in 20-30 mL Borate buffer pH 9 and 1 M Tris pH 8 for 5 minutes while rotating at room temperature to quench the reaction.

Tris was removed and antibody cross-linked beads were washed with 0.001% PBS-Tween 2-3 times and re-suspended in 500 µL 0.001% PBS-Tween with sodium azide.

2.6.6 Sample preparation for mass spectrometry

2 L cultures were harvested and lysed as in 2.2.2. Antibody coupled Dynabeads were washed once with 1 mL 0.1% PBS-Tween 20 and twice with wash buffer (50 mM Hepes pH 7.6, 75 mM KCl, 1 mM $MgCl_2$, 1 mM EGTA, 10% Glycerol, 0.02% Tween 20). The clear lysate was incubated with antibody-coupled Dynabeads for 15 minutes at 4°C. The beads were washed 3 times with wash buffer (changing eppendorf tubes twice). Beads were then washed five more times in wash buffer without detergent (50 mM Hepes pH 7.6, 75 mM KCl, 1 mM $MgCl_2$, 1 mM EGTA, 10% Glycerol) the tubes were changed in between. The wash buffer was removed and an on-bead tryptic digestion was performed (2.2.7).

2.6.7 On-bead digestion and Stage Tip Extraction

This was carried out with the help of Christos Spanos in the Rappsilber lab. Beads were re-suspended in 50 µL denaturation buffer (8 M urea in 50 mM ammonium bi-carbonate, ~ pH 8.0) and add digestion buffer (50 mM ammonium bi-carbonate in water, pH 8.0) so that beads were covered. 1 µL of reduction buffer (10 mM **di**thio**t**hreitol (DTT) in 50 mM ammonium bi-carbonate) per 10 µL digestion solution was added and incubated at room temperature for 30 minutes. 1 µL of alkylation buffer (55 mM iodoacetamide in 50 mM ammonium bi-carbonate) per 10 µL digestion solution was then added and incubated at room temperature, in the dark, for 30 minutes. 1 µg/µL LysC in 0.1% TFA (**t**ri**f**luoroacetic **a**cid) per 50 µg protein was added and incubated for at least 3-4 hours at room temperature. The sample was then diluted x4 with digestion buffer (50 mM ammonium bi-carbonate pH 8.0). 1 µg trypsin in 0.1% TFA per 50 µg protein was added and the sample was incubated overnight at room temperature. The supernatant was transferred to a new eppendorf tube and acidified to pH < 2.5 with 10% TFA to quench the trypsin digest. The peptides were then purified using C18 Stage Tips. C18-**St**op **a**nd **g**o **e**xtraction (stage) tips were used to desalt peptides prior to mass spectrometry analysis as described in Rappsilber et al., 2003. Subsequent mass spectrometry analysis was performed by Christos Spanos (Rappsilber lab) using an Orbitrap mass analyser Q Exactive™ Hybrid Quadrupole-Orbitrap™ Mass Spectrometer (IQLAAEGAAPFALGMAZR, ThermoFisher) and analysis was carried out using MaxQuant software.

2.6.8 SDS-PAGE

The protein samples were run on 10 cm x 20 cm SDS-PAGE (**s**odium **d**odecyl **s**ulphate **p**olyacryl**a**mide **g**el **e**lectrophoresis) gels, the percentage of which was determined based on the size of the protein of interest. The composition of the resolving gel was as follows:

Reagent	Gel percentage		
	10.0%	12.5%	15%
40% acrylamide	3.7 mL	4.7 mL	5.6 mL
2% Bis	0.98 mL	0.75 mL	0.64 mL
1.5M Tris-HCl pH 8.8	3.75 mL	3.75 mL	3.75 mL
Water	*to 15 mL*	*to 15 mL*	*to 15 mL*
10% ammonium persulphate*	150 µL	150 µL	150 µL
TEMED*	15 µL	15 µL	15 µL

10% ammonium persulphate and TEMED (indicated with an asterix (*)) were added immediately before the gel is poured. 1 mL of butan-1-ol was laid over the resolving gel to aid setting and removed prior to adding the stacking gel:

Reagent	Volume
40% acrylamide	6.25 mL
2% Bis	3.33 mL
1.0M Tris-HCl pH 8.8	6.25 mL
Water	*to 50 mL*
10% ammonium persulphate*	25 µL
TEMED*	250 µL

10% ammonium persulphate and TEMED (starred) were added immediately before use. Gels were typically run at a constant voltage of 120-170 V in SDS-PAGE buffer (50 mM Tris, 384 mM glycine, 2% SDS) until the protein of interest was resolved.

2.6.9 Western blot semi-dry transfer

The proteins were transferred onto nitrocellulose membranes (Amersham Protan 0.2µm nitrocellulose, GE Healthcare Lifescience) using a TE77 semi-dry transfer unit (Hoefer) at 150-220 mA for 90-150 minutes (depending on protein size). In the unit, the membrane and

gel were placed inbetween 5 pieces of 3MM Whatman® filter paper pre-soaked in transfer buffer (25 mM Tris, 130 mM glycine, 10-20% methanol (depending on protein size)). Following the transfer, the proteins on the nitrocellulose membrane were stained with Ponceau S solution to determine the efficiency of transfer. The membrane was then washed with 0.1% Tween 20 in PBS.

2.6.10 Immunoblotting

The membranes were blocked in a 0.1% Tween 20 in PBS, 5% w/v dried semi-skimmed milk (Marvel) solution while shaking for 30 minutes at room temperature. Membreanes were then incubated overnight with primary antibody while shaking at 4°C. Membranes were washed with 0.1% Tween 20-PBS 4 times for 5 mins while shaking to remove any unbound antibody. They were then incubated with the corresponding secondary antibody for 1 hour at room temperature while shaking. Membranes were re-washed with 0.1% Tween 20-PBS 4 times for 5 mins while shaking prior to protein visualisation.

2.6.11 Protein visualisation

Proteins were detected using an enhanced chemiluminescense (ECL) kit (SuperSignal West Pico or SuperSignal West Femto, Pierce) according to manufacturer's recommendations. The ECL solution was applied to the blots which were placed between clear acetate sheets and exposed to X-ray film (Agfa Healthcare). The film was developed using a SRX-101A Film Processor (Konica-Minolta).

2.6.12 List of primary and secondary antibodies used in this study

Secondary antibodies are indicated with an asterix (*)

Antibody	Species	Immunobloting concentration	Source
anti-Bub1	rabbit	1:1000	Hardwick lab
anti-FLAG M2	mouse	1:1000	Sigma-Aldrich
anti-GFP S2T	sheep	1:1000	Hardwick lab
anti-GFP G	sheep	1:1000	Hardwick lab
anti-HA 12CA5	mouse	1:1000	Kumiko Samejima
anti-Mad1 T	rabbit	1:1000	Hardwick lab
anti-Mad2	sheep	1:1000	Hardwick lab

Antibody	Species	Immunobloting concentration	Source
anti-Spc7 G	sheep	1:1000	Hardwick lab
anti-mouse, HRP conjugated*	donkey	1:10000	GE Healthcare
anti-rabbit, HRP conjugated*	sheep	1:10000	GE Healthcare
anti-sheep, HRP conjugated*	donkey	1:10000	Jackson Immuno-Research

2.7 Yeast methods

2.7.1 Yeast transformation

Transformation of DNA into yeast in this work was carried out using either lithium acetate pH 4.9 (Ito et al., 1983) or pH 7.5 (adapted from Bahler et al., 1998). The optimal method of transformation was determined empirically. An overnight 100 mL yeast culture in YES (set-up from a fresh patch and starter culture of yeast) was grown at 30°C (unless temperature sensitive) with shaking for transformation the following day. $5x10^6$ cells/mL needed from the overnight culture.

For **pH 4.9** LiAc transformation, $2x10^8$ cells were harvested by centrifuging culture at 3000 RPM for 2 minutes. The cells were resuspended in 1 mL dH2O and transferred to a sterile eppendorf tube. The suspension was then centrifuged at 6000 RPM and resuspended in 100 µL of 0.1 M LiAc pH 4.9. The cells were then incubated at 30°C (unless temperature sensitive) for 30 minutes after which it was added to 2-10 µg DNA. The tube was mixed gently and 290 µL of 50% PEG4000 in 0.1M LiAc pH 4.9 was added. This was mixed well and the tube was incubated at 30°C (unless temperature sensitive) for 2-2.5 hours. Heat shock was performed at 43°C for 15 minutes and the mixture was left to cool to room temperature. Depending on the type of selection, the mixture was either plated directly onto selection plates or plated onto YES for 24 hours to recover before replica-plating onto selection plates. Plates were incubated at 32°C (unless temperature sensitive) for 3-5 days to obtain colonies. Positives were screened by western blotting and if necessary, PCR and sequencing.

For **pH 7.5** LiAc transformation, $2x10^8$ cells were harvested by centrifuging culture at 3000 RPM for 2 minutes. The cells were resuspended in 1 mL dH2O or 1 mL 0.1M LiAc/TE pH 7.5 and transferred to a sterile eppendorf tube. The suspension was then centrifuged at 6000 RPM and resuspended in 100 µL of 0.1 M LiAc/TE pH 7.5. The cell suspension was added to 2-10 µg DNA in TE, and left at room temperature for 10 minutes. 260 µL of 40%

PEG4000 in 0.1 M LiAc/TE pH 7.5 was added, mixed well and incubated at 30°C (unless temperature sensitive) for 1-2.5 hours. Heat shock was performed at 42°C for 5 minutes and the mixture was left to cool to room temperature. The mix was then plates as described above.

2.7.2 Yeast genomic DNA extraction

Genomic DNA from yeast was extracted for testing and cloning purposes using the LiOAc-SDS lysis method described in Löoke et al., 2011.

2.7.3 Crosses and random spore analysis

Yeast were plated onto YES plates from -80°C stocks and incubated at the appropriate temperature (25°C or 32°C) for 1-2 days. Strains of opposite mating type were mixed on SPA plates (1% w/v anhydrous D-glucose, 7.3 mM monopotassium phosphate, 3% w/v agar, 1x vitamins mix, 1x minerals mix, 0.2x supplements mix) using a 5 μL inoculation loop and dH_2O. Plates were incubated at 30°C (unless temperature sensitive) overnight. The following day (2 days if incubated at 25°C), a light microscope was used to check for the formation of tetrads. If tetrads were visible, a small colony's worth of mated cells were added to a solution of 500 μL of dH_2O with 1 μL of β-glucuronidase extract (MP Biomedicals LLC) and incubated for a day at 32°C to digest the ascus (unless temperature sensitive). The spores were then vortexed and washed twice with dH_2O (while briefly vortexing in between washes). Spores were plated onto YES plates and incubated at the appropriate temperature for 3-5 days for colony formation. Colonies were patched onto selective plates (replica plating if necessary) and positives were verified by imaging if fluorescent, western blotting and/or colony PCR and sequencing . A stock of resulting strain was made in a 50% glycerol/ YES solution and stored at -80°C.

2.7.4 G2 synchronisation with *cdc25-22*

Cells in a *cdc25-22* genetic background were grown at 25°C for 1-2 days on YES (unless stated otherwise) plates. They were then pre-cultured in 10 mL of liquid YES containing amino acid supplements at 25°C over the day and inoculated into a larger culture of YES overnight. The following day, log phase cultures were shifted to 36°C for 3.5 h to block in G2. After this, cultures were briefly cooled in iced water to rapidly shift them back to 25°C and release them from the G2 block.

2.7.5 ABA arrest and silencing assay

Following a *cdc25-22* block, 250 mM ABA stock (in DMSO Sigma Aldrich A1049) was added to cultures 5 min after release (20 min if comparing to a carbendazim arrest) to achieve a final concentration of 250 μM (unless otherwise stated). Following an ABA-induced synthetic arrest, the cells were washed 2 times with 50 mL YES.

2.7.6 Carbendazim arrest

Following a *cdc25-22* block, 3.75 mg/mL stock of carbendazim (Sigma Aldrich) was added to cultures 20 min after release to achieve a final concentration of 100μg/mL.

2.7.7 Cell viability

Following an arrest assay (unless DMSO treated), cells from 1 mL of culture were harvested by centrifugation at 6000 rpm for 1 minute and re-suspended in 1 mL of distilled water. Tenfold serial dilutions were made in distilled water. Cells were diluted by factors of 100 and 1000, and 0.1 mL plated in triplicate. Colony forming units (cfu) per millilitre of culture was calculated and cell viability over time was plotted as a percentage relative to that at time zero.

2.7.8 *nda3-KM311* arrest

Cells in an *nda3-KM311* background were grown on YES plates for 1 day at 32°C and pre-cultured over the day in liquid YES while shaking after which a larger overnight culture was inoculated. Cultures were transferred to a 18°C water bath placed in a 4°C room for 6 hours to arrest cells. Time points were taken periodically and tubes were stored on ice and centrifuged in the cold before fixation in ice-cold methanol and imaging. Samples were stored at -20°C.

2.7.9 rTetR arrest assay: SynCheck

Cells were grown overnight on PMG plates containing 15μM thiamine at 32°C. Cells were then pre-cultured while shaking over the day in liquid PMG containing 15μM thiamine to repress the *nmt* promoter. After 7 hours, cultures were washed with 50 mL PMG liquid 3 times and inoculated into larger liquid PMG cultures (without thiamine) for 12-16 hours (depending on experiment) to activate the *nmt* promoter and generate an arrest.

2.7.10 Methanol fixation and fluorescence microscopy

The samples of culture (1-1.5 mL) were centrifuged for 1 min at 6000 rpm. The cell pellet was fixed in 200–500 µL of 100% ice-cold methanol. To image cells, 8 µL of the cell suspension in methanol was added to a glass slide when the methanol evaporated, 1-2 µL DAPI (0.4 µg/mL) was added to the sample and a glass cover slip was placed on top. Cells were imaged immediately using a 100Å~ oil immersion lens and a Zeiss Axiovert 200M microscope (Carl Zeiss), equipped with a CoolSnap CCD camera (Photometrics) and Slidebook 5.0 software (3i, Intelligent Imaging Innovations). Typical acquisition settings were 300 ms exposure (FITC and TRITC) and 100 ms exposure (DAPI), 2Å~ binning, Z-series over 3µm range in 0.5 µm steps (seven planes).

2.7.11 Quantifying fluorescence

This work was conducted in collaboration with the Joglekar lab. The images for quantification of the mCherry and GFP fluorescence signal were acquired on a Nikon Ti-E inverted microscope with a 1.4 NA, 100x, oil immersion objective as described in Joglekar et al., 2013. Image analysis was performed using a semi-automated graphical user interface written in MatLab as described in Joglekar et al., 2013, with the exception that fluorescence at a TetO array was being analysed (as opposed to at kinetochores).

2.8 HeLa cell methods

This work was conducted in collaboration with the Joglekar lab. The eSAC arrest assay and long term IncuCyte® imaging were carried out as described in Chen et al., 2019. Cell fate was characterised manually based on cellular morphology. The cell line used was pPS28 – MELT12-13-14-2xFKBP12, inducible:mCherry-FRB-Mps1$_{500\text{-}857}$

2.9 *S.pombe* growth media

Cells are either grown on solid or in liquid PMG (minimal) or YES (rich) media. Liquid cultures were usually grown in a 30°C (unless temperature sensitive) room/incubator while shaking at 180 RPM. Cells were usually harvested when at mid-log growth ($5x10^6$ cells/mL). Media recipes are given below with PMG and YES plates usually supplemented with 2% w/v agar. All media was autoclaved, with amino acids supplements, vitamin and mineral stocks and other additives included after autoclaving.

PMG (**p**ombe **m**inimal **g**lutamate) media :

Reagent	Final concentration
Phtalic acid	14.7 mM
Di-sodium hydrogen orthophosphate, anhydrous	15.5 mM
L-glutamic acid, monosodium salt	25.4 mM
D-glucose, anhydrous	2% w/v
Vitamins mix	1x
Minerals mix	1x
Supplements mix	1x

YES (**y**east **e**xtract **s**upplemented) media :

Reagent	Final concentration
Yeast extract	0.5 w/v
D-glucose, anhydrous	3% w/v
Supplements mix	1x

Supplements mix (amino acids):

Reagent	Final concentration
Adenine	3.75 g/L
Arginine	3.75 g/L
Histidine	3.75 g/L
Leucine	7.5 g/L
Lysine	3.75 g/L
Uracil	3.75 g/L
Water	*to 500 mL*

Vitamin stock (1000x):

Reagent	Final concentration
Pantothetic acid	1 g/L
Nicotinic acid	10 g/L

Reagent	Final concentration
Inositol	10 g/L
Biotin	10 mg/L

Mineral stock (1000x):

Reagent	Final concentration (mM)
Boratic acid	80.9
$MnSO_4$	23.7
$ZnSO_4$	13.9
$FeCl_3$	7.4
Molybic acid	2.47
KI	6.02
$CuSO_4$	1.6
Citric acid	47.6

Drug selection plates:

Reagent	Final concentration
CloNat	100 µg/mL
G418	150 µg/mL
Hygromycin	100 µg/mL

2.10 Bacterial cell media

LB media (Lysogeny broth) plates:

Reagent	Final concentration
Tryptone	20 g/L
Yeast extract	5 g/L
NaCl (pH 7.2)	5 g/L
Agar	20 g/L

Liquid SOC (**s**uper **o**ptimal broth with **c**atabolite repression) recipe:

Reagent	Final concentration
Tryptone	20 g/L
Yeast extract	5 g/L
NaCl (pH 7.2)	5 g/L
KCl	2.5 mM
$MgCl_2$	10 mM
D-glucose	20 mM

2.11 List of fission yeast strains used in this work

Strain	Genotype	Source
PA 103	*Padh15-GFP-ABI:LEU2 lys1::adh15-rTetR-mcherry-PYL:ura4 112xtetO:kanR*	this work
PA 252	*Padh41-mph1(303-678)-3xHA-ABI:LEU2 mph1Δ::nat lys1::Padh21-spc7(1-666)-PYL:ura4 cdc25-22 Z:Padh15-mCherry-atb2:natMX6 bub1-GFP:his*	this work
PA 88	*Padh15-eGFP-GID:LEU2 lys::adh15-rTetR-mCherry-GAI:ura4 112xtetO:kanR*	this work
PA 269	*Padh41-mph1(303-678)-3xHA-ABI:LEU2 mph1Δ::nat cdc25-22 Z:Padh15-mCherry-atb2:natMX6 bub1GFP:his*	this work
PA 286	*lys1::Padh21-spc7(1-666)-PYL:ura4 cdc25-22 Z:Padh15-mCherry-atb2:natMX6 bub1-GFP:his*	this work
PA 260	*mad1Δ::hyg Padh41-mph1(303-678)-3xHA-ABI:LEU2 mph1Δ::nat lys1::adh21-spc7(1-666)-PYL:ura4 cdc25-22 Z:Padh15-mCherry-atb2:natMX6 bub1-GFP:his*	this work
PA 262	*spc7Δ::G418 spc7-T12A:hyg lys1::Padh21-spc7(1-666)-PYL:ura4 Padh41-mph1(303-678)-3xHA-ABI:LEU2 mph1Δ::nat cdc25-22 Z:Padh15-mCherry-atb2:natMX6*	this work
PA317	*Padh41-mph1(303-678)-3xHA-ABI:LEU2 lys1::Padh21-spc7(1-666)12A-PYL:ura4 cdc25-22 Z:Padh15-mCherry-atb2:natMX6*	this work
PA 264	*spc7Δ::G418 spc7:hyg lys1::Padh21-spc7(1-666)-PYL:ura4 Padh41-mph1(303-678)-3xHA-ABI:LEU2 mph1Δ::nat cdc25-22 Z:Padh15-mCherry-atb2:natMX6*	this work
PA 338	*Padh41-mph1(303-678)-3xHA-ABI:LEU2 lys1::Padh21-spc7(1-666)-PYL:ura4 cdc25-22 Z:Padh15-mCherry-atb2:natMX6 cdc13-GFP:leu*	this work
PA 363	*Padh41-mph1(303-678)-3xHA-ABI:LEU2 mph1Δ::nat lys1::Padh21-spc7(1-666)-PYL:ura4 cdc25-22 Z:Padh15-mCherry-atb2:natMX6*	this work
PA 364	*Padh41-mph1(303-678)-3xHA-ABI:LEU2 mph1Δ::nat lys1::Padh21-spc7(1-666)-PYL:ura4 cdc25-22 Z:Padh15-mCherry-atb2:natMX6 cdc13-GFP:leu*	this work
PA 295	*adh41-mph1(D1-302)-3xHA-ABI:LEU2 mph1D::nat lys::adh21-spc7(1-666)-PYL:ura cdc25-22 adh15-mCherry-atb2:nat bub1-GFP:his mad2-GFP*	this work
PA 175	*lys::adh21-spc7(1-666)wt-flag-mCherry-PYL:ura adh41-mph1(D1-302)-GFP-ABI:LEU2, mph1D:Nat, cdc25-22*	this work

Strain	Genotype	Source
PA 253	*Padh41-mph1(303-678)-3xHA-ABI:LEU2 mph1D::nat lys1::Padh21-spc7(1-666)-PYL:ura4 2xflag-mad1-Δ1CC:hyg cdc25-22 Z:Padh15-mCherry-atb2:natMX6 bub1-GFP:his*	this work
PA 254	*Padh41-mph1(303-678)-3xHA-ABI:LEU2 mph1D::nat lys1::Padh21-spc7(1-666)-PYL:ura 2xflag-mad1-Δ1CC:hyg cdc25-22 Z:Padh15-mCherry-atb2:natMX6 bub1-GFP:his*	this work
PA 278	*adh41-mph1(D1-302)-3xHA-ABI:LEU2 mph1D::nat lys::adh21-spc7(1-666)-PYL:ura flag-mad1:hyg cdc25-22 adh15-mCherry-atb2:nat bub1-GFP:his*	this work
PA 299	*adh41-mph1(D1-302)-3xHA-ABI:LEU2 mph1D::nat lys::adh21-spc7(1-666)-PYL:ura cdc25-22, adh15-mCherry-atb2:nat cen2-GFP*	this work
PA 326	*adh41-mph1(D1-302)-3xHA-ABI:LEU2 mph1D::nat lys::adh21-spc7(1-666)-PYL:ura cdc25-22, adh15-mCherry-atb2:nat bub1Dkinase-GFP*	this work
PA 36	*ura4::[4xtetO:ade6+]his3D lys1::adh15-rTetR-mCherry-spc7(1-666)-9TE:ura4 pnmt81-rTetR-mph1(D1-302):leu1 mad2 GFP:his*	this work
IY 222	*lys1::Padh15-rtetR-mCherry-spc71-666-9TE:ura4 leu1+ :Pnmt81rtetR-mph1(D1-302) mad2-GFP:his3*	Ivan Yuan
IY 230	*lys1::Padh15-rtetR-mCherry-spc71-666-9TE:ura4 tetO:kanR leu1+ :Pnmt81rtetR-mph1(D1-302) mad2-GFP:his3*	Ivan Yuan
IL 250	*lys1::Padh15-rtetR-mCherry-spc71-666-9TE:ura4 tetO:kanR leu1+ :Pnmt81rtetR-mph1(D1-302) bub1-GFP:his3*	Ioanna Leontiou
IL 615	*lys1::Padh15-rtetR-mCherry-spc71-666-9TE:ura4 leu1+ :Pnmt81rtetR-mph1(D1-302) bub1-GFP:his3*	Ioanna Leontiou
IL 382	*lys1::Padh15-rtetR-mCherry-spc71-666-9TE:ura4 tetO:kanR leu1+ :Pnmt81rtetR-mph1(303-678)*	Ioanna Leontiou
IL 626	*lys1::Padh15-rtetR-mCherry-spc71-666-9TE:ura4 tetO:kanR leu1+ :Pnmt81rtetR-mph1(303-678) bub1CD1 mad2-GFP:his3*	Ioanna Leontiou
IL 266	*lys1::Padh15-rtetR-mCherry-spc71-666-9TE:ura4 tetO:kanR leu1+ :Pnmt81rtetR-mph1(303-678 bub3Δ::hygR bub1-GFP:his3*	Ioanna Leontiou
IL732	*lys1::adh15-rtTA-mCherry-bub1Δkinase:ura+,Pnmt81-mph1(303-678):leu1 mph1D:natR tetO:G418 mad2-gfp*	Ioanna Leontiou
IL 728	*lys1::adh15-rtTA-mCherry-bub1ΔkinaseΔCD1:ura+ Pnmt81-mph1(303-678):leu1 mph1Δ:natR tetO:G418 mad2-gfp*	Ioanna Leontiou
IL 725	*lys1::adh15-rtTA-mCherry-bub1:ura+ Pnmt81-mph1(303-678):leu1 mph1Δ:natR tetO:G418 mad2-gfp*	Ioanna Leontiou
PA 160	*lys::adh15-rtetR-mCherry-spc7(1-666)wt:ura nmt81-rtetR-mph1(303-678):leu mph1D:NAT mad1GFP-C2A bub1GFP*	this work
PA 158	*lys::adh15-rtetR-mCherry-spc7(1-666)wt:ura nmt81-rtetR-mph1(303-678):leu mph1Δ:NAT mad1GFP-M6A bub1GFP*	this work
PA 155	*lys::adh15-rtetR-mCherry-spc7(1-666)wt:ura nmt81-rtetR-mph1(303-678):leu mph1D:NAT mad1GFP-C8A bub1GFP*	this work
KM 382	*mad1Δ::ura4 bub1-GFP:his*	Karen May

Strain	Genotype	Source
PA 185	*flag-mad1:hyg, bub1-GFP*	this work
IL 235	*bub1Δ::ura4*	Ioanna Leontiou
IY 157	*mph1Δ::natMX6*	Ivan Yuan
IY 6	*mad2Δ::ura4*	Ivan Yuan
IY 266	*mad3Δ::ura4*	Ivan Yuan
KM332	*wt 972*	Karen May
PA 208	*flag-mad1-S598A:hyg bub1-GFP:his*	this work
PA 209	*flag-mad1-S598A:hyg bub1-GFP:his*	this work
PA 210	*flag-mad1-S598A:hyg bub1-GFP:his*	this work
PA 211	*flag-mad1-S598A:hyg bub1-GFP:his*	this work
PA 212	*flag-mad1-S598A:hyg bub1-GFP:his*	this work
PA 213	*flag-mad1-S616A:hyg bub1-GFP:his*	this work
PA 215	*flag-mad1-S616A:hyg bub1-GFP:his*	this work
PA 216	*flag-mad1-S632A/S633A/T634A:hyg bub1-GFP:his*	this work
PA 217	*flag-mad1-S632A/S633A/T634A:hyg bub1-GFP:his*	this work
PA 218	*flag-mad1-S632A/S633A/T634A:hyg bub1-GFP:his*	this work
PA 219	*flag-mad1-T659A/T668A:hyg bub1-GFP:his*	this work
PA 220	*flag-mad1-T659A/T668A:hyg bub1-GFP:his*	this work
PA 221	*flag-mad1-T659A/T668A:hyg bub1-GFP:his*	this work
PA 222	*flag-mad1-T659A/T668A:hyg bub1-GFP:his*	this work
PA 223	*flag-mad1-RLK/AAA:hyg bub1-GFP:his*	this work
PA 224	*flag-mad1-RLK/AAA:hyg bub1-GFP:his*	this work
PA 225	*flag-mad1-RLK/AAA:hyg bub1-GFP:his*	this work
PA 226	*flag-mad1-RLK/AAA:hyg bub1-GFP:his*	this work
PA 233	*flag-mad1:hyg bub1-GFP:his, nda3-KM311*	this work
PA 234	*flag-mad1-S616:hyg bub1-GFP:his nda3-KM311*	this work
PA 235	*flag-mad1-S632/S633/T634A:hyg bub1-GFP:his nda3-KM311*	this work
PA 236	*flag-mad1-T659A/T668A:hyg bub1-GFP:his nda3-KM311*	this work
PA 237	*flag-mad1-RLK/AAA:hyg bub1-GFP:his nda3-KM311*	this work
PA 293	*mad1D::ura bub1-GFP:his nda3*	this work
PA 302	*flag-mad1-T659E:hyg bub1-GFP:his nda3*	this work
PA 304	*flag-mad1-T668A:hyg bub1-GFP:his nda3*	this work
PA 306	*flag-mad1-T668E:hyg bub1-GFP:his nda3*	this work

Strain	Genotype	Source
PA 311	*flag-mad1-T659A:hyg bub1-GFP:his nda3*	this work
PA 355	*flag-mad1:hyg, slp1-HA:G418, cdc25-22, mad3-GFP*	this work
PA 358	*flag-mad1T659AT668A:hyg, slp1-HA:G418, cdc25-22, mad3-GFP*	this work
PA 360	*flag-mad1T668A:hyg, slp1-HA:G418, cdc25-22, mad3-GFP*	this work
PA 362	*flag-mad1T668E:hyg, slp1-HA:G418, cdc25-22, mad3-GFP*	this work
YLM 109	*mph1-GFP:kanR*	Judith Zich
SL 336	*leu1-32 ade6-M216 ura4-D18 mph1Δ::mph1-Δ1-302-S(GGGGS)3-GFP<<kanR*	Silke Hauf

CHAPTER 3

In vivo reconstitution of spindle assembly checkpoint activation and silencing using chemically induced dimerisation

3.1 Introduction: Chemically induced dimerisation

Cell signalling is dynamic, often involving acute spatiotemporal regulation of a protein through interactions with other proteins and post-translational modifications. Manipulating signalling pathways in a complex biological environment, without the use of gene/protein depletion or over-expression, requires a rapid and reversible control system. **C**hemically **i**nduced **d**imerisation (CID) is the process of artificially co-recruiting two proteins in the presence of a small molecule. Thus forming a ternary complex that is freely diffusible, or one that can be tethered to a specific subcellular location.

One of the first and most widely adopted heterodimerisers is the rapamycin-induced dimerisation system (Spencer et al., 1993; Rivera et al.,1996). Rapamycin was discovered as an antifungal antibiotic in *Streptomyces hygroscopicus* from a soil sample from Easter Island (Vézina et al., 1975) and was later found to be an immunosupressor in mammalian cells (Martel et al., 1977). It binds to FKBP12 (**FK**506-**b**inding **p**rotein **12**-kDa), the complex then binds to and inhibits the FRB (**F**KBP12 and **r**apamycin **b**inding) domain of TORC1 kinase (**t**arget **o**f **r**apamycin **c**omplex **1**). Therefore, tagging proteins of interest with FKBP12 and FRB will induce heterodimers in the presence of rapamycin. However, despite its popular use and rapid mode of action, this system has some limitations.

- The high affinity binding of rapamycin to FKBP (K_d = 0.2 nM) and the subsequent binding of the complex to FRB (K_d =12 nM) (Banaszynski et al., 2005) makes reversing the dimerisation impractical within short timeframes. Alternatively, using competitive binders of rapamycin is often ineffective (Putyrski and Schultz, 2012).
- The nutrient-sensing TOR pathway is highly conserved among eukaryotes and controls essential cellular functions responsible for growth (Virgilio and Loewith, 2006). To prevent cross-reaction with endogenous TORC1 and FKBP proteins, cells need to be in

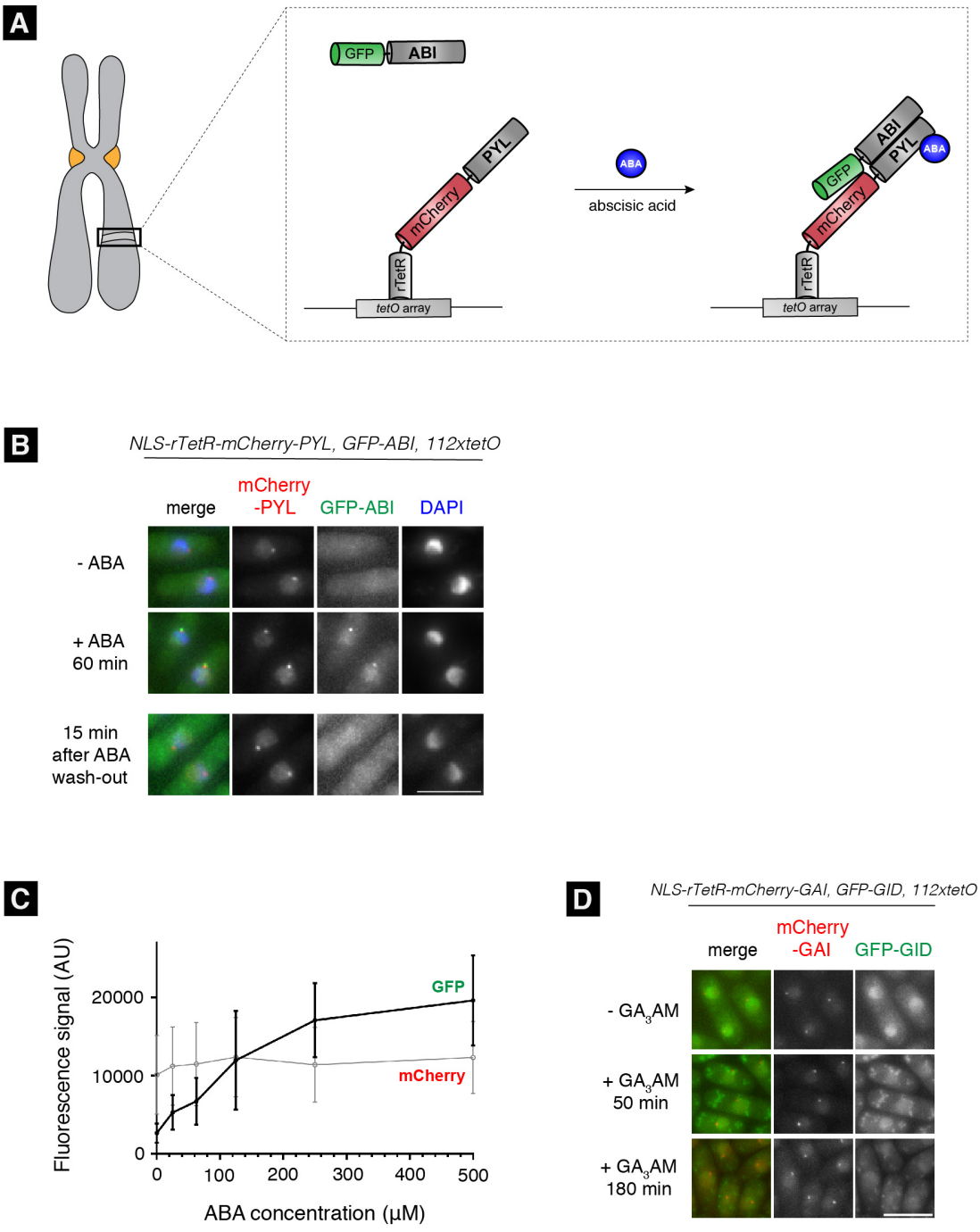

Figure 3.1: Proof of principle - Abscisic acid induces dimerisation in *S. pombe*. (A) Schematic representation of GFP-ABI and rTetR-mCherry-PYL co-localisation at a TetO array integrated on the arm of chromosome 1 in the presence of ABA. **(B)** Fixed cell images of cells after 60 minutes of 250 µM ABA addition, untreated cells are shown in the top panel. The bottom panel shows cells 15 minutes after washing out ABA (following a 1 hour treatment). rTetR-mCherry-PYL is shown in red, GFP-ABI in green and chromatin is stained with DAPI. Scale bar is 10 µm. **(C)** Quantitation of GFP and mCherry fluorescence signal at the TetO array at different concentrations (0, 25, 62.5, 125, 250, 500 µM) of ABA. The experiment was repeated twice and is plotted as mean +/- s.d. **(D)** Fixed cell images of cells treated with 100 µM gibberellic acid. Co-localisation of mCherry and GFP is not observed in the presence of GA_3AM. Scale bar is 10 µm.

a *fkh1Δ* (fission yeast homologue of FKBP), *tor1-S1834E* mutant background. Our lab and others have found that these mutations decrease mating efficiency and make *S. pombe* more sensitive to stress (Weisman et al., 2001; Ding et al., 2014).

Over the last 25 years, chemical biology research has taken to improving existing CID methods, and developing the use of novel small-molecules for studying protein interactions. Among them, plant phytohormones such as S-(+)-**ab**scisic **a**cid (ABA) (Liang et al., 2011) and **g**ibberellic **a**cid **3** analog (GA_{3}-AM) (Miyamoto et al., 2012) have successfully emerged as rapid, non-toxic, controllable systems in mammalian models. Both systems have been used to manipulate transcription initiation, signal transduction pathways and protein localisation in mammalian cells. In addition, these systems are fully orthogonal to the existing rapamycin system in mammalian cells. Thus allowing simultaneous spatiotemporal control of multiple cell circuits.

As these methods are derived from plant pathways, cross-reaction is limited to algae and phytopathogenic microbes (Dorffling et al., 1984; Shi et al., 2016). Plant hormones have been recorded as non-essential secondary metabolites in some phytopathogenic filamentous fungal species. It remains unclear whether phytopathogenic fungi are able to produce these hormones *de novo*, simply metabolise them from growth media, or both (Chanclud and Morel, 2016). This is because the majority of research in this field has been carried out *in vitro* and in addition, widely used growth media made from potato dextrose agar and yeast extract contains unknown concentrations of phytohormones. The effects of GA and ABA on fungi physiology are not well-characterised but are thought to affect processes such as hyphal growth, appressorium formation and spore germination.

In this work, we focus on the use of abscisic acid for CID.

3.2 Proof of principle: abscisic acid as a dimerisation tool in *S. pombe*

Identified in the 1960s (Eagles and Wareing 1963; Ohkuma et al., 1963), the phytohormone abscisic acid is involved in the plant stress response and plays a key role in developmental processes. Liang et al. (2011) re-engineered the ABA signalling pathway from *Arabidopsis thaliana* for use as a CID system in mammalian cells. The ABA CID system induces the heterodimerisation of the complementary surfaces of its cognate binding proteins $PYL1_{CS}$ (**py**rabactin resistance **1**-**l**ike (residues 33-209)) and $ABI1_{CS}$ (**AB**A **i**nsensitive **1** (residues 126-423)), hereafter referred to as PYL and ABI. This occurs via a sequential binding

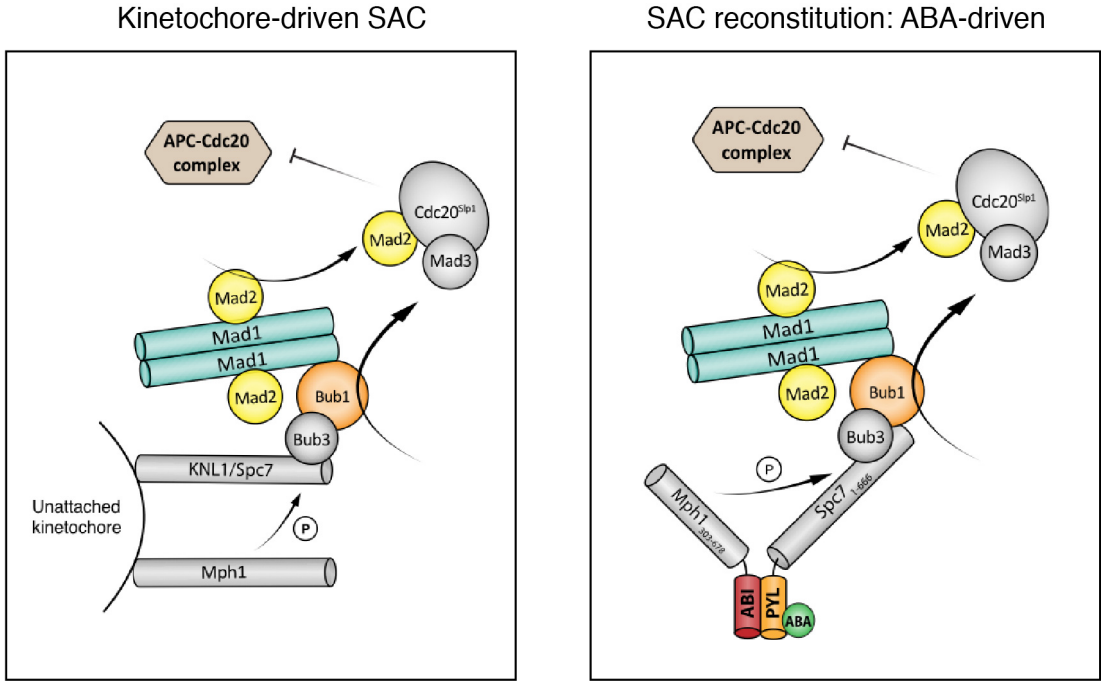

Figure 3.2: Schematic of spindle assembly checkpoint signal initiated at an unattached kinetochore (left) and that generated by ABA-dependent dimerisation of Mph1-ABI and Spc7-PYL domains (right).

mechanism where ABA binds to its receptor PYL, inducing a conformational change which then creates a binding surface for ABI. Thereby inducing proximity of proteins fused to these domains.

To test the cell permeability and effectiveness of ABA in *S. pombe,* a strain was built containing fluorophore-tagged plant domains, one of which was also anchored to a TetO array (see Fig **3.1 A**). The strain contains 3 components: GFP-ABI, NLS-rTetR-mCherry-2xFLAG-PYL and an array of **Tet**racycline **o**perators (TetO). The array is composed of 112 tandem copies of TetO integrated at the *arg3* locus of chromosome 1 (Yuan et al., 2017). The PYL domain is tagged with rTetR (**r**everse **tet**racycline **r**epressor) which allows binding to the TetO array. In the absence of ABA, NLS-rTetR-mCherry-2xFLAG-PYL is enriched on the TetO array in the nucleus, and ABI-GFP is distributed throughout the cell. Upon ABA addition, rapid association of fusion proteins is visible at the array as early as 15 minutes after addition of the drug, with equilibrium reached at approximately 60 minutes in this case (Fig **3.1 B**). Importantly, this reaction accommodates rapid on/off control as 'washing out' or putting the cells in fresh media lacking ABA reverses the interaction within 15 minutes (Fig **3.1 B**, lower panel). This level of control is an important advantage of the ABA system which is absent in others such as rapamycin, where reversing the phenotype by 'wash out' is not possible due to high affinity binding of the ligand to its receptor. The K_d of rapamycin binding to FKBP is 0.2 nM (Banaszynski et al., 2005), this is much lower than that of ABA-PYL1 which is 52 μM (Miyazono et al., 2009).

Figure **3.1 C** shows a linear increase in the fluorescent signal of GFP-ABI at the array when cells are treated with increasing concentrations of ABA, while the rTetR-mCherry-PYL signal at the array remains constant. 250 μM is used in this study as it provides near maximal effect. This wide range of linear dose response provides the possibility for more precise control of the desired effect by altering concentration. Comparatively, rapamycin exhibits more of a 'switch-like' linear dose response where activity peaks (from none) within a narrow dose range. Liang and colleagues found that for rapamycin, the full range of activity is attained when concentration is increased by a factor of 10 (2011). For ABA, this occurs over a 1000 fold change in concentration. Their experiment used CID to control luciferase expression.

When testing GA_3AM in a similar proof of principle experiment as that described above, we did not detect any co-localisation of fluorescent fusion proteins (Fig **3.1 D**). GA_3AM causes heterodimerisation of its receptor GID (**g**ibberellin **i**nsensitive **d**warf 1) and GAI

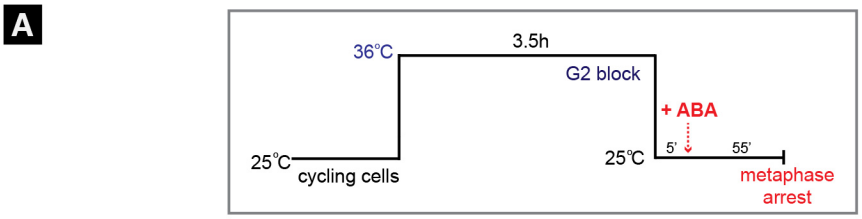

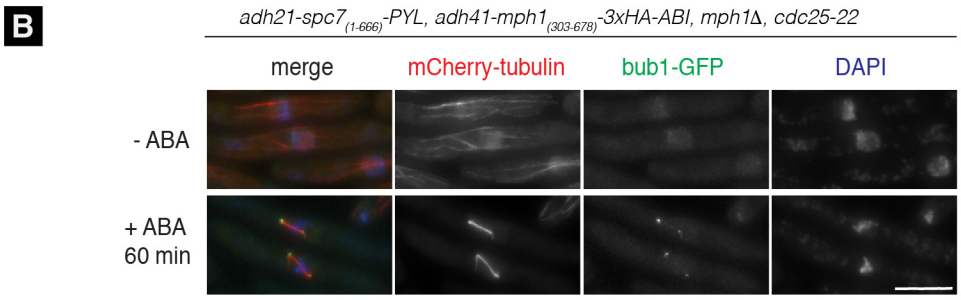

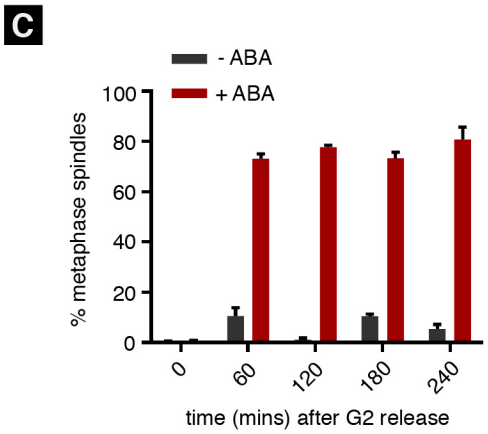

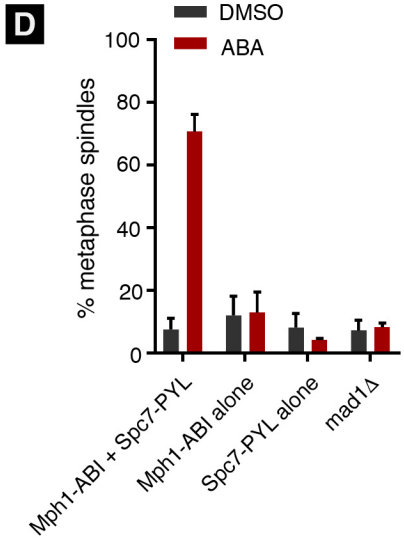

Figure 3.3: Rapid induction of spindle checkpoint arrest using abscisic acid to form Spc7-Mph1 heterodimers. (A) Work flow of the pre-synchronisation in G2 (*cdc25-22*), followed by release into mitosis at 25^{O}C and then induction of checkpoint arrest through the addition of ABA. **(B)** Fixed cell images taken of the arrested ABA-induced strain 60 minutes after ABA addition. Microtubules are seen in red (mCherry-tubulin), the checkpoint protein in green (Bub1-GFP) and chromatin is stained with DAPI. Scale bar is 10 µm. **(C)** Quantitation of cultures (+/- ABA addition) through a 4 hour time course after release from G2. Samples were fixed every 60 minutes and scored as metaphase arrested if they had short metaphase spindles and a single mass of condensed chromatin. >100 cells were analysed per strain at each time point. This experiment was repeated 3 times. Data plotted as mean +/- s.d. **(D)** Quantitation of the strains indicated at the 60 minute time point after release from the G2 block (ABA added 5 mins after release). *mad1Δ* is the Mph1-ABI Spc7-PYL strain with *mad1* deleted. >100 cells were analysed per strain at each time point. This experiment was repeated at least 2 times for each strain. Data plotted as mean +/- s.d.

(**g**ibberellin **i**nsensitive). These domains were fused to fluorophores, and GAI had an additional rTetR domain which tethered it to a TetO array. This result was unexpected especially since the cell permeability of gibberellic acid was optimised by concealing the negatively charged carboxylic acid moiety with an ester (**a**cetoxy**m**ethyl) to generate GA_3AM (Miyamoto et al., 2012). It may have been unsuccessful in *S. pombe* due to the lack of compatible esterases to cleave the ester and reveal the carboxyl group, or a result of the added complexity brought by a cell wall.

Hence we find that the ABA CID system is a valuable tool for controlling protein-protein interactions in *S. pombe*. The rest of this chapter i.) describes ABA-dependent reconstitution of SAC activation, ii.) and silencing, and iii.) broadly discusses the benefits this system in the context of others used to study the SAC.

3.3 Design: Reconstitution of the SAC

Our lab previously published a synthetic checkpoint (SynCheck) assay which is driven by rTetR dimers of rTetR-$Spc7_{1\text{-}666}$ and rTetR-$Mph1_{303\text{-}678}$ (Yuan et al., 2017). Since rTetR homodimers form spontaneously, dimerisation needs to be transcriptionally controlled. In the absence of thiamine, transcription at the *nmt81* (**n**o **m**essage in **t**hiamine **81**) promoter is activated, *rTetR-mph1* is expressed and is able to bind rTetR-Spc7. This recruits the Bub and Mad proteins, eventually leading to APC inhibition. While this arrest is effective, transcriptional control means it is time consuming as a peak mitotic index is reached in 14-16 hours. An additional factor is that since rTetR dimerisation is ligand-independent, dimerisation is constitutive, making reversal unfeasible. Due to these reasons, ABA induced dimerisation was implemented to improve efficiency and regulation.

This novel reconstitution (published in Amin et al., 2018) is designed to be independent of kinetochores with the aim to study the checkpoint without interfering with other kinetochore functions such as microtubule attachment and chromosome biorientation (see model Fig **3.2**). The complementary surface of the ABA receptor PYL (residues 33-209) was tagged to an N-terminal region of Spc7, $spc7_{1\text{-}666}$. This truncation prevents the fusion protein from localising to kinetochores since it can no longer bind to the kinetochore protein Mis12 (Petrovic et al., 2014; Petrovic et al., 2016). This recombinant protein was expressed under a constitutive adh21 promoter (Tanaka et al., 2009). Similarly, the complementary surface of the ABI domain (residues 126-423) was tagged with the C-terminus of Mph1 kinase, $mph1_{303\text{-}678}$, which prevents its localisation to kinetochores (Heinrich et al., 2012). The

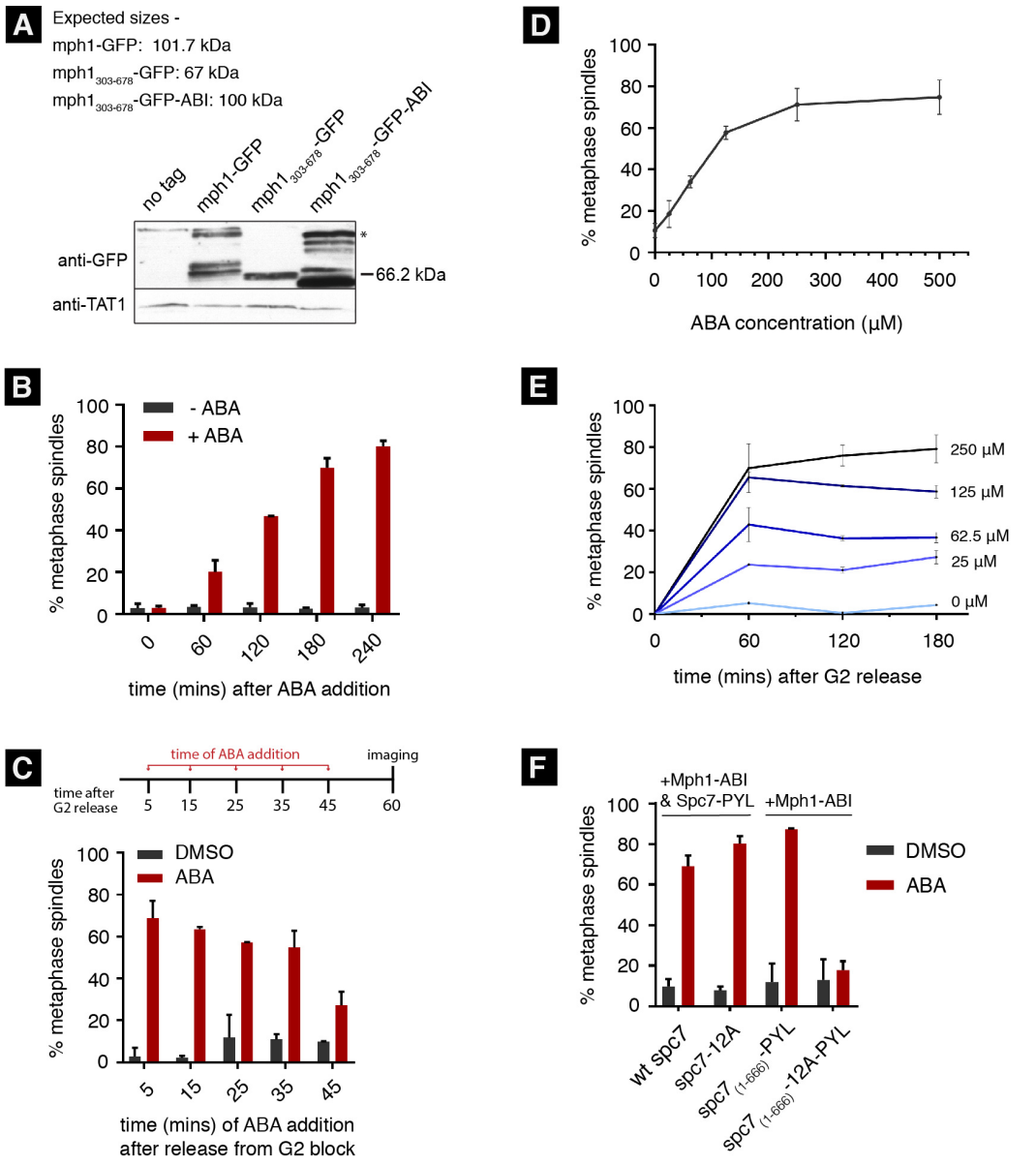

Figure 3.4: ABA-dependent CID can be tightly regulated. (A) Western blot comparing levels of full length Mph1, the N-terminal truncation and N-terminal truction with an ABI tag, using anti-GFP. The Mph1$_{303-678}$-GFP-ABI band is indicated with an asterix. The expected sizes are given above. **(B)** Quantitation of Mph1-ABI Spc7-PYL cultures +/- ABA through a 4 hour time course at 25ºC without synchronisation in G2. >250 cells were analysed per strain at each time point. This experiment was repeated 2 times. Data plotted as mean +/- s.d. **(C)** Quantitation of cultures +/- ABA 60 mins after G2 release in which ABA was added at 5,15, 25, 35 or 45 mins after release from the G2 block. >150 cells were analysed per condition at each time point. This experiment was repeated 2 times. Data plotted as mean +/- s.d. **(D)** The effect of ABA concentration on Mph1-ABI Spc7-PYL driven arrest. Different concentrations (0, 25, 62.5, 125, 250, 500 μM) of ABA were used to induce arrest in cultures 5 mins after release from the G2 block. Samples were fixed at 60 mins. >100 cells were analysed per condition at each time point. This experiment was repeated 3 times. Data plotted as mean +/- s.d. **(E)** The effect of ABA concentration on over time in a Mph1-ABI Spc7-PYL driven arrest. ABA was added 5 mins after G2 release. >170 cells were analysed per condition at 60, 120 and 180 mins. This experiment was repeated 2 times. Data plotted as mean +/- s.d. **(F)** Quantification of the strains indicated 60 mins after release from the G2 block. The spc7-12A strain has the endogenous *spc7* gene deleted and expresses this non-phosphorylatable 12A (MELA) allele from its own promoter integrated at the C locus. wt Spc7 is the wild-type control for this strain. Both strains can arrest in an Spc7$_{(1-666)}$-PYL Mph1-ABI arrest. Spc7$_{(1-666)}$-12A-PYL is a non-phosphorylatable 12A (MELA) mutant tagged with PYL, which does not generate an arrest when co-recruited with Mph1-ABI in the presence of ABA. Spc7$_{(1-666)}$-PYL is a positive control for this strain. >100 cells were analysed per strain at each time point. This experiment was repeated 3 times. Data plotted as mean +/- s.d.

endogenous *mph1* gene is deleted in most of the strains used here. This construct was expressed under a constitutive, low-strength, adh41 promoter (Tanaka et al., 2009). In addition to the above constructs, the strains used in this study also contain a temperature sensitive *cdc25-22* mutant for G2 synchronisation, mCherry-labelled microtubules (mCherry-alpha tubulin) and a GFP-tagged checkpoint protein, Bub1-GFP in some cases.

3.4 Spc7-Mph1 heterodimers trigger a robust metaphase arrest

To induce an ABA-dependent ectopic metaphase arrest, cells were first synchronised in G2 after incubating cells at 36°C for 3.5 hours using temperature-sensitive *cdc25-22* mutant. To 'release' from the G2 block, cells were moved to 25°C, resuming progression through the cell cycle. Abscisic acid was added 5 minutes after release from the G2 block to form Spc7-PYL and Mph1-ABI heterodimers (Fig. **3.3 A**). 60 minutes after release from G2, over 70% of cells have short metaphase spindles, condensed chromatin and Bub1-GFP at spindle poles (Fig. **3.3 B,C**). The arrest can be sustained for at least 4 hours (Fig. **3.3 C**).

The ABA-induced arrest is dependent on the hetero-dimerisation of Spc7-PYL and Mph1-ABI, yeast strains containing either the Mph1-ABI or Spc7-PYL component alone are unable to arrest in the presence of ABA (Fig. **3.3 D**). Deleting the downstream checkpoint protein Mad1 (*mad1Δ*) abrogates the arrest (Fig. **3.3 D**), indicating that it is checkpoint-dependent. This arrest works well in both rich (YES) and minimal (PMG) media. A comparison between different GFP-tagged Mph1 fusion proteins indicates that the N-terminal truncation and ABI tag do not significantly alter expression levels (Fig. **3.4 A**).

Without pre-synchronising in G2, mitotic index increases over time and reaches a peak 4 hours after release from the G2 block (Fig. **3.4 B**). To determine the optimal time to add ABA, ABA was added to cultures at varying times following G2 release (Fig. **3.4 C**). We found that ABA can be added up to 20 minutes after release from the G2 block without impacting the efficiency of the arrest. We note that adding ABA early does not impact entry into mitosis (demonstrated in Fig. **3.4 B, C**). Upon testing a range of concentrations of ABA, we found that 250 μM was sufficient to generate a robust arrest (Fig. **3.4 D**). When examining how the concentration of ABA affects the arrest over time, we find a positive correlation until 60 mins after release from G2 after which the % of cells arrested in a given population remains constant over time (Fig. **3.4 E**). We find a clear split in the population where a cell either arrests or it does not. This bimodal distribution in a clonal population is interesting and suggests that the phenotypic split is due to non-genetic factors. This is in

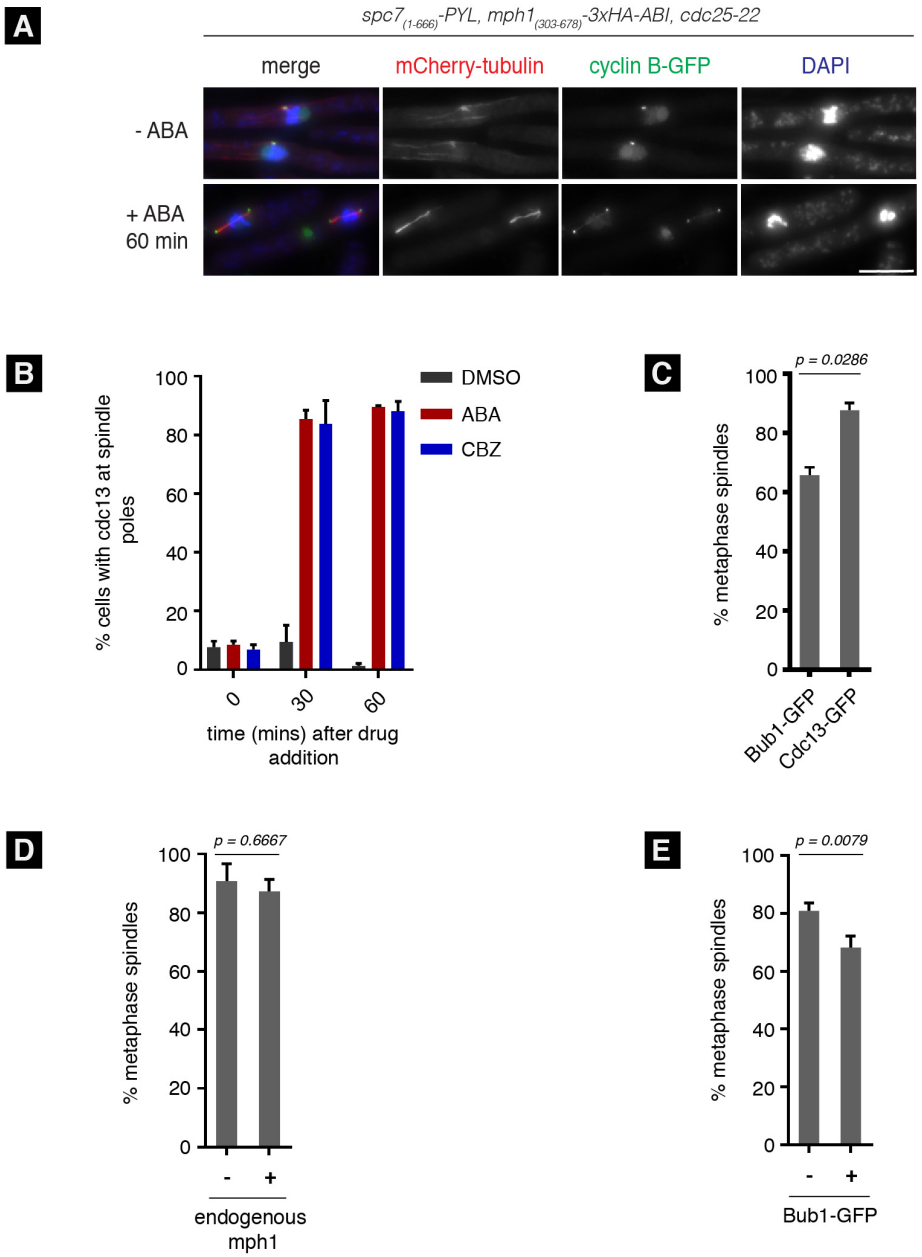

Fig 3.5: The GFP tag on Bub1 decreases the efficiency of ABA arrest. (A) Fixed cell images taken of a strain with Cdc13-GFP at spindle poles bodies 60 minutes after release from G2 block (ABA added at 5 mins). Scale bar is 10 µm. **(B)** Quantitation of strain containing Cdc13-GFP at 60 minutes after treatment with either DMSO, ABA or CBZ (added 20 minutes after release from G2 block). Cells were scored as arrested if Cdc13 was enriched at spindle poles and/or if short metaphase spindles were present. >240 cells were analysed per strain at each time point. This experiment was repeated 2 times. Data plotted as mean +/- s.d. **(C)** Quantitation comparing ABA-induced arrest in Bub1-GFP and Cdc13-GFP strain 60 minutes after release from G2 block. >160 cells analysed per strain. Mean +/- s.d. of 4 experiments is plotted. **(D)** Quantitation of ABA-induced arrest in strains with and without endogenous mph1 60 minutes after release from G2 block. >160 cells were analysed per strain at each time point. This experiment was repeated 2 times. Data plotted as mean +/- s.d. **(E)** Quantitation of ABA-induced arrest in strains with and without the GFP tag on Bub1 60 minutes after release from G2 block. >180 cells were analysed per strain at each time point. This experiment was repeated 5 times. Data plotted as mean +/- s.d. Mann-Whitney test was used to determine *p* value using Prism.

agreement with work by the Hauf group (Heinrich et al., 2013). They noticed a similar pattern in cells following a *nda3-KM311* arrest (where microtubules are depolymerised at 18°C). They concluded that this type of response in a clonal population occurs due to 'ultrasensitivity' to slight differences in checkpoint protein abundances (such as $Slp1^{Cdc20}$) which can occur in stoichiometric binding reactions like MCC formation.

To achieve an ectopic arrest, the Spc7-PYL and Mph1-ABI constructs used in this study lack their kinetochore-binding domains. The strain used above also lacks endogenous *mph1*, preventing all Mad and Bub checkpoint protein recruitment to kinetochores (Heinrich et al., 2012). To further test kinetochore independence, a strain with endogenous *spc7Δ* but supplemented with a full length copy of the unphosphorylatable MELT mutant *spc7-12A* (containing 12 MELA motifs), was used (Yamagishi et al., 2012; Mora-Santos et al., 2016). Mph1-phosphorylated MELT motifs are required for Bub3-Bub1 recruitment to kinetochores and in turn, kinetochore-dependent checkpoint activation. The *spc7-12A* mutant arrested with similar efficacy as the wild type *spc7* strain in the presence of ABA (Fig. **3.4 F**). Importantly, cells with the $Spc7_{1\text{-}666}$ MELT mutant tagged to PYL, $Spc7_{1\text{-}666}$-12A-PYL, are unable to arrest in the presence of ABA, despite dimerisation with Mph1-ABI (Fig. **3.4 F**). This strongly suggests that the ectopic arrest is driven by Mph1 phosphorylation of Spc7 MELT motifs, allowing the recruitment of downstream checkpoint effectors and MCC generation.

Taken together, the data implies that the ABA-induced SAC arrest does not require endogenous kinetochores for initiation or propagation of the checkpoint signal.

The accumulation of Cyclin B at spindle poles is an indicator of a metaphase delay. Using a modified yeast strain, we were able to observe Cdc13 (fission yeast Cyclin B) along the mitotic spindle and at spindle poles as an indicator of checkpoint arrest (Fig. **3.5 A**). These cells reached peak mitotic index 30 minutes after addition of ABA (when added at 20 minutes after G2 release), similar to when treated with the anti-microtubule drug **c**ar**b**enda**z**im (CBZ) (Fig. **3.5 B**). This strain also had endogenous *mph1* as the kinetochore binding domain of Mph1 is required for the kinetochore-dependent CBZ arrest.

We observed that the strain with Cyclin B-GFP consistently arrests more efficiently than the original strain used containing Bub1-GFP, with over 80% of cells arrested in the modified strain versus 70% in the original (Fig. **3.5 C**). To test whether this was due to the presence of endogenous *mph1* in the Cyclin B strain, it was compared to a similar strain in which endogenous mph1 was deleted. Arrest efficiency was similar in both strains (Fig. **3.5 D**).

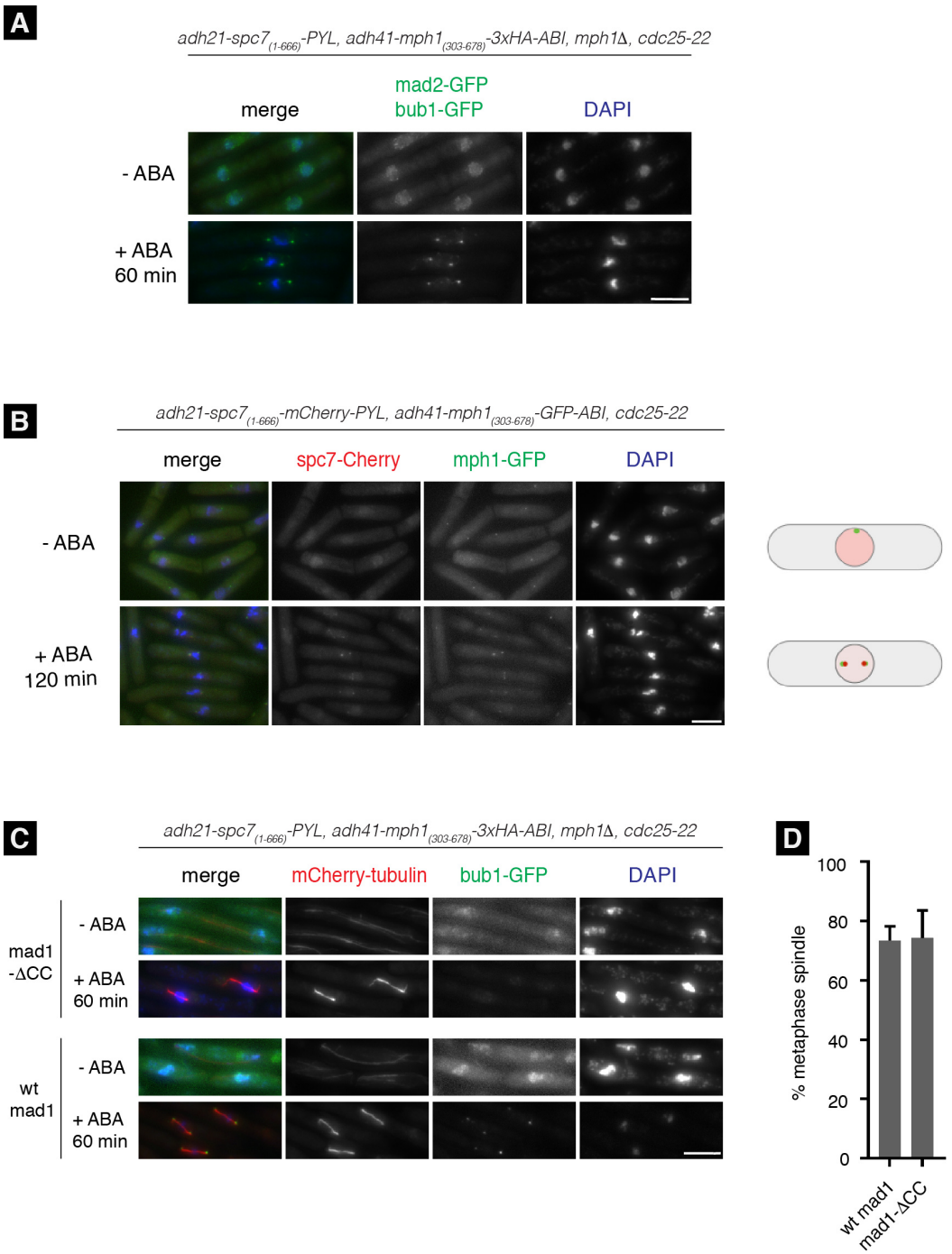

Figure 3.6: Checkpoint proteins accumulate at spindle poles in a Mad1-N terminal dependent manner. (A) Fixed cell images of a Spc-PYL Mph1-ABI strain containing Mad2-GFP and Bub1-GFP 60 minutes after release from the G2 block treated +/- ABA. Scale bar is 10 µm. **(B)** Fixed cell images of cells containing fluorescently labelled Mph1-ABI and Spc7-PYL 2 hours after release from G2 block (ABA added 5 minutes after G2 release). A schematic depicting the localisation of flurophores +/- ABA is shown on the right. Scale bar is 10 µm. **(C)** Fixed cell images of Spc-PYL Mph1-ABI strains with and without the N-terminal coil of Mad1 (wt mad1 and mad1-ΔCC respectively) treated +/- ABA. Scale bar is 10 µm. **(D)** Quantitation of Mph1-ABI Spc7-PYL arrest in strains with and without the N-terminal coiled-coil of Mad1, 60 minutes after release from G2 block . >150 cells were analysed per strain at each time point. This experiment was repeated 4 times. Data plotted as mean +/- s.d.

Further investigation revealed that the C-terminal GFP tag on Bub1 was attributing to the discrepancy in arrest efficiency (Fig. **3.5 E)**, most likely resulting in a partial loss of function. We find that C-terminal tagging of Bub1 with 3xHA (**h**em**a**gglutinin) also leads to a loss of function (unpublished).

Consistent with our previously published SynCheck assay (Yuan et al., 2017), the checkpoint proteins Bub1 and Mad2 localise at spindle poles in an ABA-controlled arrest (Fig. **3.6 A**). This movement is driven by an interaction between Mad1 and Cut7 (fission yeast homologue of Kinesin-5), a bi-directional motor protein (Edamatsu, 2014). In this ectopic arrest, we also detect Mph1 and Spc7 at spindle poles as they are, via Bub1-Bub3, associated with Mad1 which binds to the motor (Fig. **3.6 B**). Deleting the first N-terminal coiled coil of Mad1, residues 1-136 (*mad1Δ1-136*), abrogates its interaction with Cut7 (Akera et al., 2015). As a consequence preventing localisation of checkpoint proteins such as Bub1 to the spindle poles (Fig. **3.6 C**). This however does not disrupt checkpoint signalling (Fig. **3.6 D**). This confirms that location of checkpoint activation signal within in the nucleus is not important, presumably as the end product is a diffusible MCC.

Thus, using yeast genetics to simplify components and CID to control the initial step of the checkpoint signalling pathway, we are able to reconstitute SAC signalling ectopically by artificially dimerising Mph1 and Spc7 to allow Mph1 phosphorylation of the Spc7 MELT motifs. This generates a robust arrest where peak mitotic index is reached in 30 minutes. The kinetochore independence of this system gives added weight to the claim that the kinetochore is a scaffold on which Mph1-mediated phosphorylation of Spc7 can take place upon sensing incorrect microtubule attachment or lack of tension. Future work includes studying the effects of other mitotic kinases on this system by coupling it to ATP analog-sensitive alleles of Ark1 and Plk1.

3.5 A novel spindle checkpoint silencing assay

A significant advantage of the ABA CID system is that the arrest can be reversed by simply removing ABA from the media (Fig. **3.7 A**). Using this assay we are able to study how the checkpoint is silenced, which has proven to be technically challenging in the past.

In a simple assay, cells are synchronised in G2, treated with ABA, and 60 minutes following release from G2, cells are washed and put into fresh media lacking ABA (Fig. **3.7 B**). Fig **3.7 C, D, E** illustrate how Cyclin B degrades following wash-out and spindles

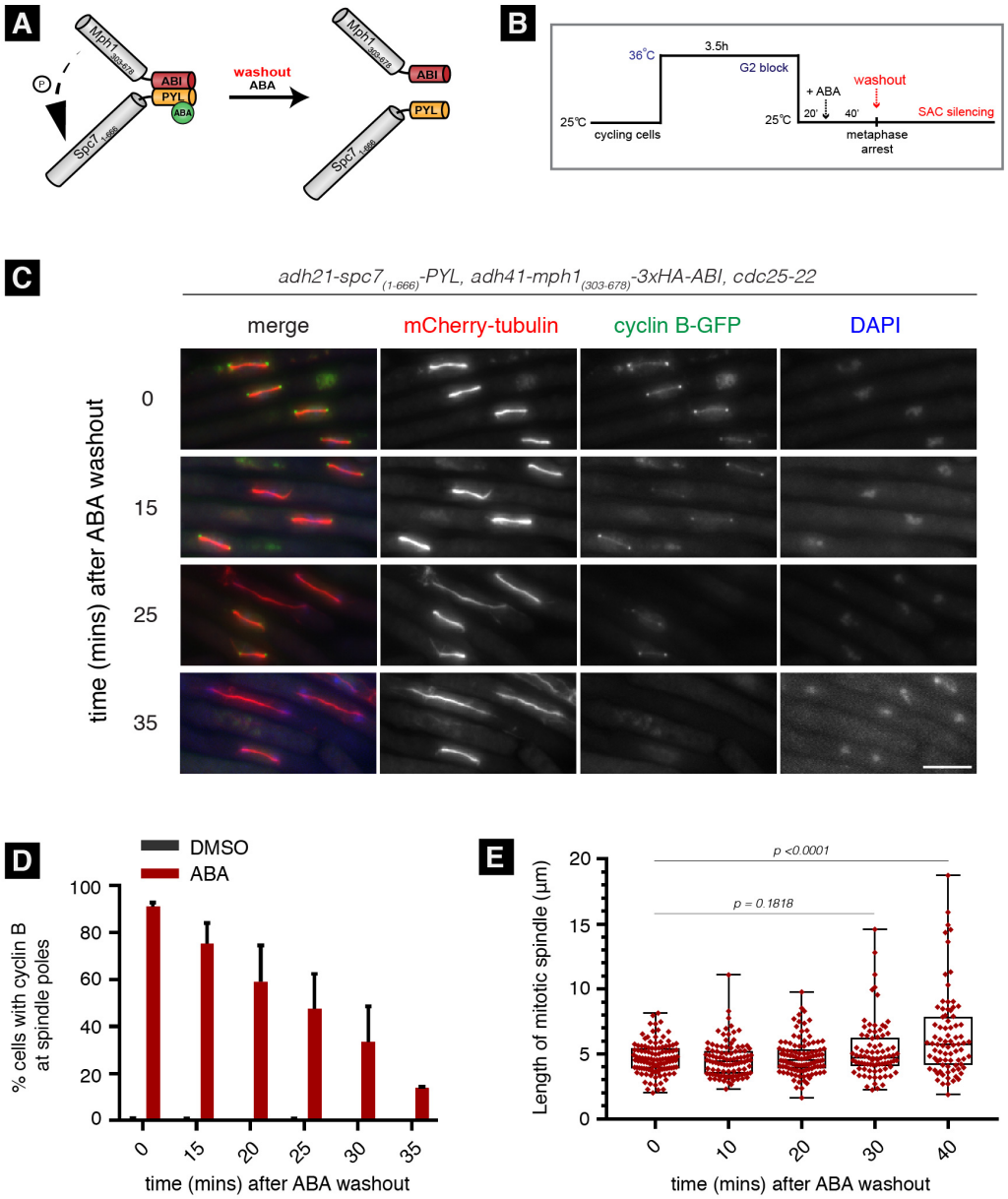

Figure 3.7: Silencing of spindle checkpoint signalling following abscisic acid wash out.
(A) Schematic representation of the dissociation of Mph1 - Spc7 heterodimers after ABA washout. **(B)** Silencing work flow: Pre-synchronisation in G2 using the temperature-sensitive *cdc25-22* mutation, induction of checkpoint arrest upon addition of ABA (20 minutes after release from G2 block), and subsequent wash-out of ABA 60 minutes after release from G2. **(C)** Fixed cell images of Mph1-ABI Spc7-PYL arrested cultures 0, 15, 25, 35 minutes after ABA wash-out. Scale bar of 10 µm. **(D)** Quantitation of cyclin B at spindles poles following a wash-out in cultures +/- ABA. The DMSO control did not arrest in metaphase. Samples were fixed and >150 cells were scored per time point for the presence of cyclin B at spindle poles. This experiment was repeated 3 times. Data plotted as mean +/- s.d. **(E)** Length of mitotic spindle was measured in cells following an ABA wash-out of cultures arrested (for 55 minutes). Cells were fixed 0, 10, 20, 30, and 40 minutes after wash-out and mitotic spindle was measured, 81-115 mitotic spindles were measured per time point. Each data point represents the length of mitotic spindle from a single cell with box plot showing the median and s.d. Mann Whitney test determined *p* value using Prism software.

elongate with the onset of anaphase B. Cells recover from an ABA wash out slower than a CBZ-induced arrest which silences almost immediately, likely due to a higher dissociation rate of CBZ from tubulin (Fig. **3.8 A**). However, this could make it difficult to capture subtle delays in silencing mutants. It is worth noting that endogenous *mph1* is required in this strain in order to directly compare the CBZ and ABA systems.

Work carried out in the last decade has identified **P**rotein **P**hosphatase **1** (PP1; Dis2 in *S. pombe*) as an important checkpoint silencing factor in yeast and humans (Pinsky et al., 2009; Vanoosthuyse and Hardwick, 2009; Meadows et al., 2011), the activity of which results in the activation of the APC and Cyclin B degradation. PP1 binds to the conserved SILK and RRVSF motifs on Spc7 (also known as the A and B motifs), and to the Kinesin 8 heterodimer (Klp 5 and 6) to mediate silencing (see Fig. **3.9**) (Meadows et al., 2011; Rosenberg et al., 2011). Work by Sadhbh Ní Chafraidh in our lab used the ABA silencing assay to confirm that the association of PP1 with Spc7 A and B motifs and kinetochore-associated Klp6 contributes to timely silencing of the checkpoint (Amin et al., 2018). The strains used to confirm this contained the endogenous *mph1* gene, enabling the recruitment of checkpoint proteins to kinetochores. This therefore allows silencing to take place at the ectopic Mph1-Spc7 scaffold and at kinetochores.

Consistent with evidence from our rTetR-based SynCheck assay, mammalian cells and budding yeast (Yuan et al., 2017; Klebig et al., 2009; Fernius and Hardwick, 2007 respectively), our investigations suggest that the kinase activity of Bub1 is not required for ABA-induced checkpoint signalling (see time 0, Fig. **3.8 A**). However we find that cells lacking the kinase domain — *bub1-Δkinase* — take longer to exit the ABA arrest (Fig. **3.8 B**). This could be a consequence of Bub1 kinase activity on error correction. Studies have shown that Bub1 phosphorylates histone H2A to recruit the inner centromere protein Shugoshin (Sgo2) which is necessary for the bi-orientation of sister chromatids (Riedel et al., 2006; Kawashima et al., 2010). It is possible that these mal-oriented sister chromatids could take more time to be resolved and segregate correctly. This may be the case as the endogenous SAC response and error correction are affected here. Future work can look at missegregation of chromosome 2 by following GFP-labelled centromere 2 (Yamamoto and Hiraoka, 2003) after ABA wash out. Previous work from our lab suggests a similar trend. Vanoosthuyse and colleagues found that 10% of cells in a Bub1 kinase-dead mutant background, *bub1K762M,* displayed lagging chromosomes while checkpoint activation remained unperturbed (2004). In addition results obtained following release from a *nda3-*

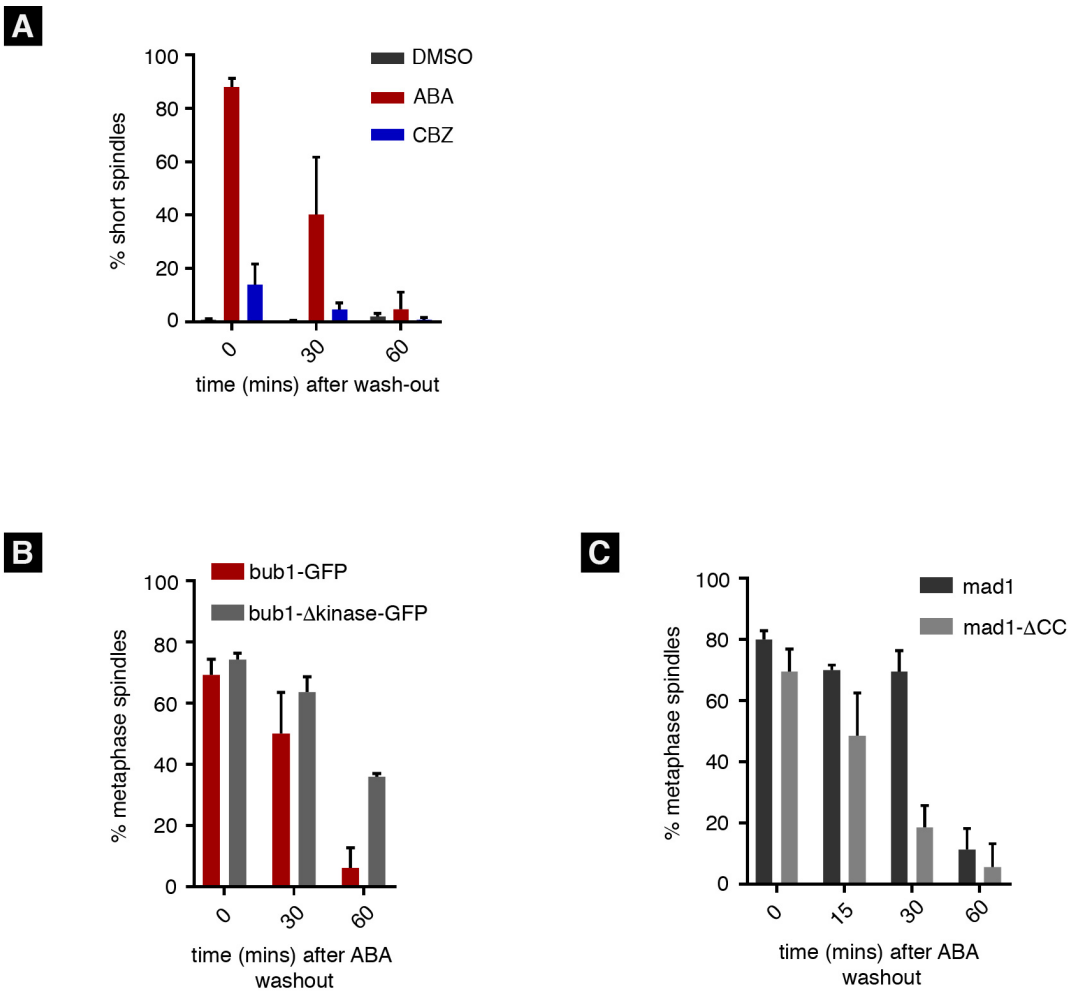

Figure 3.8: Factors affecting SAC silencing. (A) Quantitation comparing DMSO, ABA and CBZ wash-out following 60 minutes of treatment with solvent (added 20 minutes after release from G2 block). Samples were fixed 0, 30 and 60 minutes afterwash-out. >165 cells were scored per time point for the presence of cyclin B at spindle poles. This experiment was repeated at least 2 times and data is plotted as mean +/- s.d. **(B)** Graph comparing SAC silencing efficiency of Mph1-ABI Spc7-PYL strain with wild type Bub1-GFP and Bub1-Δkinase-GFP following 55 minute treatment +/- ABA and wash-out. >100 cells were scored for short metaphase spindles. This experiment was repeated 2 times and plotted as mean +/- s.d. **(C)** Graph comparing SAC silencing efficiency of wild type mad1 and an N-terminal coiled coil deletion (mad1-ΔCC) following 55 minute treatment +/- ABA and wash-out. Note that these strains also contained Bub1 GFP. >150 cells were scored for short metaphase spindles. This experiment was repeated at least 2 times and plotted as mean +/- s.d.

KM311 block, found a delay in mitotic exit as well as chromosome segregation defects in *bub1-Δkinase* (Onur Sen, unpublished).

Interestingly, we find that the *mad1-ΔCC* strain is able to exit the ABA metaphase block faster than full length Mad1 (Fig. **3.8 C**). Given that the checkpoint signalling components in *mad1-ΔCC* are unable to bind the Cut7 motor protein and localise to spindle poles, the increased silencing efficiency could occur as the PP1-Spc7 pathway alone is needed to silence the arrest. The *mad1-ΔCC* strain (also lacking endogenous *mph1*) is unable to bind to any part of the mitotic machinery and may bypass the need for the spindle-based PP1-Klp5-Klp6 silencing pathway (see model Fig. **3.9**). This is plausible since in an unperturbed mitosis, Klp5 recruitment to kinetochores is microtubule dependent (Garcia et al., 2002) and PP1-Klp5-Klp6 is likely to dephosphorylate checkpoint proteins present at the kinetochore-microtubule interface (Meadows et al., 2011). In *mad1-ΔCC*, the spindle pool of PP1 has no SAC targets (namely Spc7, and possibly other checkpoint proteins), leaving available a larger pool of PP1 for ectopic Spc7-based silencing. To test this hypothesis, further experiments include testing the above experiment in an *mph1+* background and testing the silencing behaviour of Klp mutants in *mph1Δ, mad1-ΔCC* strains (i.e. preventing localisation to kinetochore and spindle poles). It is also possible that the faster mitotic exit reflects the more efficient nature of silencing at the ectopic PP1-Spc7 pool. As an aside, it would be useful to have a direct measure of MCC levels to determine whether silencing discrepancies arise due to varying levels of MCC present in these mutant backgrounds.

This novel assay provides a way of studying SAC silencing without perturbing kinetochore-microtubule interactions. It has confirmed how PP1 recruitment to Spc7 and Kinesin-8 is needed to silence the checkpoint and allow anaphase progression. We also find that the kinase activity of Bub1 is required for timely exit possibly due to its downstream effect on chromosome bi-orientation, and use *mad1-ΔCC* to describe how bypassing the PP1-Klp5-Klp6 silencing pathway may speed up mitotic exit.

3.6 Summary and perspectives

In summary, by using yeast genetics and abscisic acid induced dimerisation to control the interaction of Spc7 and Mph1, we are able to ectopically reconstitute spindle assembly checkpoint activation and silencing in a manner which is tightly regulated and rapid. As with the rTetR-based SynCheck assay, this is dependent on the downstream checkpoint protein Mad1, and is independent of kinetochore and spindle pole localisation. The ectopic arrest has

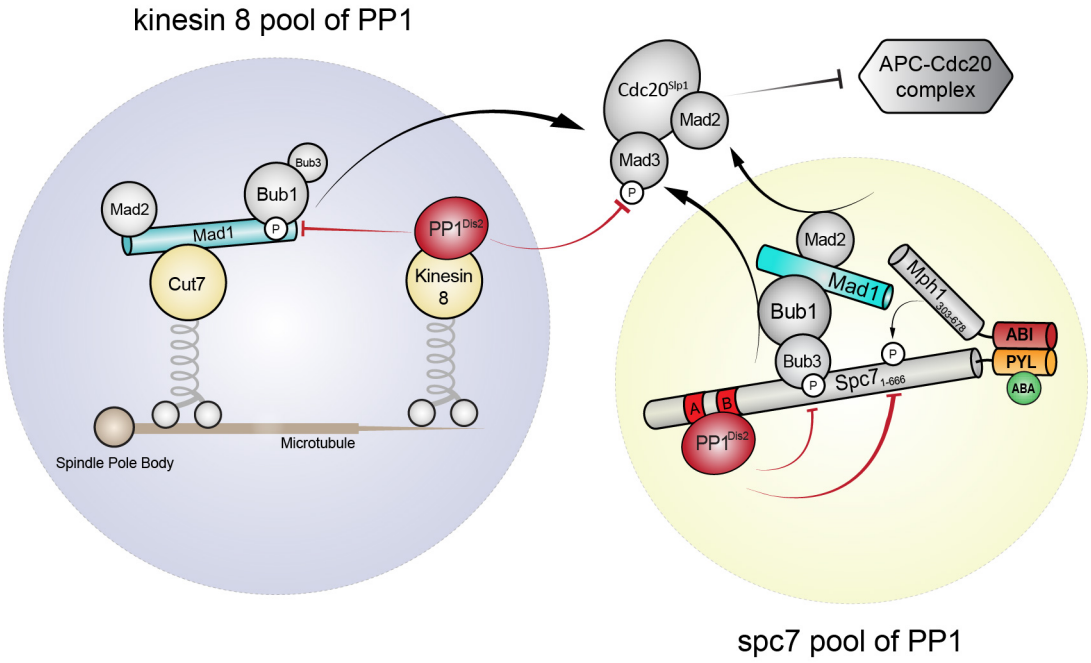

Figure 3.9: PP1-mediated SAC silencing takes place at Spc7 and Kinesin 8. Model showing a pool of PP1 associating with ectopic Spc7 and a spindle pool of PP1 associating with Kinesin 8 (Klp5-Klp6). The red arrows in the kinesin 8 pool of PP1 depict putative dephosphorylation.

reinforced the idea of kinetochores being the scaffold where sensing incorrect attachments is coupled to checkpoint activation. The contribution of the kinetochore would be difficult to dissect in an anti-microtubule arrest initiated by CBZ or a cold sensitive tubulin depolymerising *nda3-KM311* arrest or in an experiment where checkpoint proteins are anchored to kinetochores.

The ability to reverse the arrest is a major advantage of this system which, along with its lack of cross-reactivity, adds to its novelty in the '*pombe* toolkit'. We have confirmed that $PP1^{Dis2}$ needs to associate with Spc7 as well as Kinesin-8 to mediate silencing of the Mph1-Spc7 platform (Amin et al., 2018). Previous attempts at *PP1Δ* strain construction in our SynCheck system (Yuan et al., 2017) were hindered by synthetic lethality as a result of 'leaky' expression from the nmt81 promoter controlling *rTetR-mph1*.

We believe that the controllability of this system is a significant improvement over our existing SynCheck assay, in particular with regard to reversibility. Whereas silencing has been studied using *nda3-KM311*, carbendazim (Meadows et al., 2011), nocodazole wash-out (Liu et al., 2010), or following reversal of a Mph1 over-expression block (Karen May, unpublished), this method provides an alternative that preserves kinetochore-microtubule attachments and comes without the technical challenges of reversing a prolonged mitotic block.

ABA CID also has potential as an anchor away system (Haruki et al., 2008). This would enable the depletion of a protein from its subcellular location and also allow for rescue of the phenotype by reversing the dimerisation. Anchor away using ABA was successfully used in budding yeast where the nuclear protein Nab3 (**N**uclear poly**a**denylated RNA-**b**inding protein **3**) was tagged with ABI and relocated to the cytoplasm in the presence of ABA via binding to PYL-tagged **r**ibosomal **p**rotein **L13A** (Rpl13A-PYL) (Sander Granneman, personal communication). This allows a reversible way to study signalling pathways where gene deletions are lethal or which are location-specific, in a way that has a broad linear range of responsiveness to changes in concentration.

Joglekar and colleagues published the first use of CID to study the SAC activation in budding yeast (Aravamudhan et al., 2015). They used rapamycin to dimerise fragments of Mps1 and Spc105 and demonstrated that this is sufficient for a cell cycle delay. Although their intention was not to achieve kinetochore-independence, they used a temperature sensitive *ndc10-1* kinetochore mutant to show that the kinetochore does not contribute to the

rapamycin induced arrest. More recently, they used this method to achieve an ectopic arrest in HeLa cells (detailed in Chapter 4) to study the switch-like mechanism of SAC activation (Chen et al., 2019). Other reconstitutions of the SAC have been done *in vitro* using Xenopus egg extracts (Minshull et al., 1994) and purified recombinant proteins (Faesen et al., 2017).

Different methods of studying the checkpoint are necessary for a multifaceted understanding of how checkpoint signalling is regulated in the greater context of mitosis with its various feedback loops. This simple assay for studying checkpoint mutants, and silencing factors and regulators *in vivo* adds to the repertoire of tools. It has applications beyond the checkpoint. By regulating metaphase entry and exit, it can be used to study different aspects of the mitotic machinery such as chromosome segregation and kinetochore-microtubule attachment, without disrupting kinetochore and microtubule physiology or over-expressing components of a given pathway.

CHAPTER 4

S. pombe and HeLa cell fate following prolonged mitotic arrest

4.1 Introduction

The previous chapter described a novel, ectopic method used to regulate checkpoint activation and silencing. To follow, we wanted to study the subsequent effects of a prolonged ectopic arrest on yeast and mammalian cells. This chapter describes the response of *S. pombe* to ABA-induced arrest and extends this work to HeLa cells using a recently published ectopic arrest assay (Chen et al., 2019). We compare cell fate profiles of HeLa cells in an ectopic arrest and an anti-microtubule nocodazole arrest. Using single cell analysis, we attempt to gauge the full complexity of responses between and within cell populations treated with different drugs and discuss the responses and trends observed.

4.2 Prolonged ABA-induced arrest leads to untimely septation in *S. pombe*

To test the viability of cells following an ectopic metaphase arrest, we used the method described in the previous chapter. Cells were synchronised in G2 using a temperature sensitive *cdc25-22* mutant. ABA, CBZ or DMSO was added 20 minutes after release from the G2 block and cells were plated on rich media (without solvent) 0, 60, 120, 180 and 240 minutes after addition of solvent to determine which were able to form colonies. While nearly 80% of cells plated 30 minutes after solvent addition were able to form colonies, we find that cell viability gradually decreases to approximately 30% 4 hours after ABA addition (Fig. **4.1**). Cells treated with the anti-microtubule drug CBZ responded similarly. Therefore, the longer cells spend in an ABA-induced metaphase block, the less viable they become.

Next, we wanted to determine why *S. pombe* cells lose viability in a protracted arrest. We followed the segregation of chromosome 2 using GFP-labelled cen2 (**cen**tromere **2**) (Yamamoto and Hiraoka, 2003) to test whether the decrease in cell viability was a result of chromosome segregation errors during nuclear division. Cells were arrested with ABA for 0, 60, 120, 180 and 240 minutes and 'washed out' to induce anaphase and follow the

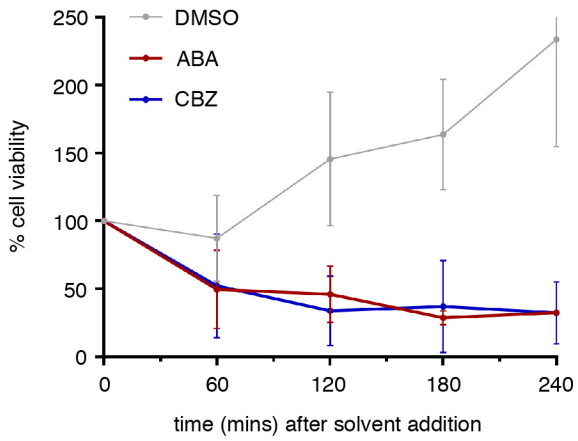

Figure 4.1: Cell viability decreases in a prolonged metaphase arrest. The viability of cells was determined by plating cells 0, 60, 120, 180 and 240 min after addition of DMSO, ABA or CBZ, where solvent was added 20 minutes after release from the G2 block. Cell viability over time was plotted as a percentage relative to that at time zero. Cells were plated in triplicate. The experiment was repeated 3 times. All data are plotted as mean +/- s.d.

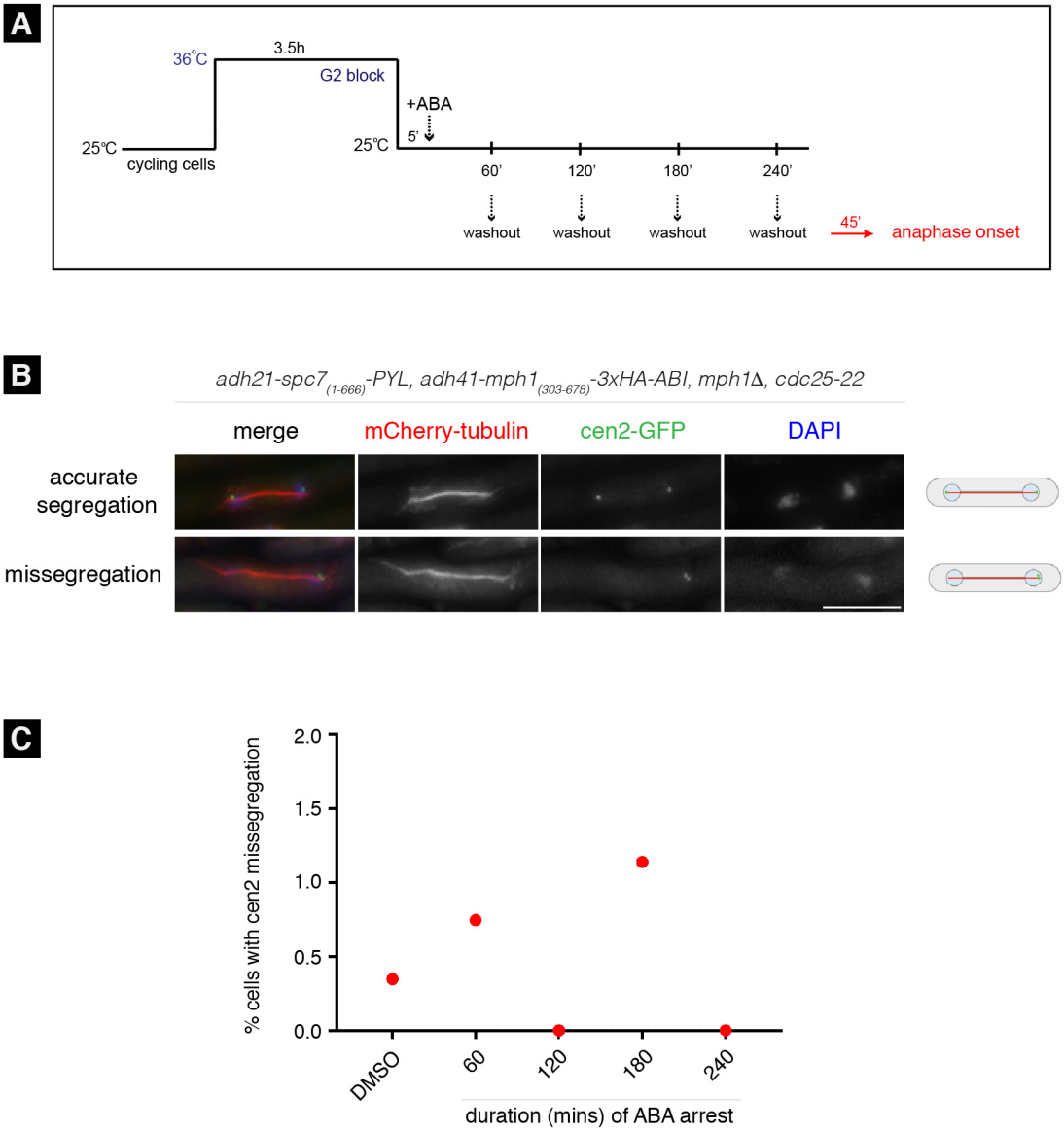

Figure 4.2: Loss of cell viability is not caused by nuclear division errors. (A) Experimental set-up to study Chromosome 2 segregation during anaphase B. Cells were synchronised in G2, treated with ABA for 60, 120, 180 or 240 minutes after which ABA was washed-out to allow anaphase onset. **(B)** Microscopy of fixed cells in anaphase B with correctly and incorrectly segregated chromosome 2. The centromere of chromosome 2 is marked with GFP and shown in green (cen2-GFP), microtubules in red (mCherry-tubulin) and DAPI stain for chromatin in blue. Scale bar represents 10 μm. A cartoon of the cells is shown on the right. **(C)** Quantitation of anaphase B cells with missegregated cen2 following an ABA-induced arrest and wash-out (described in panel A). DMSO treated cells captured in anaphase B 60 minutes after release from G2 block were used as controls. n= 367, 391,133, 88, 53 respectively.

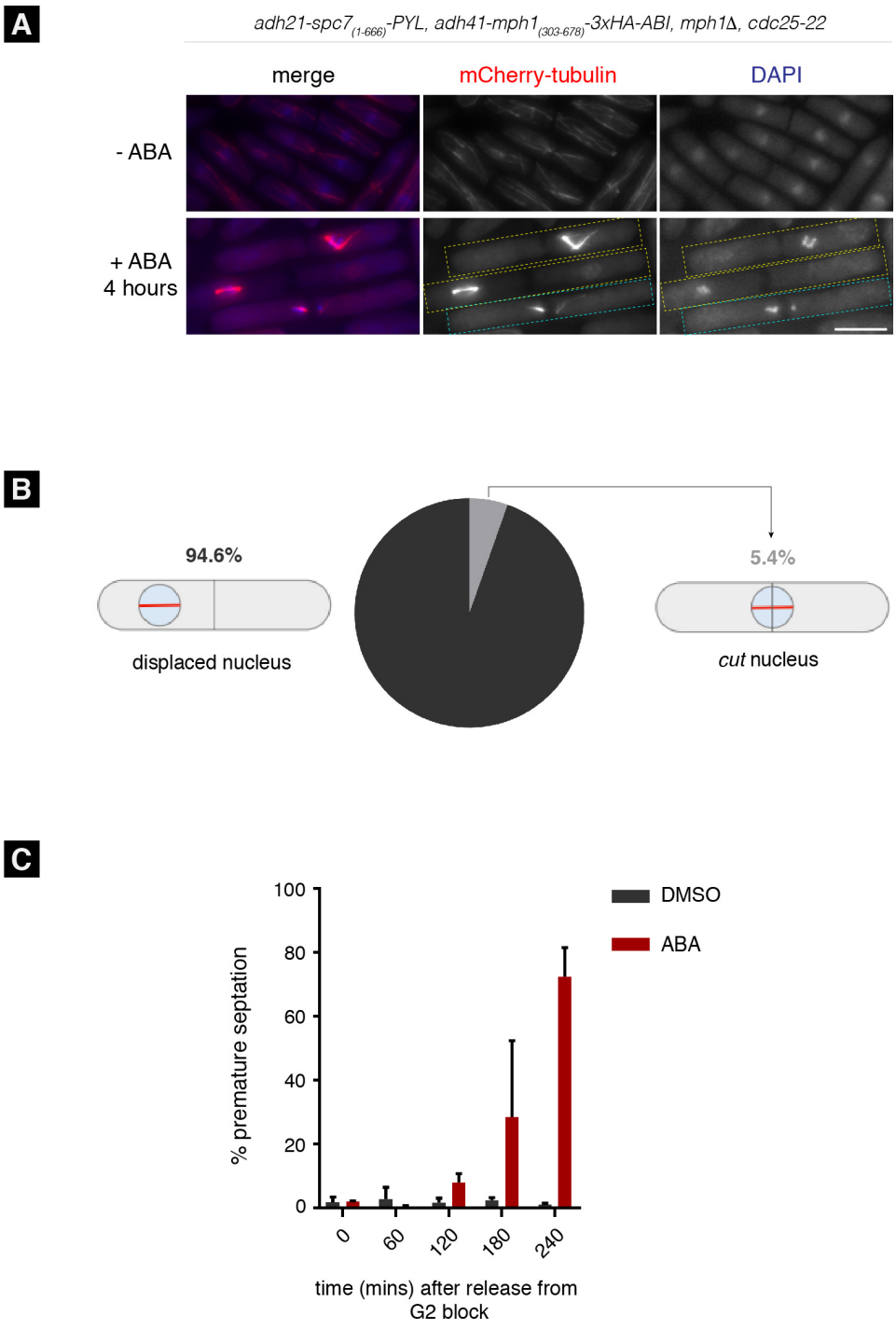

Figure 4.3: Prolonged metaphase arrest leads to cytokinesis before nuclear division in *S. pombe*. (A) Microscopy showing prematurely septated fixed cells following a 4-hour ABA-induced arrest. An untreated population (-ABA) is used as a control (top panel). Microtubules are shown in red (mCherry-tubulin) and DAPI stain for chromatin in blue. Cells with a displaced nucleus are surrounded by a yellow box and *cut* cells by a cyan box. Scale bar is 10 μm. **(B)** Pie chart depicting the porportion of prematurely septated cells with a displaced nucleus versus a cut nucleus following a 4 hour ABA-induced arrest. The mean of 3 experiments is plotted (n=234). **(C)** Graph showing an increase in premature septation of mitotic cells over time in an ABA arrest. ≥100 cells counted in each condition per experiment. Data is plotted as the mean of 3 experiments +/- s.d.

segregation of cen2-GFP (Fig. **4.2 A**). In cultures treated with ABA, anaphase B was captured 45 minutes after wash-out. In control cultures treated with DMSO, anaphase B was captured 60 minutes after release from the G2 block. Accurate segregation of chromosome 2 would lead to one cen2-GFP dot at each end of the anaphase spindle whereas, incorrect segregation would lead to two cen2-GFP dots at one end of the spindle and none at the other (Fig. **4.2 B**). We found that missegregation of chromosome 2 during nuclear division occurred at a low frequency of between 0 and 1.2% in both DMSO-treated and the ABA-treated cultures (Fig. **4.2 C**). This suggests that chromosome segregation errors during nuclear division are not causing a decrease in cell viability. This experiment explored the segregation of cen2 to individual nuclei, rather than to daughter cells. We observe that after 2 hours of arrest many cells displace their nucleus and undergo septation before anaphase is complete. After ABA wash-out, these cells are still able to complete nuclear division, usually resulting in a daughter cell with 2 haploid nuclei and another which is aploid (lacking chromosomes). This phenotype is also observed when cells leak out of a prolonged SynCheck arrest.

We hereby refer to the untimely occurrence of septation before nuclear division as 'premature septation', depicted in Fig. **4.3 A**. Following a 4 hour ABA-induced arrest, 94.6% of prematurely septated cells displace their SAC-arrested nucleus before septation and 5.4% of cells display the *cut* (**c**ell **u**ntimely **t**orn) phenotype where the septum cuts through the undivided nucleus (Fig. **4.3 B**) (Yanagida, 1998). In a given population, the percentage of cells that have prematurely septated increases with time spent in mitosis (Fig. **4.3 C**). Around 10% of cells are prematurely septated 2 hours after release from G2 (when ABA is added at 5 minutes). This increases to nearly 80% 4 hours after G2 release, inversely correlating with the loss of cell viability observed over time. Additionally, we find that when prematurely septated cells are plated individually on rich media without ABA, they are unable to divide. Together, this data supports the hypothesis that the loss of *S. pombe* cell viability during a prolonged mitotic arrest is due to the consequences of prematurely septated cells.

This phenotype has been observed in temperature sensitive *S. pombe* APC mutants *cut4*, *cut9*, *nuc2*, *lid1/cut20*, *cut23* and *apc10* where a septum either cuts through an undivided nucleus or in such a way that DNA is segregated to one only daughter cell (Chang et al., 2001). Surprisingly, the Gould group found that in the APC mutant *lid1-6,* $Cdc13^{cyclin\ B}$-$Cdc2^{CDK1}$ levels still oscillate and decrease prior to septation, while $Cut2^{Securin}$ levels are seemingly stable as chromosomes remain unsegregated (Chang et al., 2001). They reasoned

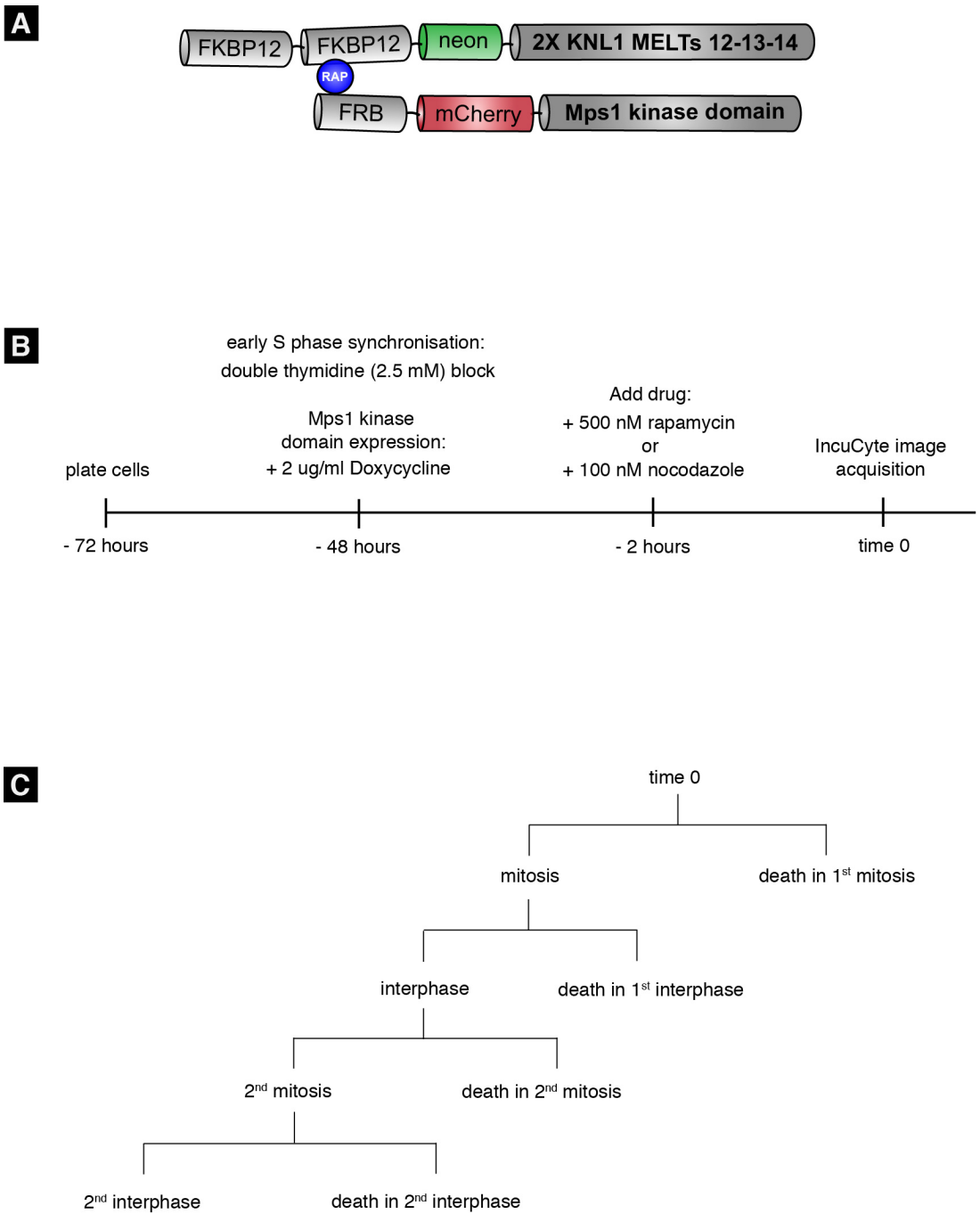

Figure 4.4: eSAC experimental set-up for long-term single analysis of HeLa cell fate. (A) Cartoon of eSAC dimerisation constructs used in HeLa cells. 2 copies of the KNL1 MELT motifs 12, 13, 14 are fused with mNeon green and 2 copies of FKBP12 for dimerisation with the kinase domain of Mps1 which is tagged with mCherry and FRB in the presence of rapamycin. **(B)** Experimental workflow of eSAC arrest. 48 hours prior to experiment, HeLa cells are pre-synchronised in S phase and the expression of the kinase domain is induced. The drug (500 mM rapamycin, or 100 mM nocodazole as a control) is added and live cell images are acquired over a 65 hour period. **(C)** Schematic showing possible cell fates.

that APC *cut* mutants are hypomorphic to Cdc13 degradation (and not to Cut2^{Securin}) as in APC-null mutants, Cdc13 levels remain stable and cells do not septate prior to nuclear division. A similar phenotypic trend has been reported in *cut4* temperature sensitive and null mutants (Yamashita et al., 1996). This supports the established hypothesis that septation can only occur if CDK1-cyclin B activity is inhibited. To further support this theory, in early mitotic arrests where tubulin is inhibited, such as in *nda3-KM311,* cells do not septate prematurely and Cyclin B levels remain high (McCollum and Gould, 2001). This suggests that septation prior to nuclear division could occur due to a decrease in Cyclin B levels during a prolonged ABA arrest.

4.3 Complex variation of HeLa cell fate in response to prolonged mitotic arrest

To study the effect of a prolonged metaphase arrest in mammalian cells, this work was extended to HeLa cells in collaboration with Ajit Joglekar's lab. They have engineered a rapamycin dependent method of generating an ectopic arrest in HeLa cells, named 'eSAC' (**e**ctopic **SAC**) (Chen et al., 2019). In a bi-cistronic cassette integrated at a LoxP site in the HeLa cell genome, the kinase domain of Mps1 (residues 500-857) was fused to the C-terminus of FRB-mCherry, and placed under the control of a doxycycline induced promoter. The same cassette was used to constitutively express 2 copies of the KNL1 MELT motifs 12, 13 and 14 (residues 800-1014) C-terminal to a 2xFKBP12-mNeonGreen tag (Fig. **4.4 A**). Positive colonies from the Cre-recombinase integration were pooled. They consequently built a system that allows for inter-cell variation in eSAC activity. This results in variation in the time spent in mitosis. In the presence of rapamycin, cells spend approximately 0-24 hours in mitosis. Therefore, this system allows the study of HeLa cell behaviour as a consequence of different levels of eSAC activity and mitotic durations.

To compare how HeLa cells respond to an arrest with and without microtubule interference, eSAC cells were treated with either nocodazole or rapamycin and tracked individually by long term live cell imaging. 48 hours before the time course, HeLa cells were synchronised in early S (**s**ynthesis) phase using a double thymidine block and Mps1$_{500\text{-}857}$ kinase expression was induced (Fig. **4.4 B**). Cells were then treated with either 500 mM rapamycin or 100 mM nocodazole 2 hours before long term IncuCyte live cell imaging where images were taken every 10 minutes for approximately 65 hours.

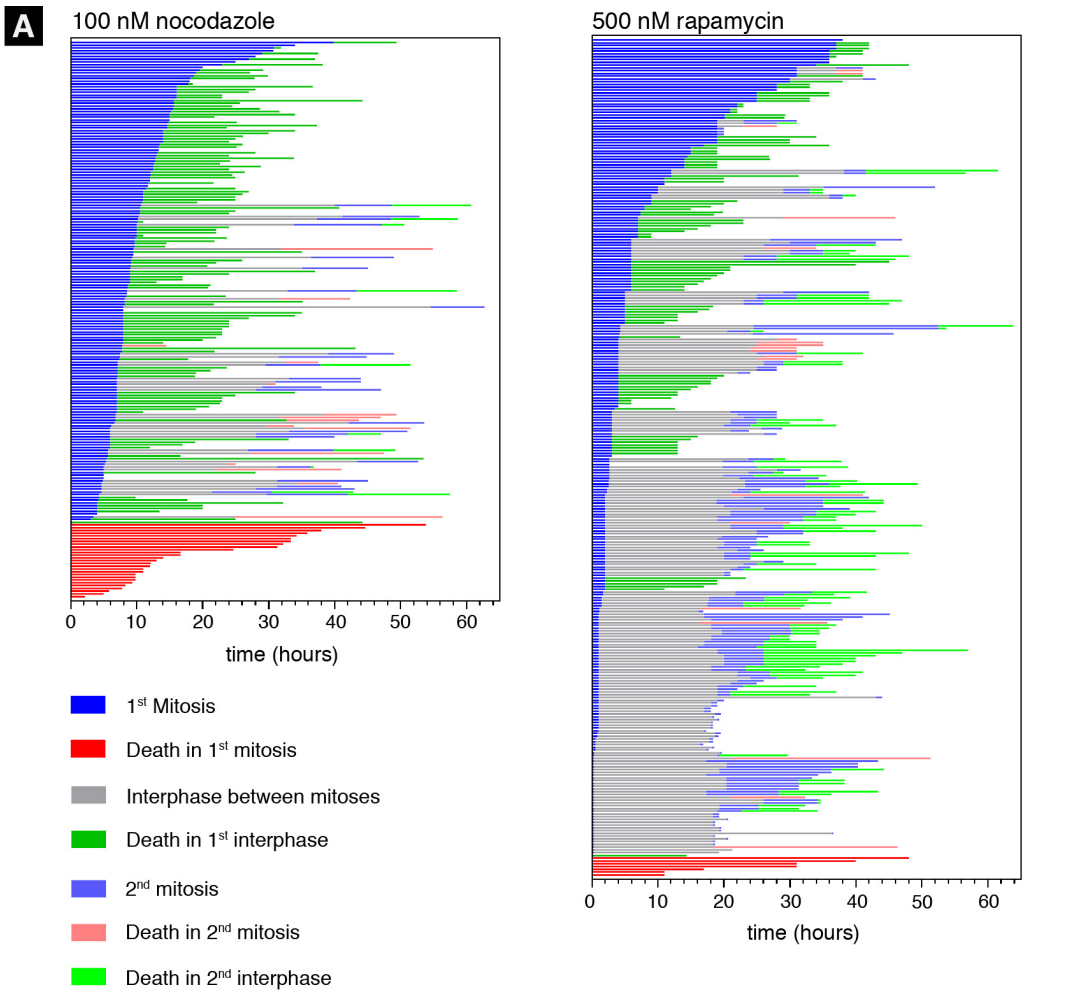

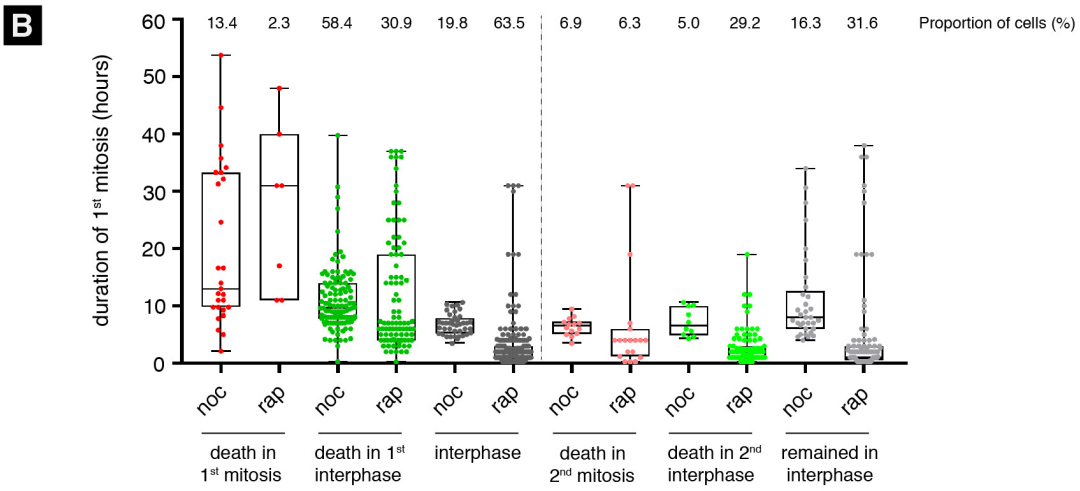

Figure 4.5: Mitotic duration determines cell fate following slippage. (A) Cell fate profiles of HeLa cells treated with 100 nM nocodazole (top panel) and 500 nM rapamycin (bottom panel). Each bar represents an individual cell (n= 202 and 301 for nocodazole and rapamycin respectively) and length of bar indicates duration of cell cycle stage in hours. **(B)** Box and whisker plots showing the distribution of mitotic duration in cells that met indicated fates. Box shows mean and upper and lower quartiles. Whiskers indicate range. The proportion of the population (%) that experienced a particular fate is given above the graph. The dotted line separates the 1st and 2nd cell cycle.

Studies published in 2008 were amongst the first to use single cell analysis to study the response of cancer cell lines to antimitotic drugs (Brito et al., 2008; Gascoigne and Taylor, 2008; Orth et al., 2008; Shi et al., 2008). Consistent with what they reported, we find that there is intra- and inter-cell population variation in the response to antimitotic drugs. Most cells enter mitosis in the first few hours of the time course. These cells either die or exit mitosis. Cells which exit the 1st mitosis either die in interphase, stay in interphase for the rest of the time course or survive interphase and enter a 2nd mitosis where they either die or survive (Fig. **4.4 C**). The fate of individual cells following treatment with either nocodazole (top panel) or rapamycin (lower panel) is depicted in Fig. **4.5 A**. Each bar represents the history of a single daughter cell, the colours denote behaviour, and the length of bars indicates duration of a particular stage. In cases where mitotic slippage occurred, defined as gradual cyclin B degradation and mitotic exit despite checkpoint arrest (Brito and Rieder, 2006), bars are arranged in order of increasing mitotic duration.

We find significant variation in cell behaviour. Cells treated with nocodazole spent between 0.3 to 53.4 hours in the initial mitosis, with an average of 11.7 hours. A wide range was also observed in rapamycin treated cells which spent 0.3 to 48 hours in mitosis, or 6.94 hours on average. In agreement with findings from Brito and colleagues (2008), we find that the presence of microtubules does not affect duration of mitotic arrest. While 13.4% of nocodazole treated cells died in the 1st mitosis, only 2.3% did so when treated with rapamycin. Perhaps surprisingly, and similar to other published analyses, there is no apparent correlation in this minority population between death in mitosis and time spent in mitosis in either drug (Fig. **4.5 B**). A larger sample size would be useful in this case.

Severe defects in cytokinesis were found in cells treated with nocodazole, which binds to β-tubulin and inhibits microtubule polymerisation. In most cases, cells were unable to undergo cytokinesis. A few divided unequally and of these, a small proportion of daughter cells merged after dividing incorrectly. These cytokinesis defects led to endoreduplication (DNA replication without cell division), resulting in polyploid cells. This could provide an explanation for why the fate of the largest subpopulation — around 58% —was death in 1st interphase. In addition, the inability to undergo cytokinesis could explain why more nocodazole-treated cells died in metaphase, and earlier as a population in general, when compared to rapamycin treated cells. On the other hand, cells treated with rapamycin display lower instances of abnormal cytokinesis. 24 out of 150 1st mitotic events led to abnormal

cytokinesis. Of these, cells died in the 1st interphase in 19 cases. Therefore, abnormal cytokinesis negatively correlates with time taken for apoptosis in HeLa cells.

Rapamycin treated cells tend to die later than nocodazole treated cells (Fig. **4.5 B**). This could be because apoptosis is triggered more quickly in response to nocodazole treated cells where abnormal cytokinesis causes severe aneuploidy (discussed later in this chapter). 63.5% of cells survived the 1st interphase (compared to 19.8% in nocodazole). While nearly a third of the population dies in the 1st interphase, 29.2% die in the 2nd interphase and 31.6% remained in interphase for the remainder of the experiment, the fate of which was not captured in the duration of this time course. Interestingly, rapamycin and nocodazole treated cells that survived the 1st interphase arrested in mitosis for a shorter period of time on average than those that had died in interphase (Fig. **4.5 B**). This indicates a link between the duration of mitosis and apoptosis.

4.4 Discussion and future work

This chapter aimed to study the effects of a prolonged checkpoint arrest in yeast and HeLa cells. We found that fission yeast lose viability over time in mitosis due to an increased incidence of septation before nuclear division. Fission yeast cytokinesis is regulated by GTPase-dependent protein kinases which form the **s**eptation **i**nitiation **n**etwork (SIN) (reviewed in McCollum and Gould, 2001). SIN signalling is temporally coordinated with late mitosis in order for septation to occur after mitotic exit (Goyal et al., 2011). In an unperturbed mitosis, high CDK1 (Cdc2 in *S. pombe*) activity during metaphase inhibits septation, with the APC playing an important role in SIN activation as the APC is responsible for Cyclin B degradation and the subsequent lowering of CDK1 activity in anaphase (Yamano et al., 1996; Chang et al., 2001; Rachfall et al., 2014). It has been found that inhibiting the **G**TPase **a**ctivating **p**rotein (GAP) Cdc16 leads to $Cdc2^{CDK1}$ inactivation and septation (Fankhauser et al., 1993). This provides a link between the SIN and the SAC.

It is possible that the uncoupling of septation from an ABA-dependent mitotic delay occurs due to slow degradation of Cyclin B during a prolonged ectopic mitotic arrest (slippage). This degradation may be sufficient to lower CDK1 activity to a threshold where the SIN can be activated. This could occur due to limitations in SAC protein abundance which could allow low levels of APC activation — sufficient to lower CDK1 activity and initiate SIN signalling. This can be tested by quantifying Cyclin B levels in cells over time in a mitotic arrest, achievable by measuring Cyclin B-GFP fluorescence at spindle pole bodies

and immunoblotting. A comparison between an ectopic, *nda3-KM311* and APC mutant arrest would provide insight on how timing or the phase of the mitosis perturbed affects the coordination of septation with nuclear division.

To test the hypothesis that decreased CDK1-cyclin B activity is required for SIN and septation, a non-destructible Cyclin B N-terminal D-box mutant (Yamano et al., 1996) could be tested in the ABA arrest and should prevent premature septation if the hypothesis is true. A SIN null mutant or over-expression of Cdc16 can be used to determine whether this phenotype is SIN-dependent.

The **m**itotic **e**xit **n**etwork (MEN) is a similar pathway that exists in budding yeast that promotes septation through $Cdc14^{Clp1}$ phosphatase-dependent Cyclin B proteolysis and mitotic exit (Visintin et al., 1998). However, an additional pathway exists which may explain why the *cut* phenotype is common in fission yeast but not in budding yeast, for example in the DNA topoisomerase II mutant *top2* (Uemura and Yanagida, 1984; Mendoza et al., 2009).

Budding yeast and mammalian cells appear to have an additional abscission checkpoint, termed 'NoCut', which delays septation in response to chromatin at the spindle midzone, detected by $Cdc14^{Clp1}$-dependent Aurora B localisation (Norden et al., 2006; Steigmann et al., 2009, Amaral et al., 2016). This therefore ensures that septation only occurs after anaphase. It would be interesting to elucidate why the NoCut delay, evident in budding yeast and higher eukaryotes, is not seemingly conserved in *S. pombe*. It could be the case that a similar delay exists in *S. pombe* but is insufficient to sustain a prolonged delay in response to a protracted metaphase arrest (Norden et al., 2006). The contribution of this Aurora B-mediated delay can be tested in *S. pombe* using an ATP analogue-sensitive allele of $Ark1^{Aurora\ B}$ in an ABA arrest and the inhibitor 1NMPP1 to suppress $Ark1^{Aurora\ B}$ during mitosis and observe whether premature septation in a synchronous population occurs earlier (than at 3 hours as observed here).

In contrast to the clear bimodal distribution of an ABA-treated population of *S. pombe*, where cells either arrest or remain cycling followed by increased premature septation over time in arrest, HeLa cells exhibit variation. This variation exists within and between populations treated with the anti-microtubule polymerising drug nocodazole or rapamycin, for kinetochore-independent eSAC activation. Variation within a population, occurring in terms of mitotic duration and cell fate, is likely due to differences in eSAC expression. Whereas cell fate between nocodazole treated and rapamycin treated cells varied due to the

mechanism of action of the drugs. Nocodazole led to severe defects in cytokinesis, causing most cells to die within the 1st interphase. This is in contrast to rapamycin which mostly caused cell death in the subsequent cell cycle. The competing fates model suggests that whether a cell dies in a prolonged mitosis or undergoes mitotic slippage depends on two competing networks — activation of apoptotic pathways (likely due to Caspase-9 dephosphorylation, discussed in the next paragraph) versus decreasing Cyclin B levels (slippage) — each of which have thresholds (Gascoigne and Taylor, 2008). Once a threshold is breached by the competing network, it dictates the fate of the cell. Therefore according to the competing fates model, in the nocodazole arrest, apoptotic pathways may have been activated before Cyclin B levels could drop to a level which allowed sister chromatid separation and slippage.

An interesting trend emerged where the mitotic duration of cells that died in interphase was higher than those that survived interphase and continued to the next cell cycle. The link between mitotic duration and apoptosis onset after mitotic slippage is novel as although other single cell analyses have found cell fate to depend on the drug used and its concentration, a relationship with mitotic duration has not been observed (Gascoigne and Taylor, 2008). A possible explanation for mitotic-linked death in interphase is CDK1 phosphorylation-dependent inhibition of Caspase-9. This is lost after mitotic exit, increasing Caspase-9 activity to a level that allows apoptosis to ensue (Allan and Clarke, 2007). Additionally, mitotic slippage, a symptom of a prolonged metaphase block, would gradually relieve CDK1-dependent inhibition of Caspase-9. This could explain the temporal link between mitotic duration and onset of apoptosis in interphase. Interestingly, apoptotic regulating genes such as those in the Bcl-2 family, namely Mcl1, are controlled by CDK1 phosphorylation and APC/C ubiquitination (Harley et al., 2010; Terrano et al., 2010). Therefore, it is likely that the regulatory requirement of APC/C ubiquitination and CDK1 phosphorylation for both mitosis and apoptosis is responsible for the link between apoptosis and mitosis.

Although cell culture experiments mirror some of the complexity observed when anti-mitotics are administered for cancer therapy, existing cell culture methods are unable to emulate the fluctuations in drug concentration that occur due to bioavailability and clearance in complex living systems (Gascoigne and Taylor, 2009). To mimic bioavailability by a greater extent, future studies could implement the more controllable ABA system in cell culture experiments to be able to better regulate mitotic duration, mitotic exit (through wash

out) and alter concentration. Given that variation in response is expected, this method could enhance control of the input (drug) to better understand the resulting effects and predict how cells may respond to a particular type of anti-mitotic treatment. It could also provide a useful tool to directly monitor the links between the SAC, which impacts mitotic duration, and cell death.

CHAPTER 5

The roles of the Mad1 C-terminus in spindle assembly checkpoint signalling

5.1 Introduction: **m**itotic **a**rrest **d**eficient **1**

Mad1 is essential for mitotic checkpoint signalling and was first isolated in 1991 (Li and Murray; Hardwick and Murray, 1995) from a genetic screen in the budding yeast *Saccharomyces cerevisiae*. They found that Mad1 mutants divide faster when exposed to low doses of benomyl, a drug that perturbs microtubule polymerisation, but also exhibit increased rates of chromosome loss which causes cell death. Mad1 is evolutionarily well conserved in eukaryotes (Vleugel et al., 2012).

S. pombe Mad1 has 676 amino acids and is 78.49 kDa in size. Crystal structures of the human protein show that it consists of a long coiled coil region and a well conserved C-terminal globular head which has a similar structure to the kinetochore binding domains Spc25 and Csm1 (Kim et al., 2012). It is a homodimer that forms a constitutive 1:1 heterotetramer with Mad2 (Chen et al., 1999; Sironi et al., 2002; Kim et al., 2012). Similar to other eukaryotes, the *S. pombe* Mad1-Mad2 complex localises to the nuclear periphery in interphase and translocates to kinetochores in prometaphase in a Mad1-dependent manner (Ikui et al., 2002). This complex is then transported to the spindle pole bodies via the Kinesin-5 motor Cut7 (Eg5 homologue) (Akera et al., 2015), a bi-directional motor protein (Edamatsu, 2014). We have shown that localisation of Mad1 to the nuclear periphery is dispensable for an ectopic checkpoint response in *S. pombe* (Chapter 3; Yuan et al., 2016; Amin et al., 2018). In humans cells, MCC is reportedly generated at **n**uclear **p**ore **c**omplexes (NPCs) in interphase, decreasing segregation errors and improving efficiency of SAC signalling in early mitosis, before kinetochores are fully assembled and able to generate MCC (Rodriguez-Bravo et al., 2014). Studies in budding yeast implicate Mad1 in regulating nuclear trafficking, ultimately impacting spindle dynamics during mitosis (Cairo et al., 2013).

Mad1 is also involved in chromosome alignment (Akera et al., 2015). The N-terminus of *S. pombe* Mad1 recruits Cut7 to the kinetochores of misaligned chromosomes in early mitosis and aids chromosome gliding to the spindle equator to achieve biorientation. It has

been found that artificially anchoring Cut7 to kinetochores partially reduces the chromosome biorientation defects of *mph1Δ*, *bub1Δ* and *bub3Δ*. This could account for the Shugoshin-independent bi-orientation function of Bub1-Bub3 (Windecker et al., 2009). In budding yeast, Kinesin-5 motors proteins Cin8 and Kip1 mediate chromosome alignment (Gardner et al., 2008), although it is unknown whether this is Mad1-directed. In human cells, this function is carried out by Mad1-dependent recruitment of Kinesin-7/CENP-E to kinetochores (Akera et al., 2015). Downstream members of the SAC via Mad1 and CENP-E subsequently localise to spindle poles in a dynein-dependent fashion (Silva et al., 2014). This is thought to facilitate SAC silencing in mammalian cells by 'stripping' Mad1-Mad2 from the kinetochore, thus preventing MCC formation (Howell et al., 2001; Gassmann et al., 2008; Gassmann et al., 2010; Barisic et al., 2010).

More recent data from mammalian cell studies finds that the Mad1 recruits Cyclin B-CDK1 to unattached kinetochores in an Mps1 kinase-dependent manner, via a complex between the N-terminus of Mad1 and Cyclin B-CDK1 (Alfonso-Pérez et al., 2019; Hayward et al., 2019). Thus establishing a positive feedback loop as CDK1 in turn promotes Mps1 recruitment to unattached kinetochores, for a sustained mitotic delay.

This Chapter focuses on the roles of Mad1 in SAC signalling, mediated by the C-terminus. It aims to uncover the long standing question of how the Mad1-C-Mad2 (Mad1-**c**losed-Mad2) complex is recruited to kinetochores and how it contributes to propagating the SAC signal. We confirm the Mad1-Bub1 interaction as a mechanism of kinetochore recruitment and provide evidence which suggests that Mad1 contributes to MCC formation through C-Mad2-Slp1 binding.

5.2 Mad1 and Bub1 form a complex in *S. pombe*

Some focus in the field and in our lab has been on the importance of Bub1-recruited Mad1-C-Mad2 to unattached kinetochores for SAC activation. Although this interaction has previously proved to be quite labile in *S. pombe*, evidence of a Mad1:C-Mad2-Bub1:Bub3 complex has been reported in *Saccharomyces cerevisiae* (*S. cerevisiae*). The first indications of a link were seen when a **c**o-**i**mmuno**p**recipation (co-IP) of Mad1 revealed Mad1p-Bub1p-Bub3p complex formation in nocodazole-treated cells (Brady and Hardwick, 2000). They additionally identified that this interaction occurs via the conserved Mad1 RLK motif and is dependent on the presence of Mad2 and Mph1 kinase. This was confirmed by a more recent

budding yeast study that found a direct Mad1-Bub1 interaction, mediated by Mph1-phosphorylated Bub1 and dependent on Mad2 (London and Biggins, 2014).

Previous efforts by our lab to capture the Mad1-Bub1 complex in *nda3*-arrested fission yeast cells following IP and mass spectrometry analysis have been unsuccessful. Furthermore, attempts to capture this transient complex in mammalian cells has also proven challenging (Kim et al., 2012; Faesen et al., 2017). The complex has been detected in *Caenorhabditis elegans (C. elegans),* where Mad1 has been found to bind the kinase domain of Bub1, although there are fundamental differences in how the SAC is regulated as they lack Mps1 kinase (Moyle et al., 2014; Espeut et al., 2015).

We used our previously published SynCheck (**syn**thethic **check**point) assay, described in Chapter 3 (and Yuan et al., 2017), to arrest cells in metaphase for co-IP. This assay uses rTetR dimerisation to co-recruit rTetR-Spc7$_{1\text{-}666}$-9TE and rTetR-Mph1$_{303\text{-}678}$. The *spc7$_{1\text{-}666}$-9TE* allele is a phosphomimetic mutant of *spc7$_{1\text{-}666}$* where 9 threonine residues within MEL**T** motifs are mutated to glutamic acid. Although this is sufficient to recruit downstream SAC proteins Bub1, Bub3 and Mad3, the dimerisation with rTetR-Mph1 kinase is required for checkpoint activation (London et al. 2012; Shepperd et al. 2012; Yamagishi et al., 2012; Zhang et al., 2014; Yuan et al., 2017). Dimerisation occurs when rTetR-Mph1$_{303\text{-}678}$ is expressed, which is driven by a thiamine-repressible nmt81 promoter (Fig. **5.1 A**). A peak mitotic index of around 85% is reached 16 hours after growing cells in the absence of thiamine. rTetR domains are also able to spontaneously bind to a tandem array of TetO repeats integrated at the *arg3* locus of chromosome 1. Despite that being the case, we have found that co-localisation of rTetR-Spc7 and rTetR-Mph1 to a TetO array is not required for a robust arrest, regardless of the number of TetO repeats (Fig. **5.1 B**, Yuan et al., 2017).

To test whether Mad1 and Bub1 form a complex in *S. pombe*, we immunoprecipitated Bub1-GFP from cells (with and without a TetO array) following 16 hours of SynCheck rTetR-Mph1 expression, and DSP (**d**ithiobis(**s**uccinimidyl **p**ropionate)) crosslinking. We found that significantly more Mad1 co-immunoprecipitated with Bub1-GFP following an anti-GFP pull down in arrested cultures (when rTetR-Mph1 is expressed), in the presence and absence of a TetO array (Fig. **5.1 C** and Yuan et al.; 2017 Fig. 4). We are also able to detect this complex in *nda3* arrested cells and without DSP crosslinking (data not shown). We propose that harvesting cells at room temperature improves the detection of these complexes in *in vivo* extracts. Our data is in accordance with that from Mora-Santos and colleagues (2016) who immunoprecipitated Mad2-GFP from *nda3-KM311* arrested fission

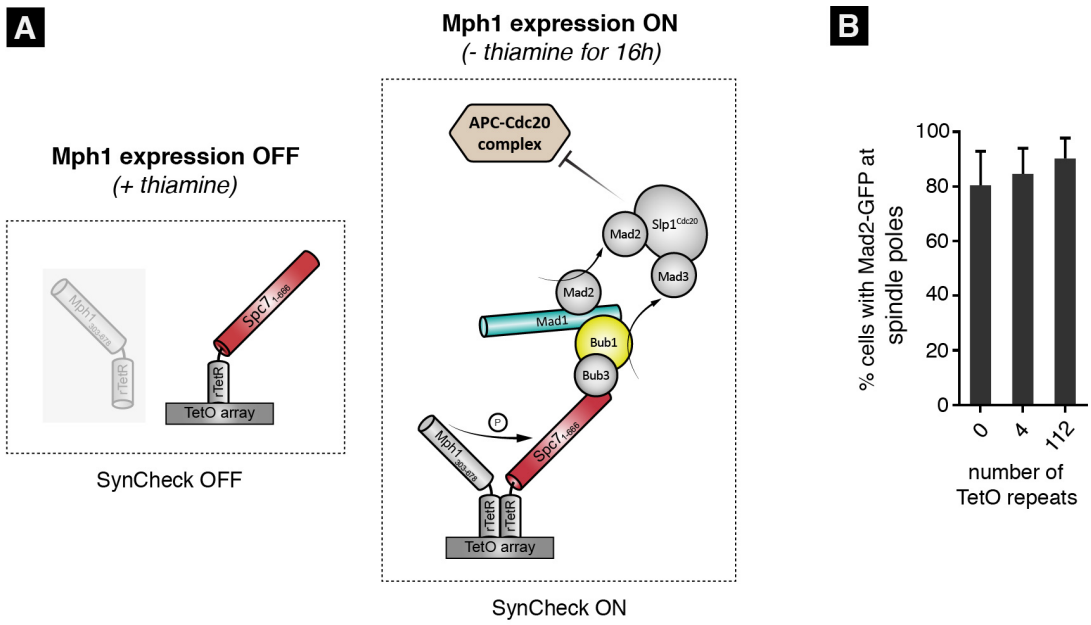

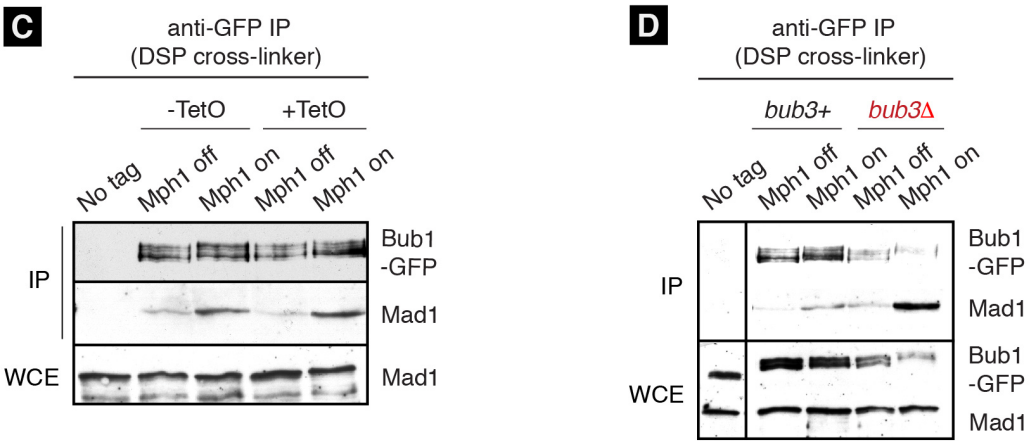

Fig. 5.1: Mad1 and Bub1 form a complex. (A) Schematic (adapted from Ioanna Leontiou) showing rTetR dependent SynCheck arrest driven by rTetR-Mph1$_{303-678}$ and rTetR-Spc7$_{1-666}$ interacting when rTetR-Mph1 is expressed (in the absence of thiamine). **(B)** Quantitation of SynCheck arrest comparing strains with 0, 4 and 112 TetO repeats following 16 hours of rTetR-mph1 expression. Live images were taken of samples which were scored for the presence of Mad2 at spindle pole bodies. This experiment was repeated 4 times. Data is plotted as mean +/- s.d. **(C)** Anti-GFP co-immunoprecipitation in cells +/- a TetO array harvested following a 16h induction of rTetR-mph1 expression and DSP crosslinking. Mad1 co-immunoprecipitates with Bub1-GFP in arrested cells in the presence and absence of a TetO array. Bub1-GFP was detected with an anti-GFP antibody and Mad1 with anti-Mad1. IP was repeated >3 times. **(D)** Anti-GFP co-immunoprecipitation in cells +/- bub3 harvested following a 12h induction of rTetR-Mph1 expression and DSP crosslinking. In the absence of Bub3, Mad1 co-immunoprecipitates with Bub1-GFP earlier - after 12 hours of Mph1 expression. Immunoprecipitated Bub1-GFP was detected with an anti-GFP antibody and the whole cell extract with anti-Bub1. Mad1 was detected as above.

yeast cells and detected Bub1 and Mad1 in the complex. In addition, it is supported by later work in HeLa cells showing a direct interaction between Bub1 and the C-terminus of Mad1 (Zhang et al., 2017).

It has been shown that Bub3 is not required for checkpoint activation in fission yeast (Tange and Niwa, 2008; Vanoosthuyse et al., 2009; Mora-Santos et al., 2016) and acts to prevent premature activation of the checkpoint by inhibiting ectopic activation of Bub1 (Yamagishi et al., 2012; Mora-Santos et al., 2016). This is supported by Yuan and colleagues (2017) who observed that SynCheck is still active in a *bub3Δ* background and that the Spc7-9TE and Mph1 SynCheck arrest occurred faster in the absence of *bub3,* where peak mitosis is reached after 12 hours of rTetR-Mph1 expression, 4 hours earlier. Thus implying that a lower threshold of rTetR-Mph1 kinase activity is required for rTetR-Spc7-9TE based SynCheck activation. Consistent with this, we find that the Mad1-Bub1 complex is detected earlier, after 12 hours of rTetR-Mph1 induction, in *bub3Δ* cells (Fig. **5.1 D)**, and Bub1 is likely hyperphosphorylated as the Bub1-GFP band appears to run slower through the polyacrylamide gel. Therefore, Mad1-Bub1 complex formation is not dependent on Bub3 in the SynCheck arrest.

The CD1 (**C**onserved **D**omain **1**) was first characterised in HeLa cells as a conserved Bub1 motif and has been identified as being essential for the checkpoint function of Bub1 in humans and yeast (Klebig et al., 2009; Heinrich et al., 2014; London and Biggins, 2014; Zhang et al., 2017). Mph1-mediated phosphorylation of CD1 is the proposed mechanism responsible for Mad1 kinetochore recruitment in yeast and humans (Brady and Hardwick, 2000; London and Biggins, 2014; Heinrich et al., 2014; Yuan et al., 2017; Zhang et al., 2017). We carried out an anti-flag co-IP after arresting cells using an ectopic SynCheck assay developed in our lab by Ioanna Leontiou where Spc7 was by-passed by co-recruiting rTetR-flag-Bub1 and rTetR-Mph1$_{303\text{-}678}$ (Fig. **5.2 A**; manuscript under revision). A Mad2:Mad1-Bub1 complex was found in arrested cells with full length *rTetR-flag-bub1* and *rTetR-flag-bub1-Δkinase* (residues 1-398; still containing CD1) when rTetR-Mph1 is expressed (Fig. **5.2 B**). Although there appears to be more Mad1 pulled down with full length Bub1 than *Δkinase*, the mitotic indices are similar. This is consistent with the ABA arrest described in chapter 3 where we also found that the absence of Bub1 kinase activity does not measurably impact mitotic index. However in *C. elegans,* which lacks a Bub1-CD1 domain (Zhang et al., 2017) and a *mps1* homologue, the Bub1 kinase domain is essential for its interaction with Mad1 (Moyle et al., 2014).

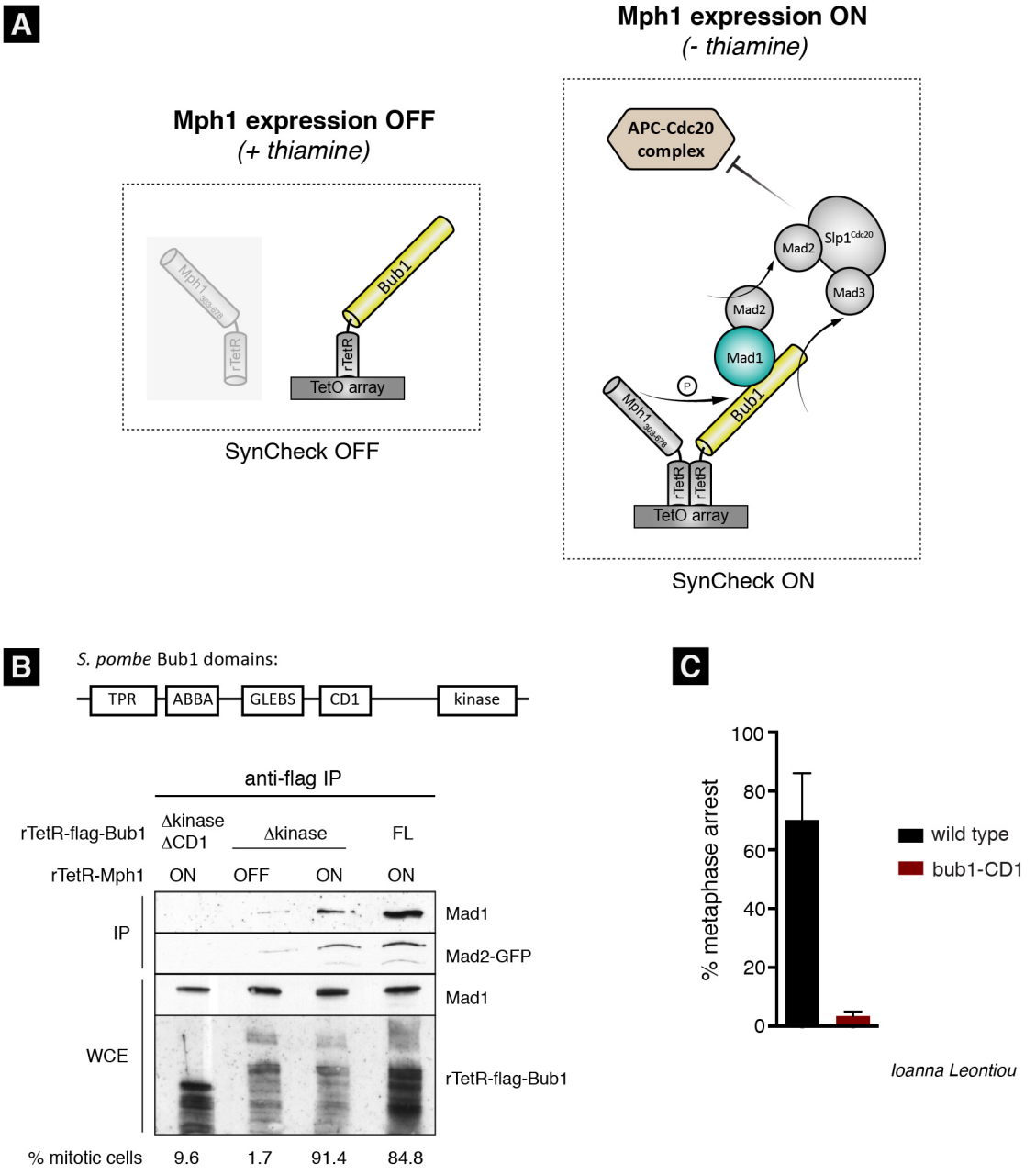

Fig 5.2: Bub1 Conserved Domain 1 is required for a Mad1-Bub1 interaction. (A) Depiction of rTetR dependent rTetR-Bub1 rTetR-Mph1303-678 SynCheck arrest, initiated by expression of rTetR-Mph1 (adapted from Ioanna Leontiou). **(B)** Anti-flag co-immunoprecipitation of cells containing rTetR-Mph1 and either rTetR-flag-Bub1 full length, Bub1 Δ-kinase or an N-terminal fragment of Bub1 consisting of the TPR, ABBA and GLEBS motif. Mad1 and Mad2 co-immunoprecipitate with rTetR-flag-Bub1 Δ-kinase and full length when rTetR-mph1 expression is induced for 16 hours. Bub1 was detected with an anti-flag antibody, Mad1 with anti-Mad1 and Mad2 with anti-GFP. IP was repeated 4 times. A schematic of *S. pombe* Bub1 domains is shown above. The % cells in mitosis (scored using Mad2-GFP at soindle poles as an indicator) from an independent time course are given below (at least 150 cells counted) **(C)** Graph showing that the mutating conserved domain 1 of Bub1 leads to a checkpoint null phenotype in a rTetR-Mph1 rTetR-Spc7 driven SynCheck arrest (following 16 hours of rTetR-Mph1 expression). This experiment was repeated 3 times (by Ioanna Leontiou). Data plotted as the mean +/- s.d.

We also found that the Mad2:Mad1-Bub1 complex is undetectable in cells co-recruiting an N-terminal fragment of Bub1 (residues 1-289; not containing the CD1 and the kinase domain) and rTetR-Mph1 (Fig. **5.2 B**). Consistently, we find that mutating conserved phosphosites to alanine in the CD1 (residues 380-398 in *S. pombe* Bub1) predicted to be necessary for Mad1 interaction (Heinrich et al., 2014), abrogates Spc7-Mph1 based SynCheck signalling (Fig. **5.2 C**; Yuan et al., 2017 Fig 4). Additionally, a recent HeLa cell study by-passed the need for CD1 by fusing a C-terminal fragment of Mad1 with an N-terminal fragment of Bub1 in which CD1 was deleted but still retained its Bub3 and Cdc20 binding motifs (Zhang et al., 2017). This suggests that the major function of CD1 is Mad1 recruitment.

Using a potent mitotic arrest and improved Co-IP protocol, we have discovered a Mad1-Bub1 interaction, mediated by Mph1-phosphorylation of CD1, in fission yeast. We have also found that this interaction is not dependent on Bub3, Spc7 or Bub1 kinase activity in an ectopic arrest. These results indicate that Bub1 is the kinetochore receptor for Mad1 in a manner dependent on Mph1 kinase and that this interaction is crucial for a mitotic delay.

5.3 Mutations at the very C-terminus of Mad1 impede the SAC

It has been proposed that Mad1 has an additional role in the checkpoint aside from recruiting Mad2 to kinetochores via an interaction with Bub1. In a fission yeast study by the Hauf laboratory, a Mad1 C-terminal mutant (E670 D673 D676) artificially tethered to kinetochores was found to be checkpoint null despite preserving Mad2 and Bub1 at kinetochores (Heinrich et al., 2014). In conjunction, the Nilsson lab found that human Mad1 C-terminal truncations were unable to activate the checkpoint despite Mad2 presence at kinetochores (Kruse et al., 2014). A more recent study from their lab found that human Mad1 C-terminal mutants (E710 F712 R714) were checkpoint defective despite Bub1 binding (Zhang et al., 2017). Studies from both groups implicate conserved residues exposed on the globular head at the very C-terminus of Mad1 in this additional function.

In light of these findings, I aimed to test the importance of the C-terminal region of Mad1 and attempt to uncover its additional function. 3 groups of Mad1 mutants based on phosphorylation data from mass spectrometry (carried out by Sjaak JA van der Sar, unpublished) and conserved putative phosphorylation sites were synthesised. 6 alanine mutations were made in the middle region of Mad1 — M6A, 8 mutations at the C-terminus (C8A), of which two sites (S633A, T634A) were used to make a double mutant C2A (see

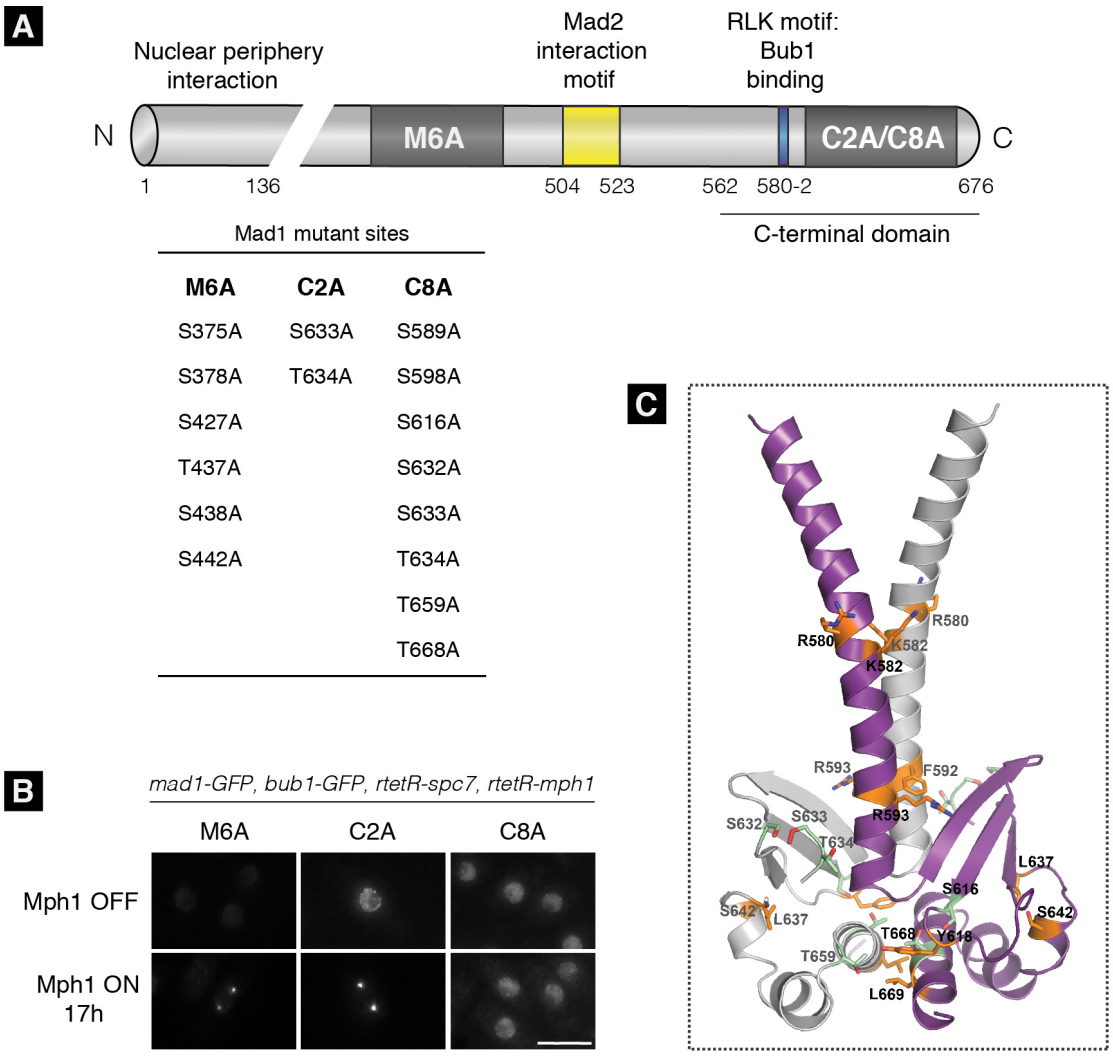

Figure 5.3: Mutations at the C-terminus of Mad1 impair the checkpoint. (A) Representation of Mad1 binding domains and M6A, C2A and C8A mutated residues. **(B)** Fluorescent microscopy images of cells after 17h of rTetR-mph1 induction was used to activate SynCheck. Cells with no rTetR-mph1 being expressed were used as controls. Mad1-GFP and Bub1-GFP accumulate at spindles poles in cells arrested in mitosis.The C8A mutant cells are unable to arrest in SynCheck, whereas C2A and M6A are unperturbed. Scale bar is 10 µm. **(C)** *S. pombe* Mad1 C-terminal domain (residues 562-676) homology model (made by Jeyaprakash Arulanandam) based on the human crystal structure published by *Kim S. and Sun H., 2012*. The C8A mutant residues and the RLK motif are labelled in green and mutations from Kim S. and Sun H., 2012 are shown in orange. **(D)** Alignment of *S. pombe* and *H. sapiens* C-terminal Mad1. The C8A mutant residues are highlighted in green and the RLK motif in blue.

Fig. **5.3 A**). Consistent with aforementioned studies, the C-terminal C8A mutant failed to arrest in a SynCheck arrest with rTetR-Spc7$_{1\text{-}666}$ (wild type) and rTetR-Mph1$_{303\text{-}678}$ (Fig. **5.3 B**). Figure **5.3 C and D** show the position of residues in the C8A mutant in green in a *S. pombe* homology model based on the human crystal structure of the Mad1 C-terminus (Kim et al., 2012), and a sequence alignment.

The C8A mutant was split into 4 groups depending on positioning to elucidate which region is responsible for the checkpoint defect and were constructed with an N-terminal flag tag for future biochemistry work. These new mutant strains contained Bub1-GFP and flag tagged Mad1 at its endogenous locus, under the control of its endogenous promoter. Upon testing these mutants on plates containing the microtubule poison benomyl, we found that the T659A T668A double alanine mutant at the very C-terminus of the protein conferred a checkpoint defect to a similar extent of the RLK<AAA mutant which is deficient in Bub1 binding and the *mad1Δ bub1-GFP* parent strain (Fig. **5.4 A**). These strains were then crossed into an *nda3-KM311* background where microtubules depolymerise at 18ºC. Consistently, the T659A T668A mutant was unable to activate a checkpoint response in the absence of microtubules (Fig. **5.4 B, C**).

To determine which, if either, of the double mutant residues is responsible for the checkpoint null phenotype, single alanine and glutamic acid mutations of T659 and T668 were made. We found that the T668A (**a**lanine) and E (glutamic acid) mutants were unable to grow on plates containing a low concentration benomyl, similar to the double mutant (Fig. **5.5 A**). In strains bearing the cold sensitive tubulin mutant *nda3-KM311*, where no kinetochore-microtubule attachments can be formed, T668E was unable to activate the SAC similarly to *mad1Δ*, the RLK mutant and the double T659A T668A mutant. Alternatively 55% of T668A cells were able to mount a checkpoint response, albeit to a lesser extent than wild type Mad1 and the T659 mutants where over 70% of cells were arrested after 6 hours at 18ºC (Fig. **5.5 B, C**). This confirms that the conserved T668 residue is important for the function of the C-terminus of Mad1.

We initially expected the phosphomimetic T668E mutant to reverse the SAC defect of T668A. We instead find that it impedes SAC function to a higher degree. It is possible that the E mutation is distorting the structure of the C-terminus and/or significantly reducing protein levels. We find that T668A cells are more sensitive to minor spindle perturbation brought on by a low dose of benomyl (5µg/ml), than a major disruption to kinetochore microtubule attachment caused by *nda3-KM311*. This could be due to increased redundancy

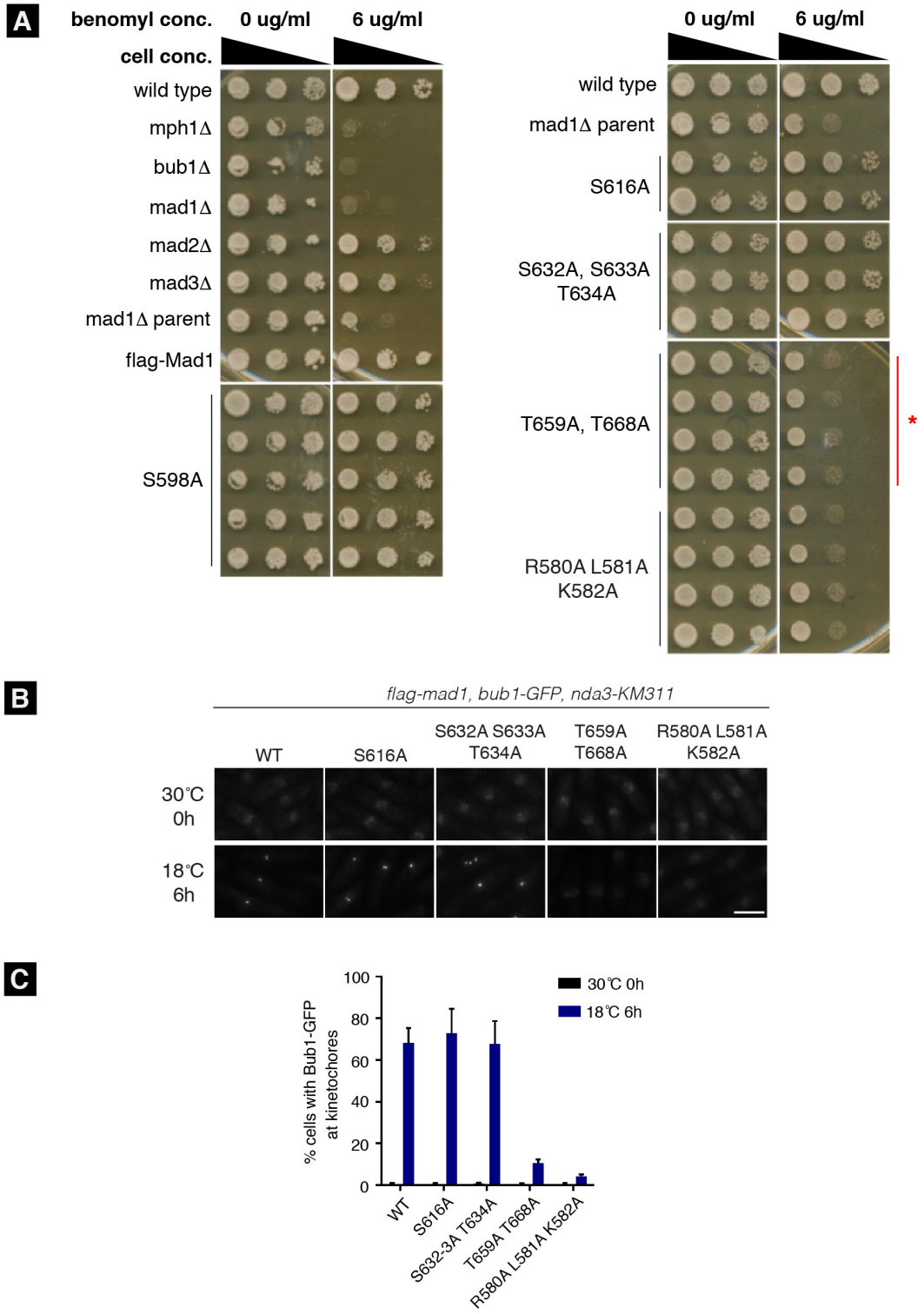

Figure 5.4: Mutations at the very C-terminus of Mad1 affect the SAC. (A) Serial dilutions of cells plated on rich growth medium contaning 0 µg/ul and 6 µg/ul of benomyl. The T659A T668A double mutant, marked in red, is benomyl sensitive. This was repeated 2 times. **(B)** Fluorescent microscopy images of cells containing Bub1-GFP. Cells were grown at 18°C for 6 hours to activate the cold-sensitive *nda3-KM311* arrest. Bub1-GFP localises to kinetochores in cells with a functional checkpoint. Scale bar is 10 µm. **(C)** Quantitation of *nda3-KM311* arrest shown in panel B. >200 cells were counted per strain in each condition. The experiment was repeated 2 times and plotted as the mean +/- s.d.

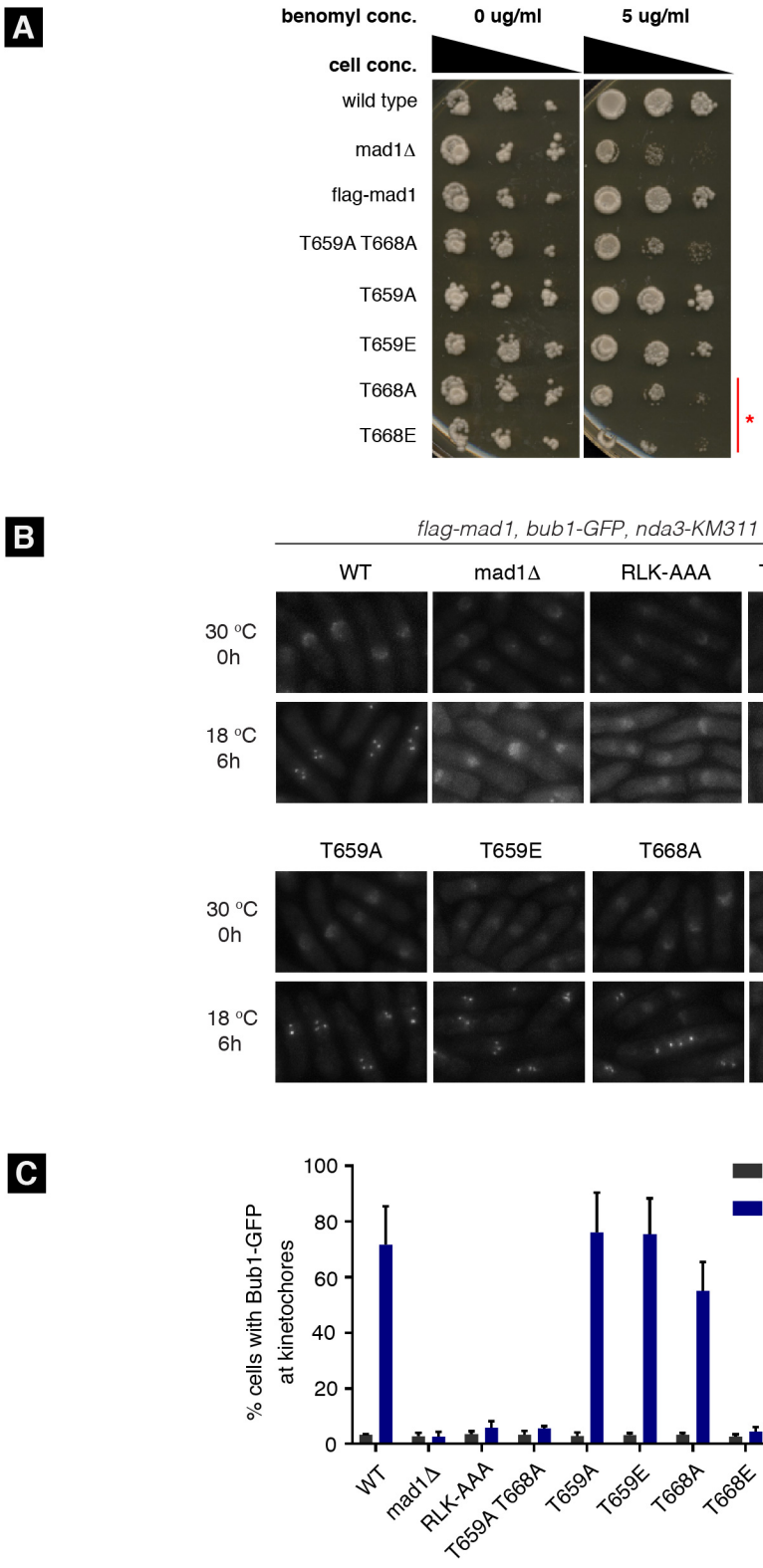

Figure 5.5: Mad1 T668 mutations impair SAC function. (A) Serial dilutions of cells plated on rich growth medium contaning 0 µg/ul and 5 µg/ul of benomyl. T668A and E, marked in red, are benomyl sensitive.This was repeated 3 times. **(B)** Fluorescent microscopy images of fixed cells containing Bub1-GFP. Cells were grown at 18°C for 6 hours to activate the cold-sensitive *nda3-KM311* mutation. Bub1-GFP localises to kinetochores in cells with a functional checkpoint. Scale bar is 10 µm. **(C)** Quantitation of panel B. >195 cells were analysed per strain in each condition. The experiment was repeated 3 times and plotted as the mean +/- s.d.

in C-terminal phosphorylation caused by 'stronger' upstream signalling generated by many unattached kinetochores. Despite the likelihood that the Mad1 C-terminal mutants are affecting a process occurring downstream of the Mad1-Bub1 interaction, a caveat of this *nda3* assay is that kinetochore recruitment of Bub1, a Mad1 interactor, was used as a read-out for an active checkpoint response. This *nda3-KM311* experiment could be performed in a strain using a marker such as cyclin B^{cdc13}-GFP in future.

While both T659 T668 residues are conserved, T659 was identified as a phosphorylated residue in *S. pombe* (Sjaak JA van der Sar, unpublished). Intriguingly, this residue has also been found to be phosphorylated in human Mad1 - residue S699 - following an *in vitro* Mps1 kinase assay. Notwithstanding that the sequence surrounding T659 (RK**T**) in *S. pombe* meets the Aurora B consensus site $[R/K]_{1-3}$-X-S/T (Meraldi et al., 2004; Ferrari et al., 2005). It is possible that there is redundancy in phosphorylation at the C-terminus of Mad1 and detecting multiple phosphorylation sites on the same peptide using mass spectrometry could be challenging.

Both T659 and T668 residues are present at the dimerisation interface of the protein, implying that phosphorylation in this region may cause the globular head region to come apart slightly and possibly facilitate a protein-protein interaction. Further phospho-mass spectrometry analysis comparing the different C-terminal mutants would provide useful insight into the phospho-regulation of Mad1.

As a side note, Kim and colleagues (2012) crystallised the C-terminal domain of human Mad1 and mutated buried hydrophobic residues. They found that these mutants were unable to homodimerise following *in vitro* co-translation and IP of differently tagged copies of Mad1 and displayed defective in kinetochore targeting. This suggests that disruptions to the Mad1 homodimer negatively impact the SAC response.

This still leaves the possibility for a subtle conformational change of the head driven by phosphorylation of surface residues, or those at the dimerisation interface when the SAC is active. Localised unfolding of the C-terminal globular head is technically difficult to capture using biochemistry. Our attempts to purify a C-terminal fragment (residues 559-676) of *S. pombe* wild type and mutant Mad1 from bacteria to confirm this and test dimerisation using native PAGE were unsuccessful due to protein purification issues. Troubleshooting this remains interesting work for the future.

In summary, a T668 mutant at the very C-terminus of Mad1, away from the Bub1 binding motif RLK and the **M**ad2 **i**nteraction **m**otif (MIM) confers a defective SAC response, suggesting a yet to be characterised role for the C-terminal globular head. At this stage we contend that it could aid an interaction with Mad2 or Bub1, or even mediate a novel Slp1 (Cdc20 in humans) interaction to facilitate MCC formation.

5.4 The C-terminus of Mad1 forms a complex with Slp1^{Cdc20}

To test whether the C-terminal mutations were affecting protein-protein interactions between Mad1 and other checkpoint proteins, we needed a method to harvest mitotic cells despite the mutants being SAC defective and unable to maintain a mitotic delay. For this reason, we used the microtubule depolymerising drug CBZ to capture cells in mitosis, as they have active Mph1 kinase, Bub1 at kinetochores and Slp1^{Cdc20} expression. In addition, a CBZ arrest tests the response of the T668 single mutant to minor spindle perturbations in liquid medium.

Cells were synchronised in G2 using a temperature sensitive *cdc25-22* block for 3.5 hours, and CBZ was added 20 minutes after release from the block to arrest cells (Fig. **5.6 A**). 30 minutes after CBZ addition, we find Mad3-GFP localised at kinetochores in 70% of cells with wild type Mad1. Comparatively in the T659A T668A double mutant and the T668A and T668E single mutants, approximately 45% of cells with Mad3-GFP at kinetochores (Fig. **5.6 B and C**). This went down to around 15% 60 minutes after CBZ addition. Therefore, Mad1 C-terminal mutants are less able to delay in mitosis. Despite this, this method allows us to harvest a larger population of mitotic cells than usual in these mutants.

An immunoblot (Mad1 has an N-terminal flag tag) revealed lower expression levels of C-terminal mutants, around 25% of that of wild type Mad1 (Fig. **5.6 D**). A follow-up co-IP in cycling cells found that Mad2 levels corresponded to that of Mad1. Although it is possible that the checkpoint defect of T668A is caused by low protein abundance, it is unlikely as this mutant is still able to mount a checkpoint arrest in *nda3-KM311* despite reduced levels. The Hauf lab determined that time spent in prometaphase following an *nda3-KM311* arrest is identical between strains with 30% and wild type levels of Mad1 (Heinrich et al., 2013). They found that a reduction to 10% severely affected but did not fully abrogate the checkpoint, making it likely that a ~25% abundance of Mad1 is sufficient for some checkpoint delays. An immunoblot using an anti-Mad1 antibody to compare flag-Mad1 to

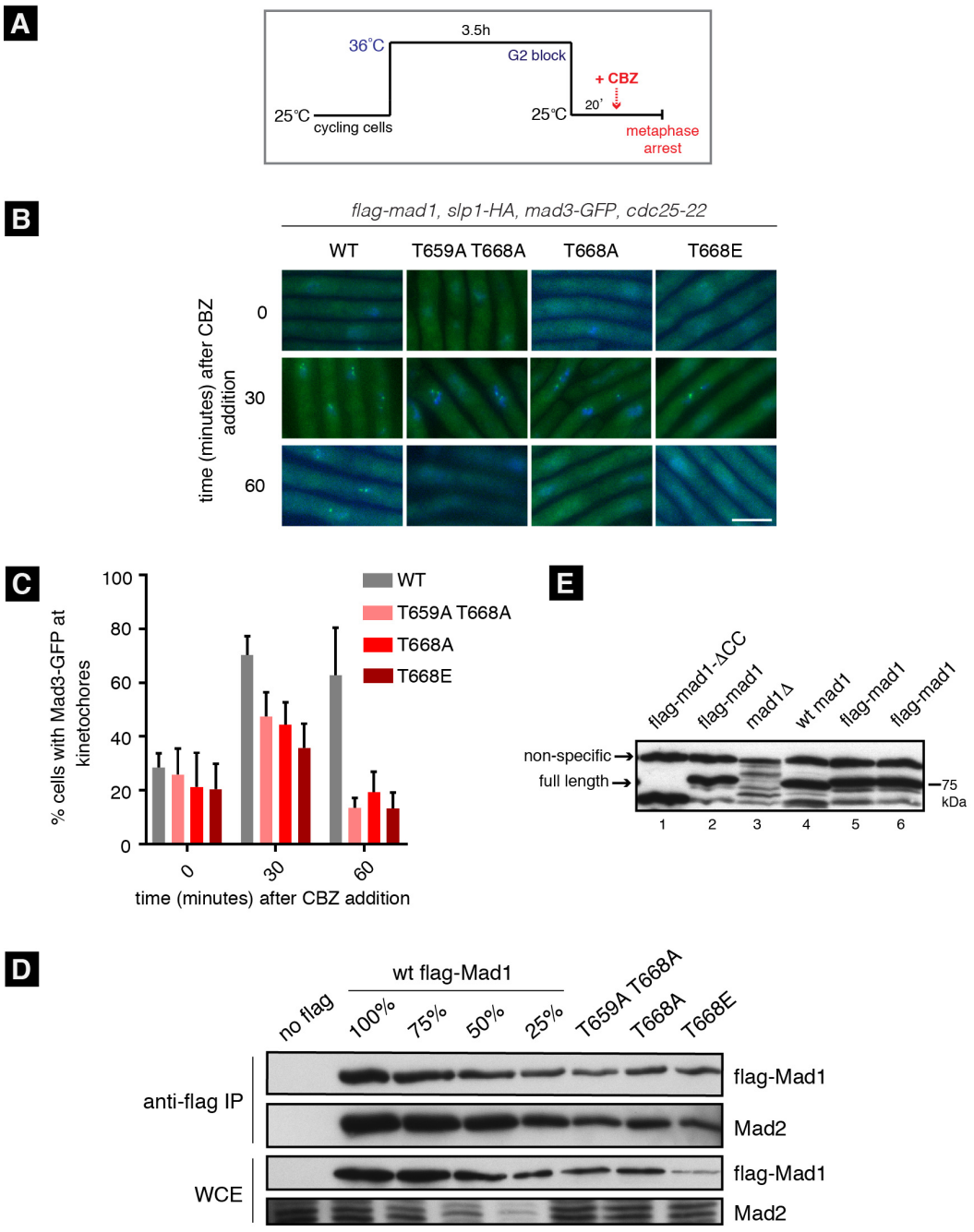

Figure 5.6: Mad1 mutants cannot sustain a carbendazim arrest. (A) Schematic showing experimental workflow of G2 block using the temperature sensitive *cdc25-22* mutation followed by addition of CBZ 20 minutes after release from the G2 block. **(B)** Flourescent microscopy images showing fixed cells with Mad3-GFP and DAPI staining. Cells were blocked in G2 and treated with CBZ (100 µg/ml final). In cells with wild type Mad1, Mad3 remains at kinetochores 60 minutes after CBZ is added. All of the mutants exit the mitotic block wthin 60 minutes. Scale bar is 10 µm. **(C)** Quantitation of panel B. >130 cells were analysed per strain at each time point. The mean of 3 experiments is plotted +/- s.d. **(D)** Immunoblots showing expression levels and a co-IP of wt and mutant Mad1 and corresponding levels of Mad2 in cycling cells. Dilutions of wt flag-Mad1 were loaded as a comparison with mutant Mad1 levels. Mad1 was detected with anti-flag antibody and Mad2 with anti-Mad2. **(E)** Western blot comparing expression levels of different isolates of full length flag-Mad1 (lanes 2,5,6) with flag-mad1ΔCC (lane 1), full length untagged mad1 (wild type, lane 4) and mad1Δ (lane 3). Blots were probed with anti-Mad1.

untagged Mad1 showed that protein levels were similar in the two, ruling out a negative impact of the N-terminal flag tag (Fig. **5.6 E**).

A flag co-IP comparing a cycling and CBZ arrested population found that wild type Mad1 associates with the MCC components Mad2, Slp1^{Cdc20} and Mad3, as well as Bub1 in an arrest (Fig. **5.7 A**). We find Bub1 harder to detect by this method, possibly due to the Bub1 antibody used for detection. Tagging Bub1 (with GFP for example) may make it more apparent. However, we are able to detect a Slp1-Mad1 complex from *in vivo* extracts for the first time. Previous attempts by our lab to capture this interaction may have been hindered by the use of C-terminal GFP and TAP tags which may have led to a subtle perturbation of function, making it difficult to capture Bub1 and Slp1^{Cdc20} binding. Where other work on Cdc20-Mad1 has been conducted *in vitro* (Ji et al., 2017), by using a small N-terminal flag tag and IP protocol we have been able to capture a Mad1-Slp1^{Cdc20} complex from *in vivo* extracts.

Slp1^{Cdc20} expression oscillates during the cell cycle with levels increasing upon mitotic onset and decreasing in late mitosis in an APC and 26S proteasome dependent manner (Yamada et al., 2000). Here, we find that Slp1^{Cdc20} levels are stabilised in cycling cells and attribute this to its HA tag. It is possible that Slp1^{Cdc20} persistence in cycling cells may also contribute to the presence of Mad3 in the complex. It is important to note that these cycling cells do not exhibit a checkpoint arrest — these cells were not synchronised in G2 or treated with CBZ and did not present Mad3-GFP at kinetochores. To supplement this finding, mass spectrometry analysis in these samples confirmed Mad2, Bub1 and Slp1^{Cdc20} peptides in complex with Mad1 in arrested cells, but not in cycling cells, re-affirming a Mad1-Slp1^{Cdc20} association in mitosis (Fig. **5.7 B**).

We find that T668A protein levels are close to 25% of wild type Mad1 and interestingly, this mutant displays relatively reduced Mad2 binding but increased Slp1^{Cdc20} binding in mitosis (Fig. **5.7 C**) while Bub1 levels remain unaffected. The same is true for the T659A T668A double mutant. In essence, the nature of Mad2 and Slp1^{Cdc20} binding to Mad1 is impacted when the very C-terminus of Mad1 is perturbed and as a result, cells cannot sustain a mitotic arrest. This implies a functional link between the C-terminus of Mad1, Mad2 and Slp1^{Cdc20}. It is possible that the C-terminus of Mad1 transiently interacts with Slp1^{Cdc20} to facilitate the formation of C-Mad2-Cdc20. We suggest that the single T668A and double A mutants inhibit localised ‘splaying’ of the C-terminal globular head and enable Mad1 to stably ‘capture’ Slp1, therefore perturbing the formation of C-Mad2-Slp1. As Mad1-C-Mad2

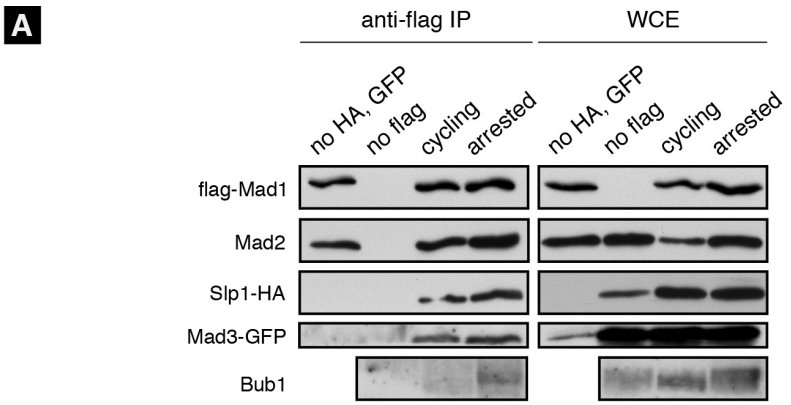

B

Protein	Unique peptides		Score	
	cycling	arrested	cycling	arrested
Mad1	33	82	323.31	323.31
Mad2	4	6	240.14	168.63
Slp1	-	6	-	80.374
Bub1	-	2	-	11.235
Mad3	-	-	-	-

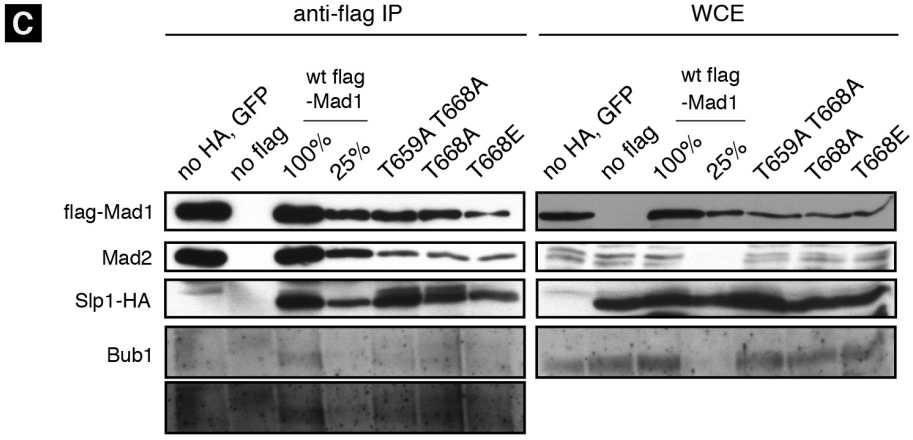

Figure 5.7: Mad1 co-immunoprecipitates with Slp1. (A) Anti-flag co-IP comparing a cycling and CBZ arrested population of cells. Arrested cells were harvested 30 minutes after addition of CBZ. A strain lacking a flag tag and another lacking both GFP and HA tags were used as negative controls, both were arrested with CBZ. In cycling cells, Mad1 co-immunoprecipitates with Mad2, Slp1 and Mad3. In arrested cells, Mad1 co-immunoprecipitates with Mad2, Slp1, Mad3 and Bub1. Mad1 was detected with an anti-flag anitbody, Mad2 with anti-Mad2, Slp1 with anti-HA, Mad3 with anti-GFP and Bub1 with anti-Bub1. **(B)** Table showing unique peptides of SAC proteins detected by mass spectrometry following a flag-Mad1 co-IP. Unique peptides refer to amino acid sequences that can only be found in a specific protein. A population of cycling cells was used as a control. The arrested sample was synchronised in G2 and treated with CBZ for 30 minutes before harvesting. The score is determined by comparing the theoretical (perfect) spectra from an *in silico* digestion to the actual spectra. A high score indicates that the peptide/protein identified is present in the complex.
(C) Anti-flag co-IP comparing CBZ arrested wild type and mutant Mad1 strains. A 25% dilution of wild type Mad1 was loaded for comparison of protein levels. Mutants show increased Slp1 binding and decreased Mad2 binding. 3 independent repeats of this CBZ arrest and co-IP were carried out.

is the site of Mph1-dependent conversion of O-Mad2 (**o**pen-**Mad2**) to C-Mad2 (**c**losed-**Mad2**) (described in Chapter 1 section 11; Mapelli and Musacchio, 2007; Luo and Yu, 2008), these results propose that the globular head dynamically binds Slp1 when phosphorylated in mitosis, bringing it in proximity to Mad1-bound Mad2 to facilitate C-Mad2-Slp1 formation.

Catalysis of the rate-limiting C-Mad2-Cdc20 interaction in human cells has been proposed to occur via phosphorylated Mad1 (Faesen et al., 2017). An *in vitro* reconstitution by the Musacchio group using FRET (**F**örster **r**esonance **e**nergy **t**ransfer) sensors on purified human SAC proteins to detect MCC production determined that the C-Mad2-Cdc20 interaction was catalysed by Mps1 phosphorylated Mad1-C-Mad2 (Faesen et al., 2017). This data is also in agreement with another *in vitro* reconstitution study which found that Mps1-mediated phosphorylation of human Mad1 at a C-terminal T716 residue following a kinase assay is implicated in binding to the N-terminus of $Cdc20^{Slp1}$ (residues 26-37) (Ji et al., 2017). As the T716 region does not match the consensus sequence of Mps1 substrates, it is likely that this region can bind Mps1 through tertiary contacts, although the possibility that it is phosphorylated by another kinase cannot be excluded (Ji et al., 2017).

To conclude, these results suggest that Mph1 phosphorylation of Spc7 MELT motifs enables Bub3-Bub1 binding to unattached kinetochores with phosphorylation of Bub1 recruiting Mad1-C-Mad2 via a CD1-RLK interaction. Successive phosphorylation of the very C-terminus of Mad1, most likely by Mph1 kinase, enables dynamic $Slp1^{Cdc20}$ binding proximal to the site of Mad2 conversion. This catalyses the formation of rate-limiting C-Mad2-Slp1, enabling subsequent MCC formation.

5.5 Perspectives and future work

Here we examined the checkpoint roles of Mad1 and found that Bub1 is the kinetochore receptor for Mad1 using co-IP following a SynCheck arrest. This interaction is dependent on Mph1 phosphorylation and Bub1-CD1, and independent of the Bub1 kinase domain and Bub3. Mad2 dependency is discussed in Chapter 6.

Using co-IP and mass spectrometry, we found that wild type Mad1 was able to form a complex with $Slp1^{Cdc20}$ in mitosis. This is the first indication of a Mad1-$Slp1^{Cdc20}$ complex *in vivo* and may relate to the additional, uncharacterised role of the Mad1 C-terminus. We find that mutating the very C-terminus of Mad1 at the homo-dimerisation interface of the

globular head affects its checkpoint function. A conserved C-terminal T668A mutation increased the levels of Slp1^{Cdc20} binding to Mad1 in mitosis. It is very likely that the inability to 'release' Slp1 from Mad1 perturbed the formation of diffusible C-Mad2-Slp1 and MCC by extension.

It was proposed that the Mad1 C-terminus 'folds back' onto itself, near the Mad2 interaction motif to possibly facilitate Mad1-C-Mad2 or O-Mad2-C-Mad2 binding (Sironi et al., 2002), although there is no evidence for the functional relevance. Unpublished cross-linking data of the Mad1-Mad2 tetramer from our lab (Sjaak JA van der Sar) supports the structural hypothesis of 'folding back' although it is not known what function, if any, this structural configuration supports. We propose that the 'folding back' of the C-terminus of Mad1 positions Slp1^{Cdc20} close to Mad2 to enable C-Mad2-Slp1 binding. This dependency can be tested by studying Slp1-C-Mad2 binding in predicted 'folding back' mutants. In addition, cross-linking co-IP could be performed with N-terminally flag tagged Mad1 to minimise changes to the C-terminus. The above cross-linking study (Sjaak JA van der Sar, unpublished) was done using a C-terminal Mad1-TAP tag which may have impacted its association with Slp1^{Cdc20} and Bub1. Albeit a technically challenging and ambitious undertaking in practice, further structural analysis would provide valuable insight into the conformational arrangement of Mad1 along with its binding partners Mad2, Bub1 and Slp1^{Cdc20}.

Therefore, we hypothesise that the additional role of the C-terminus of Mad1 in SAC activation is to facilitate formation of C-Mad2-Slp1 through a direct interaction with Slp1^{Cdc20}. We propose that in mitosis, the Mad1 C-terminal head is phosphorylated, causing subtle conformational change or 'splaying' of the globular head dimer. Slp1^{Cdc20} is able to transiently bind to this region where, as a result of 'folding back' it is brought in proximity to Mad1-associated C-Mad2 - the site of O-Mad2 conversion to C-Mad2. As a result, C-terminally phosphorylated Mad1 facilitates C-Mad2-Slp1 binding.

Future experiments to supplement these findings include:

1. Adding an extra copy of Mad1-T668A into the existing mutant strain to increase protein levels and assess whether this alters the checkpoint defect of this mutants. We expect it will not rescue the checkpoint defect due to the largely preserved SAC function of the mutant in an *nda3-KM311* arrest, observed effects on levels of binding partners (such as increased Slp1 abundance) in addition to results by the Hauf group suggesting that 30% of

Mad1 protein abundance maintains SAC ability in an *nda3-KM311* arrest (Heinrich et al., 2013). This can also be done with the T668E mutant where levels are lower and the checkpoint more severely abrogated. We find that interpretation of the phenotype of this mutant is marred by the low protein levels, which are suggestive of structural perturbation. It is possible that adding an extra copy to this strain may relieve the SAC defect.

2. We observe in our co-IPs that Slp1-HA is present in cycling cells and attribute this stabilisation to the HA tag which may hinder degradation of Slp1. Future co-IPs can be done using Slp1^{Cdc20} with an internal GFP tag that is present in a non-conserved N-terminal loop (made by Onur Sen and Ioanna Leontiou unpublished). This protein is recognised by western blotting although it is not detected using a fluorescent microscope in cycling cells as Slp1 turnover does not provide sufficient time for the GFP to mature.

3. Testing Slp1^{Cdc20} mutants required for the checkpoint and Mad1 binding by CBZ arrest followed by co-IP. In human Cdc20, the N-terminus (residues 26-37) is implicated in Mad1 binding (Ji et al., 2017).

4. It is not known whether the conserved Mad1 T668 residue is phosphorylated, and if so, by which kinase. It is likely that multiple residues in C-terminal region of Mad1 are phosphorylated and contribute to its SAC function. Attempts to determine this and gather additional phosphorylation data of mitotic Mad1 by mass spectrometry from *in vivo* samples have been unsuccessful. Phospho-mass spec can be optimised in the future. Phosphorylated Mad1 can be enriched for mass spectrometry from bacterial purification of Mad1, following an *in vitro* kinase assay comparing Mph1^{Mps1}, Ark1$^{Aurora\ B}$, Cdc2^{CDK1} and Plo1^{Plk1} samples. Albeit technically difficult, *in vitro* kinase assays can also be carried out on short C-terminal fragments of Mad1 and run on a native PAGE gel to indicate whether dimers comes apart or 'splay' upon phosphorylation.

5. It would be interesting to test Slp1^{Cdc20} binding in the T668A mutant during an *nda3-KM311* arrest as it is able to arrest to a large extent. This could be due to redundant phosphorylation at the C-terminus of Mad1 caused by higher Mph1 activity in a 'stronger' arrest where no kinetochore-microtubule attachments can form. To test whether this interaction is influenced by the attachment state of the kinetochore, Mad1 mutants and Mad1-Slp1 binding can be tested in an ectopic ABA arrest (described in Chapter 3) assay and co-IP in cells where microtubules remain intact.

The possible dependencies of Mad2 and Bub1 on the Mad1-Slp1 complex is discussed in Chapter 6.

CHAPTER 6

Final discussion

The spindle assembly checkpoint (SAC) is a conserved mechanism in eukaryotes that enables the correct segregation of chromosomes during anaphase. Upon incorrect kinetochore-microtubule attachment or lack of tension at kinetochores, SAC signalling is initiated at these kinetochores, inhibiting the APC/C through formation of the diffusible mitotic checkpoint complex. In this way, the SAC is able to delay anaphase onset until chromosomes are properly attached and biorientated.

6.1 Reconstituting SAC signalling using ABA-induced dimerisation

The first aim of this work was to reconstitute SAC activation and silencing ectopically using a novel chemically induced dimerisation (CID) tool in *S. pombe*. Chapter 3 demonstrated that abscisic acid (ABA) is an effective tool for co-recruiting proteins in *S. pombe*. Using ABA to form heterodimers of minimal fragments of Spc7 and Mph1, we were able to recapitulate upstream checkpoint signalling rapidly and independently of kinetochores and spindle pole body localisation. Similarly to the SynCheck arrest (Yuan et al., 2017), this co-recruitment was sufficient to trigger SAC signalling, suggesting that kinetochores act as scaffolds for coupling attachment defects with checkpoint signalling. It would be interesting to test the effects of other mitotic kinases on the ectopic arrest using the ATP-analogue sensitive drug 1NMPP1 to regulate Aurora B^{Ark1} and Plk1^{Plo1} activity. This would resolve the functions of these kinases in error correction and SAC signalling. The Joglekar lab used rapamycin to dimerise Plk1 with KNL1^{Spc7} MELT motifs in HeLa cells and found that mitotic duration was not prolonged despite MELT phosphorylation (Chen et al., 2019). This emphasises the importance of Mps1 phosphorylation for SAC signalling downstream of the initial trigger. An ABA-dependent Plk-Spc7 and Aurora B-Spc7 arrest could also be tested in *S. pombe* although we predict it is unlikely to result in a mitotic delay.

Using an ABA-induced arrest to test whether Mph1 and Bub1 heterodimers can bypass Spc7 in the same way as in the rTetR system (explained in chapter 5) found that 60% of cells in a given population can arrest transiently (for approximately 30 minutes) (Ioanna Leontiou, manuscript under revision). This emphasises the role of Spc7 MELTs in amplifying the checkpoint signal for a robust arrest. Reducing the number of Spc7 MELTs in the Mph1-

Spc7 ABA arrest would be interesting future work. One would expect that dimerising 1-2 MELT motifs with Mph1 would mimic the Bub1-Mph1 arrest behaviour if signal amplification was the difference. In addition, it is possible that the ability of Bub1 (and or Mph1) to homodimerise contributed to signal amplification in the Bub1-Mph1 rTetR arrest, although differing protein levels could also be the cause.

A major advantage of the ABA-induced checkpoint is the ability to reverse dimerisation and capture SAC silencing. This novel silencing assay confirmed that silencing is mediated by PP1 localisation to Spc7 and Kinesin-8. This method induces silencing without affecting with kinetochore-microtubule attachments, as is the case with *nda3-KM311*, CBZ and nocodazole assays, therefore separating the events of biorientation and error correction from the SAC signalling pathway. Reversal is not possible in SynCheck rTetR or the widely used rapamycin system. Less is known about how the SAC is silencing compared to its activation. In future, this silencing assay can be used to test regulators of PP1 and other potential silencing candidates such as Bub3 (Vanoosthuyse et al., 2009) and PP2A (Schmitz et al., 2010; Espert et al., 2014) to further understand the SAC silencing pathway.

The ABA-induced signalling method provides a more controllable method of inducing SAC signalling *in vivo* than the existing SynCheck rTetR-based system used by our lab (Yuan et al., 2017). While the rTetR system is effective at generating an ectopic arrest, ABA-induced dimerisation has significantly improved the time frame to achieve peak mitosis from a 14-16 hour transcriptional induction in the rTetR system to 30 minutes in ABA (in cells pre-synchronised in G2). Expression of rTetR-mph1 at the *nmt* promoter for SynCheck induction can be leaky, which can add complications to strain construction. Whereas with ABA, the desired response can be modulated by varying the concentration of drug used or the number of spc7 MELT motifs dimerised with mph1 in this case. A limitation to the rTetR system is that since rTetR forms homodimers, one cannot be certain that the resulting phenotype is a result of a 1:1 ratio of heterodimers, or a combination of hetero- and homo-dimers. As ABA generates heterodimers of PYL and ABI, it is more likely to cause 1:1 binding, unless the protein of interest itself exists as a dimer.

There is limited cross-reactivity with endogenous proteins in the plant-based ABA system. This is particularly important for *S. pombe,* where the *fkh1Δ*, *tor1-S1834E* mutant background required for rapamycin sensitivity has been found to increase stress and reduce mating efficiency. It is also promising as an anchor away technique and can be used in conjunction with other CID systems to allow control of multiple cell circuits. For example,

rapidly and reversibly depleting an essential protein from its subcellular location to study its effect on a particular process which is under the control of another CID. This avoids the need for deleting genes or altering their expression levels.

6.2 How do cells respond to a prolonged mitotic block?

Chapter 4 follows on to study the effects of prolonged ectopic checkpoint activation in *S. pombe* and HeLa cells. We observe that cell viability in fission yeast decreases in a prolonged metaphase arrest due to loss of temporal coordination between septation and nuclear division. This is consistent with findings from APC mutants where septation occurs before nuclear division. They found that this occurred due to a decrease in Cyclin B^{cdc13} levels while $Securin^{cut2}$ levels remained stable (Chang et al., 2001). Similar to our studies, they also found cell death to occur in these prematurely septated cells. This suggests that septation ensues before nuclear division due to gradual degradation of Cyclin B in a prolonged ABA arrest which results in lower $CDK1^{cdc2}$ activity and SIN activation. This hypothesis can be tested in future experiments by i) monitoring Cyclin B levels in a prolonged arrest using microscopy and quantitative western blotting - is there a decrease prior to septation? ii) using a non-destructible $Cdc13^{cyclin\ B}$ D-box mutant and iii) a SIN null mutant. Therefore, we propose that in a prolonged arrest, Cyclin B^{cdc13} levels decrease (due to limited SAC protein abundance) to a threshold which allows septation while the cell is able to remain 'arrested'. We suggest this occurs as the ABA-generated arrest is independent of $CDK1^{cdc2}$ once cells have entered mitosis. This can be tested using the CDK1as allele.

Using single cell analysis in HeLa cells we found variation in cell fate within and between populations treated with either the anti-microtubule drug nocodazole or rapamycin (for ectopic activation of the checkpoint (eSAC) through KNL1-Mps1 dimers) (Chen et al., 2019). Intra population differences in mitotic duration in eSAC most likely to arise due to varying Mps1 expression levels, which in turn affects the level of MCC formation. We observed that the severe defects in cytokinesis and aneuploidy likely trigger apoptosis sooner in nocodazole treated cells. Comparatively, in rapamycin treated cells, cytokinesis defects were not as apparent and cells took longer to undergo apoptosis. This suggests that severe aneuploidy increases the likelihood of apoptosis.

A link between mitotic duration and timing of apoptosis onset following mitotic exit (or slippage) emerged from our single cell analysis. Broadly, cells that arrested in mitosis for longer died sooner following mitotic slippage than those that arrested for a short duration.

Mitotic-linked death in interphase could occur as mitotic slippage gradually releases the inhibitory CDK1-mediated phosphorylation of pro-apoptotic Caspase-9. An additional link is that apoptotic regulating genes such as Mcl1 are involved in pathways which are regulated by CDK1 and APC/C. Future experiments include quantifying eSAC activator and cyclin B levels in these cells and comparing these with mitotic duration and time of apoptosis. This could be possible using a similar MATLAB program to that developed by Chen and colleagues (2019) to quantify fluorescence of cyclin B as well as eSAC components. This would allow clearer correlations between these variables.

Single cell analyses conducted here and by others demonstrate the complexity and variation within and between cell lines, drugs used and drug concentrations. Cell culture studies have important implications in understanding the variability in cancer cell response to anti-mitotic drugs. Understanding the molecular links between the SAC and apoptosis would provide valuable insight into the basis of variation observed in cell culture as well as in complex living systems. While investigating the molecular link is beyond the scope of this study, we suggest that ABA-dependent regulation of mitosis provides a useful tool for tight regulation of mitosis timing, 'strength' of checkpoint, as well as mitotic exit. Therefore enabling a more direct study of how the SAC and mitosis affect apoptosis as well as more accurate indicators of how cells may react to different types and concentrations of anti-mitotic drugs.

These 2 chapters employed novel, ectopic methods for regulation of the spindle assembly checkpoint in space and time. They illustrated results from its direct implementation to studying SAC signalling as well as discussed its broader applications.

6.3 Contribution of the Mad1 C-terminus to SAC signalling

Chapter 5 aimed to uncover the kinetochore receptor for Mad1 as well as identify the additional role of its C-terminus. Co-immunoprecipitation following a SynCheck rTetR arrest revealed that Bub1-CD1 is the kinetochore receptor of Mad1 in *S. pombe*, similar to budding yeast and later confirmed in mammalian cells. We find that this interaction is crucial for the fission yeast checkpoint function and is dependent on Mph1 phosphorylation of Bub1. It is independent of the kinase domain of Bub1, and Bub3.

Unsurprisingly, as Mad2 is a stable binder of Mad1, we find that Mad2 co-IPs with Bub1 and Mad1. It has been demonstrated that the Mad1-Bub1 interaction is dependent on Mad2

in budding yeast *in vivo* and *in vitro* (Brady and Hardwick, 2000; London and Biggins, 2014), although this may not be conserved as there are indications that it is not required in human cells (Hewitt et al., 2010; Kim et al., 2012; Ji et al., 2017). Testing the Mad2 dependency for the Mad1-Bub1 binding in *S. pombe* could be conducted in future by performing a Bub1-GFP and/or flag-Mad1 co-IP in *mad2Δ* cells captured in mitosis using the *cdc25-22* CBZ arrest assay described in Chapter 5 section 4.

To test the additional function of the Mad1 C-terminus, we mutated putative phosphorylation sites and conserved sites at the C-terminus and found that mutating the very C-terminus of Mad1 disrupts the checkpoint response. A conserved T668A mutation present at the dimerisation interface of the C-terminal globular head region, caused sensitivity to minor spindle perturbation induced by benomyl and CBZ.

Co-IP and mass spec revealed that Mad1 co-immunoprecipates with Slp1^{Cdc20}, Mad2 and Bub1, providing the first indication of a Mad1-Slp1^{Cdc20} complex *in vivo*. To our surprise, we found that more Slp1 associates with Mad1 T668A in the IP from CBZ arrested cells, despite lower expression levels of the mutant. We suggest that the T668A mutant abrogates the SAC as it is unable to 'release' Slp1^{Cdc20}, impeding C-Mad2-Slp1 binding. We hypothesise that the C-terminal globular head of Mad1 undergoes subtle splaying upon checkpoint activation, possibly as a result of phosphorylation, which enables dynamic Slp1^{Cdc20} association. This positions Slp1 close to Mad2, facilitating C-Mad2-Slp1^{Cdc20} formation.

To dissect the dependencies of the Mad1-Slp1 complex, the following are suggested:

- The co-IP in Figure 5.7 C suggests that in an arrest, Mad2 levels in the alanine mutants are disproportionately lower than Mad1. This is at odds with Mad1-Mad2 levels in a cycling population of these mutants 5.6 C where levels of Mad2 seem proportional to wild type Mad1 at approximately 25%. The reduction of Mad2 could be a consequence of stabilised Slp1 binding to Mad1 which could spatially perturb Mad2 binding. Careful assessment of Mad2 levels in these mutants during an arrest is important future work, as chemiluminescence is indicative and does not provide quantitative comparisons. To improve accuracy when comparing protein levels in the IPs, quantitative western blots with a LI-COR could be used as an alternative to chemiluminescence. Although not strongly supported by this work, we cannot exclude the possibility that Slp1 binds to Mad1 via Mad2. To test whether Mad1-Slp1 binding is dependent on the presence of Mad2, co-IP can be carried out in a *mad2Δ* background. Additionally, to test whether it is dependent on

Mad2 dimerisation (C-Mad2-O-Mad2), the co-IP can be performed in a Mad2 αC region mutants, such as *mad2*^{R133A}, which are unable to dimerise and abrogate the SAC (DeAntoni et al, 2005; Mapelli et al., 2006, Sironi et al., 2001).

- *In vitro* reconstitution studies have reported that Bub1-Bub3, along with Mad1-Mad2 contribute to the formation of C-Mad2-Cdc20 (Faesen et al., 2017). Additionally they found that MCC formation in a Mad1 triple mutant (at the very C-terminus) was completely abrogated in the absence of Bub1. This suggests a requirement for Bub1 in Mad2-Cdc20 formation. This need could arise as the Bub1-ABBA and, to a lesser extent, its KEN motif have been found to be a key recruiter of Cdc20 to the kinetochore (Lischetti et al., 2014; Di Fiore et al., 2015; Vleugel et al., 2015). The BubR1-ABBA motif can also recruit Cdc20 but redundancy with Bub1-ABBA could make it less crucial. Nevertheless, whether Bub1-ABBA motif is the key receptor for Slp1 has not been determined in *S. pombe*. Due to the labile interaction between Mad1 and Slp1 (previous efforts to detect this complex were unsuccessful), it is not obvious that Mad1 is the principle kinetochore receptor of Slp1, although the possibility exists. However, to test the requirement of Bub1 on the Mad1-Slp1 complex, co-IPs could be conducted in *mad1-RLK* and *bub1-CD1* mutants which hinder the Mad1-Bub1 interaction.

In conclusion, our predicted model (Fig. **6.1**) for the additional function of Mad1 in the SAC is as follows. The Mad1 C-terminus, which folds back over the Mad1-C-Mad2 tetramer, is able to bind C-Mad2 throughout the cell cycle via its MIM (Mad2 interacting motif). In mitosis, Mad1-C-Mad2 is recruited to kinetochores via a Mph1-dependent interaction between the Mad1-RLK motif and Bub1-CD1. Additional phosphorylation at the dimerisation interface of the C-terminal globular head domain of Mad1 by Mph1 kinase causes subtle splaying of the head. This spatial rearrangement reveals a charged surface (due to phosphorylation) on Mad1 that dynamically interacts with Slp1. Thus bringing Slp1 close to the MIM and in proximity to the site of Mad2 conversion, enabling formation of C-Mad2-Slp1.

Figure 6.1: SAC roles of the Mad1 C-terminus

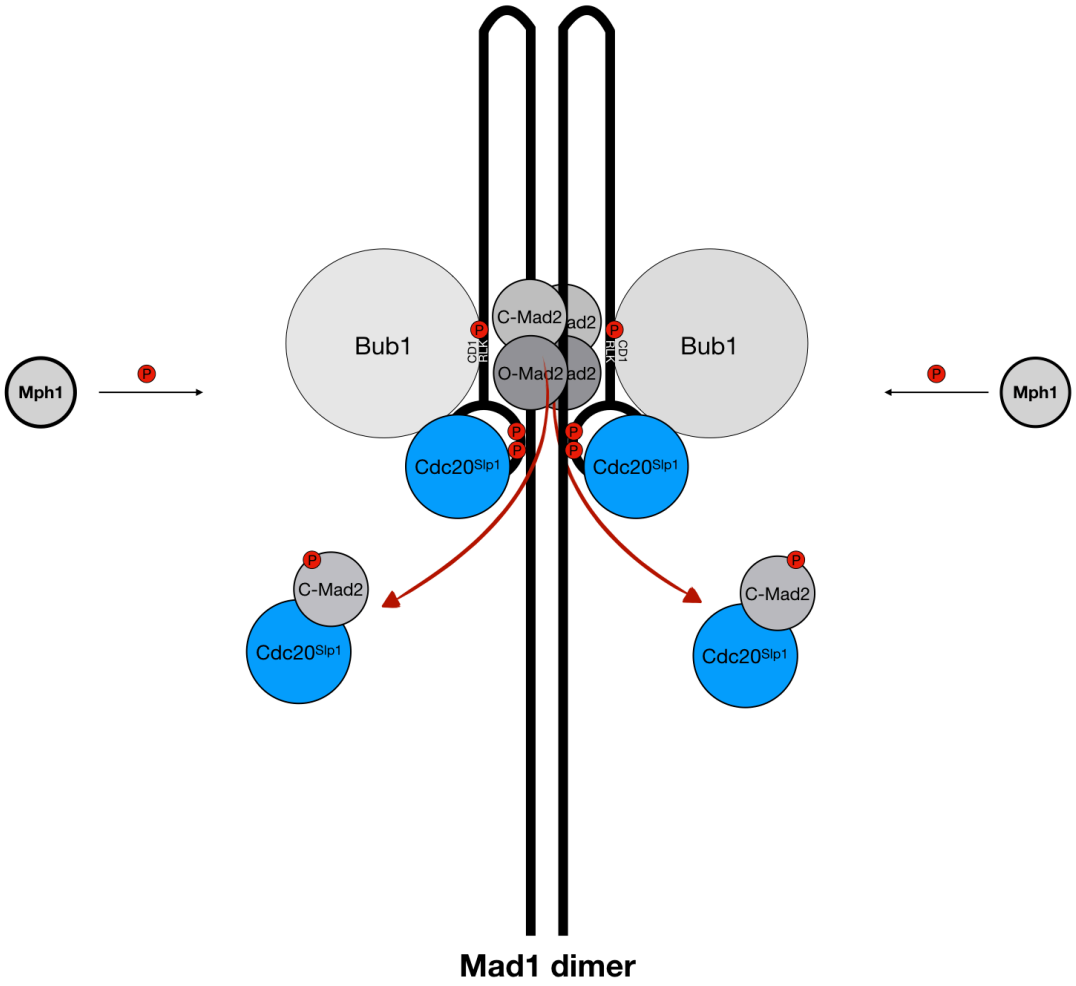

Bibliography

Akera, T., Goto, Y., Sato, M., Yamamoto, M., & Watanabe, Y. (2015). Mad1 promotes chromosome congression by anchoring a kinesin motor to the kinetochore. Nat Cell Biol, 17(9), 1124-1133. doi:10.1038/ncb3219

Alfieri, C., Chang, L., Zhang, Z., Yang, J., Maslen, S., Skehel, M., & Barford, D. (2016). Molecular basis of APC/C regulation by the spindle assembly checkpoint. Nature, 536(7617), 431-436. doi:10.1038/nature19083

Alfonso-Perez, T., Hayward, D., Holder, J., Gruneberg, U., & Barr, F. A. (2019). MAD1-dependent recruitment of CDK1-CCNB1 to kinetochores promotes spindle checkpoint signaling. J Cell Biol, 218(4), 1108-1117. doi:10.1083/jcb.201808015

Allan, L. A., & Clarke, P. R. (2007). Phosphorylation of caspase-9 by CDK1/cyclin B1 protects mitotic cells against apoptosis. Mol Cell, 26(2), 301-310. doi:10.1016/j.molcel.2007.03.019

Amaral, N., Vendrell, A., Funaya, C., Idrissi, F. Z., Maier, M., Kumar, A., . . . Mendoza, M. (2016). The Aurora-B-dependent NoCut checkpoint prevents damage of anaphase bridges after DNA replication stress. Nat Cell Biol, 18(5), 516-526. doi:10.1038/ncb3343

Amin, P., Soper Ni Chafraidh, S., Leontiou, I., & Hardwick, K. G. (2018). Regulated reconstitution of spindle checkpoint arrest and silencing through chemically induced dimerisation *in vivo*. J Cell Sci, 132(4). doi:10.1242/jcs.219766

Amor, D. J., Bentley, K., Ryan, J., Perry, J., Wong, L., Slater, H., & Choo, K. H. (2004). Human centromere repositioning "in progress". Proc Natl Acad Sci U S A, 101(17), 6542-6547. doi:10.1073/pnas.0308637101

Aravamudhan, P., Goldfarb, A. A., & Joglekar, A. P. (2015). The kinetochore encodes a mechanical switch to disrupt spindle assembly checkpoint signalling. Nat Cell Biol, 17(7), 868-879. doi:10.1038/ncb3179

Bahler, J., Wu, J. Q., Longtine, M. S., Shah, N. G., McKenzie, A., 3rd, Steever, A. B., . . . Pringle, J. R. (1998). Heterologous modules for efficient and versatile PCR-based gene targeting in Schizosaccharomyces pombe. Yeast, 14(10), 943-951. doi:10.1002/(SICI)1097-0061(199807)14:10<943::AID-YEA292>3.0.CO;2-Y

Ballister, E. R., Riegman, M., & Lampson, M. A. (2014). Recruitment of Mad1 to metaphase kinetochores is sufficient to reactivate the mitotic checkpoint. J Cell Biol, 204(6), 901-908. doi:10.1083/jcb.201311113

Banaszynski, L. A., Liu, C. W., & Wandless, T. J. (2005). Characterization of the FKBP.rapamycin.FRB ternary complex. J Am Chem Soc, 127(13), 4715-4721. doi:10.1021/ja043277y

Barisic, M., Sohm, B., Mikolcevic, P., Wandke, C., Rauch, V., Ringer, T., . . . Geley, S. (2010). Spindly/CCDC99 is required for efficient chromosome congression and mitotic checkpoint regulation. Mol Biol Cell, 21(12), 1968-1981. doi:10.1091/mbc.E09-04-0356

Brady, D. M., & Hardwick, K. G. (2000). Complex formation between Mad1p, Bub1p and Bub3p is crucial for spindle checkpoint function. Curr Biol, 10(11), 675-678.

Brito, D. A., Yang, Z., & Rieder, C. L. (2008). Microtubules do not promote mitotic slippage when the spindle assembly checkpoint cannot be satisfied. J Cell Biol, 182(4), 623-629. doi:10.1083/jcb.200805072

Burton, J. L., & Solomon, M. J. (2007). Mad3p, a pseudosubstrate inhibitor of APCCdc20 in the spindle assembly checkpoint. Genes Dev, 21(6), 655-667. doi:10.1101/gad.1511107

Cairo, L. V., Ptak, C., & Wozniak, R. W. (2013). Mitosis-specific regulation of nuclear transport by the spindle assembly checkpoint protein Mad1p. Mol Cell, 49(1), 109-120. doi:10.1016/j.molcel.2012.10.017

Camasses, A., Bogdanova, A., Shevchenko, A., & Zachariae, W. (2003). The CCT chaperonin promotes activation of the anaphase-promoting complex through the generation of functional Cdc20. Mol Cell, 12(1), 87-100.

Campbell, C. S., & Desai, A. (2013). Tension sensing by Aurora B kinase is independent of survivin-based centromere localization. Nature, 497(7447), 118.

Carmena, M., Wheelock, M., Funabiki, H., & Earnshaw, W. C. (2012). The chromosomal passenger complex (CPC): from easy rider to the godfather of mitosis. Nat Rev Mol Cell Biol, 13(12), 789-803. doi:10.1038/nrm3474

Chanclud, E., & Morel, J. B. (2016). Plant hormones: a fungal point of view. Mol Plant Pathol, 17(8), 1289-1297. doi:10.1111/mpp.12393

Chang, F., Woollard, A., & Nurse, P. (1996). Isolation and characterization of fission yeast mutants defective in the assembly and placement of the contractile actin ring. J Cell Sci, 109 (Pt 1), 131-142.

Chang, L., Morrell, J. L., Feoktistova, A., & Gould, K. L. (2001). Study of cyclin proteolysis in anaphase-promoting complex (APC) mutant cells reveals the requirement for APC function in the final steps of the fission yeast septation initiation network. Mol Cell Biol, 21(19), 6681-6694.

Chao, W. C., Kulkarni, K., Zhang, Z., Kong, E. H., & Barford, D. (2012). Structure of the mitotic checkpoint complex. Nature, 484(7393), 208-213. doi:10.1038/nature10896

Cheeseman, I. M., Chappie, J. S., Wilson-Kubalek, E. M., & Desai, A. (2006). The conserved KMN network constitutes the core microtubule-binding site of the kinetochore. Cell, 127(5), 983-997. doi:10.1016/j.cell.2006.09.039

Cheeseman, I. M., & Desai, A. (2008). Molecular architecture of the kinetochore-microtubule interface. Nat Rev Mol Cell Biol, 9(1), 33-46. doi:10.1038/nrm2310

Chen, C., Whitney, I. P., Banerjee, A., Sacristan, C., Sekhri, P., Kern, D. M., . . . Joglekar, A. P. (2019). Ectopic Activation of the Spindle Assembly Checkpoint Signaling Cascade Reveals Its Biochemical Design. Curr Biol, 29(1), 104-119 e110. doi:10.1016/j.cub.2018.11.054

Chen, R. H., Brady, D. M., Smith, D., Murray, A. W., & Hardwick, K. G. (1999). The spindle checkpoint of budding yeast depends on a tight complex between the Mad1 and Mad2 proteins. Mol Biol Cell, 10(8), 2607-2618. doi:10.1091/mbc.10.8.2607

Ciferri, C., Pasqualato, S., Screpanti, E., Varetti, G., Santaguida, S., Dos Reis, G., . . . Musacchio, A. (2008). Implications for kinetochore-microtubule attachment from the structure of an engineered Ndc80 complex. Cell, 133(3), 427-439. doi:10.1016/j.cell.2008.03.020

Clute, P., & Pines, J. (1999). Temporal and spatial control of cyclin B1 destruction in metaphase. Nat Cell Biol, 1(2), 82-87. doi:10.1038/10049

Collin, P., Nashchekina, O., Walker, R., & Pines, J. (2013). The spindle assembly checkpoint works like a rheostat rather than a toggle switch. Nat Cell Biol, 15(11), 1378-1385. doi:10.1038/ncb2855

Coudreuse, D., & Nurse, P. (2010). Driving the cell cycle with a minimal CDK control network. Nature, 468(7327), 1074-1079. doi:10.1038/nature09543

Currie, C. E., Mora-Santos, M., Smith, C. A., McAinsh, A. D., & Millar, J. B. A. (2018). Bub1 is not essential for the checkpoint response to unattached kinetochores in diploid human cells. Curr Biol, 28(17), R929-R930. doi:10.1016/j.cub.2018.07.040

Davenport, J., Harris, L. D., & Goorha, R. (2006). Spindle checkpoint function requires Mad2-dependent Cdc20 binding to the Mad3 homology domain of BubR1. Exp Cell Res, 312(10), 1831-1842. doi:10.1016/j.yexcr.2006.02.018

De Virgilio, C., & Loewith, R. (2006). The TOR signalling network from yeast to man. Int J Biochem Cell Biol, 38(9), 1476-1481. doi:10.1016/j.biocel.2006.02.013

DeAntoni, A., Sala, V., & Musacchio, A. (2005). Explaining the oligomerization properties of the spindle assembly checkpoint protein Mad2. Philos Trans R Soc Lond B Biol Sci, 360(1455), 637-647, discussion 447-638. doi:10.1098/rstb.2004.1618

DeLuca, J. G., Gall, W. E., Ciferri, C., Cimini, D., Musacchio, A., & Salmon, E. D. (2006). Kinetochore microtubule dynamics and attachment stability are regulated by Hec1. Cell, 127(5), 969-982. doi:10.1016/j.cell.2006.09.047

Desai, A., Rybina, S., Muller-Reichert, T., Shevchenko, A., Shevchenko, A., Hyman, A., & Oegema, K. (2003). KNL-1 directs assembly of the microtubule-binding interface of the kinetochore in C. elegans. Genes Dev, 17(19), 2421-2435. doi:10.1101/gad.1126303

Di Fiore, B., Davey, N. E., Hagting, A., Izawa, D., Mansfeld, J., Gibson, T. J., & Pines, J. (2015). The ABBA motif binds APC/C activators and is shared by APC/C substrates and regulators. Dev Cell, 32(3), 358-372. doi:10.1016/j.devcel.2015.01.003

Dick, A. E., & Gerlich, D. W. (2013). Kinetic framework of spindle assembly checkpoint signalling. Nat Cell Biol, 15(11), 1370-1377. doi:10.1038/ncb2842

Ding, R., West, R. R., Morphew, D. M., Oakley, B. R., & McIntosh, J. R. (1997). The spindle pole body of Schizosaccharomyces pombe enters and leaves the nuclear envelope as the cell cycle proceeds. Mol Biol Cell, 8(8), 1461-1479.

Dorffling, K., Petersen, W., Sprecher, E., Urbasch, I., & Hanssen, H. P. (1984). Abscisic-Acid in Phytopathogenic Fungi of the Genera Botrytis, Ceratocystis, Fusarium, and Rhizoctonia. Zeitschrift Fur Naturforschung C-a Journal of Biosciences, 39(6), 683-684.

Eagles, C. F., & Wareing, P. F. (1963). Experimental Induction of Dormancy in Betula Pubescens. Nature, 199(489), 874-&. doi:DOI 10.1038/199874a0

Edamatsu, M. (2014). Bidirectional motility of the fission yeast kinesin-5, Cut7. Biochem Biophys Res Commun, 446(1), 231-234. doi:10.1016/j.bbrc.2014.02.106

Elledge, S. J. (1996). Cell cycle checkpoints: preventing an identity crisis. Science, 274(5293), 1664-1672.

Elowe, S., Dulla, K., Uldschmid, A., Li, X., Dou, Z., & Nigg, E. A. (2010). Uncoupling of the spindle-checkpoint and chromosome-congression functions of BubR1. J Cell Sci, 123(Pt 1), 84-94. doi:10.1242/jcs.056507

Espert, A., Uluocak, P., Bastos, R. N., Mangat, D., Graab, P., & Gruneberg, U. (2014). PP2A-B56 opposes Mps1 phosphorylation of Knl1 and thereby promotes spindle assembly checkpoint silencing. J Cell Biol, 206(7), 833-842. doi:10.1083/jcb.201406109

Evans, T., Rosenthal, E. T., Youngblom, J., Distel, D., & Hunt, T. (1983). Cyclin: a protein specified by maternal mRNA in sea urchin eggs that is destroyed at each cleavage division. Cell, 33(2), 389-396.

Eytan, E., Wang, K., Miniowitz-Shemtov, S., Sitry-Shevah, D., Kaisari, S., Yen, T. J., . . . Hershko, A. (2014). Disassembly of mitotic checkpoint complexes by the joint action of the AAA-ATPase TRIP13 and p31(comet). Proc Natl Acad Sci U S A, 111(33), 12019-12024. doi:10.1073/pnas.1412901111

Faesen, A. C., Thanasoula, M., Maffini, S., Breit, C., Muller, F., van Gerwen, S., . . . Musacchio, A. (2017). Basis of catalytic assembly of the mitotic checkpoint complex. Nature, 542(7642), 498-502. doi:10.1038/nature21384

Fang, G. (2002). Checkpoint protein BubR1 acts synergistically with Mad2 to inhibit anaphase-promoting complex. Mol Biol Cell, 13(3), 755-766. doi:10.1091/mbc.01-09-0437

Fankhauser, C., Marks, J., Reymond, A., & Simanis, V. (1993). The S. pombe cdc16 gene is required both for maintenance of p34cdc2 kinase activity and regulation of septum formation: a link between mitosis and cytokinesis? EMBO J, 12(7), 2697-2704.

Fernius, J., & Hardwick, K. G. (2007). Bub1 kinase targets Sgo1 to ensure efficient chromosome biorientation in budding yeast mitosis. Plos Genetics, 3(11), 2312-2325. doi:ARTN e21310.1371/journal.pgen.0030213

Ferrari, S., Marin, O., Pagano, M. A., Meggio, F., Hess, D., El-Shemerly, M., . . . Pinna, L. A. (2005). Aurora-A site specificity: a study with synthetic peptide substrates. Biochem J, 390(Pt 1), 293-302. doi:10.1042/BJ20050343

Fisher, D. L., & Nurse, P. (1996). A single fission yeast mitotic cyclin B p34cdc2 kinase promotes both S-phase and mitosis in the absence of G1 cyclins. EMBO J, 15(4), 850-860.

Flemming, W., 1882. Zellsubstanz, kern und zelltheilung. Vogel.

Foe, I. T., Foster, S. A., Cheung, S. K., DeLuca, S. Z., Morgan, D. O., & Toczyski, D. P. (2011). Ubiquitination of Cdc20 by the APC occurs through an intramolecular mechanism. Curr Biol, 21(22), 1870-1877. doi:10.1016/j.cub.2011.09.051

Foley, E. A., & Kapoor, T. M. (2013). Microtubule attachment and spindle assembly checkpoint signalling at the kinetochore. Nat Rev Mol Cell Biol, 14(1), 25-37. doi:10.1038/nrm3494

Fraschini, R., Beretta, A., Sironi, L., Musacchio, A., Lucchini, G., & Piatti, S. (2001). Bub3 interaction with Mad2, Mad3 and Cdc20 is mediated by WD40 repeats and does not require intact kinetochores. EMBO J, 20(23), 6648-6659. doi:10.1093/emboj/20.23.6648

Garcia, M. A., Koonrugsa, N., & Toda, T. (2002). Spindle-kinetochore attachment requires the combined action of Kin I-like Klp5/6 and Alp14/Dis1-MAPs in fission yeast. EMBO J, 21(22), 6015-6024.

Gascoigne, K. E., & Taylor, S. S. (2008). Cancer cells display profound intra- and interline variation following prolonged exposure to antimitotic drugs. Cancer Cell, 14(2), 111-122. doi:10.1016/j.ccr.2008.07.002

Gassmann, R., Essex, A., Hu, J. S., Maddox, P. S., Motegi, F., Sugimoto, A., . . . Desai, A. (2008). A new mechanism controlling kinetochore-microtubule interactions revealed by comparison of two dynein-targeting components: SPDL-1 and the Rod/Zwilch/Zw10 complex. Genes Dev, 22(17), 2385-2399. doi:10.1101/gad.1687508

Gassmann, R., Holland, A. J., Varma, D., Wan, X., Civril, F., Cleveland, D. W., . . . Desai, A. (2010). Removal of Spindly from microtubule-attached kinetochores controls spindle checkpoint silencing in human cells. Genes Dev, 24(9), 957-971. doi:10.1101/gad.1886810

Ge, S., Skaar, J. R., & Pagano, M. (2009). APC/C- and Mad2-mediated degradation of Cdc20 during spindle checkpoint activation. Cell Cycle, 8(1), 167-171. doi:10.4161/cc.8.1.7606

Goyal, A., Takaine, M., Simanis, V., & Nakano, K. (2011). Dividing the spoils of growth and the cell cycle: The fission yeast as a model for the study of cytokinesis. Cytoskeleton (Hoboken), 68(2), 69-88. doi:10.1002/cm.20500

Grew, N. (2010). 1682. The anatomy of plants: With an idea of a philosophical history of plants, and several other lectures, read before the Royal Society. *Printed by W. Rawlins, for the author,[London]*.

Habu, T., Kim, S. H., Weinstein, J., & Matsumoto, T. (2002). Identification of a MAD2-binding protein, CMT2, and its role in mitosis. EMBO J, 21(23), 6419-6428.

Hadwiger, J. A., Wittenberg, C., Richardson, H. E., de Barros Lopes, M., & Reed, S. I. (1989). A family of cyclin homologs that control the G1 phase in yeast. Proc Natl Acad Sci U S A, 86(16), 6255-6259.

Harashima, H., Dissmeyer, N., & Schnittger, A. (2013). Cell cycle control across the eukaryotic kingdom. Trends Cell Biol, 23(7), 345-356. doi:10.1016/j.tcb.2013.03.002

Hardwick, K. G., Johnston, R. C., Smith, D. L., & Murray, A. W. (2000). MAD3 encodes a novel component of the spindle checkpoint which interacts with Bub3p, Cdc20p, and Mad2p. J Cell Biol, 148(5), 871-882.

Hardwick, K. G., Weiss, E., Luca, F. C., Winey, M., & Murray, A. W. (1996). Activation of the budding yeast spindle assembly checkpoint without mitotic spindle disruption. Science, 273(5277), 953-956.

Harley, M. E., Allan, L. A., Sanderson, H. S., & Clarke, P. R. (2010). Phosphorylation of Mcl-1 by CDK1-cyclin B1 initiates its Cdc20-dependent destruction during mitotic arrest. EMBO J, 29(14), 2407-2420. doi:10.1038/emboj.2010.112

Hartwell, L. H., Culotti, J., Pringle, J. R., & Reid, B. J. (1974). Genetic control of the cell division cycle in yeast. Science, 183(4120), 46-51.

Hartwell, L. H., & Weinert, T. A. (1989). Checkpoints: controls that ensure the order of cell cycle events. Science, 246(4930), 629-634.

Hayward, D., Alfonso-Perez, T., Cundell, M. J., Hopkins, M., Holder, J., Bancroft, J., . . . Gruneberg, U. (2019). CDK1-CCNB1 creates a spindle checkpoint-permissive state by enabling MPS1 kinetochore localization. J Cell Biol, 218(4), 1182-1199. doi:10.1083/jcb.201808014

Heinrich, S., Geissen, E. M., Kamenz, J., Trautmann, S., Widmer, C., Drewe, P., . . . Hauf, S. (2013). Determinants of robustness in spindle assembly checkpoint signalling. Nat Cell Biol, 15(11), 1328-1339. doi:10.1038/ncb2864

Heinrich, S., Windecker, H., Hustedt, N., & Hauf, S. (2012). Mph1 kinetochore localization is crucial and upstream in the hierarchy of spindle assembly checkpoint protein recruitment to kinetochores. J Cell Sci, 125(Pt 20), 4720-4727. doi:10.1242/jcs.110387

Hewitt, L., Tighe, A., Santaguida, S., White, A. M., Jones, C. D., Musacchio, A., . . . Taylor, S. S. (2010). Sustained Mps1 activity is required in mitosis to recruit O-Mad2 to the Mad1-C-Mad2 core complex. J Cell Biol, 190(1), 25-34. doi:10.1083/jcb.201002133

Hiruma, Y., Sacristan, C., Pachis, S. T., Adamopoulos, A., Kuijt, T., Ubbink, M., . . . Kops, G. J. (2015). CELL DIVISION CYCLE. Competition between MPS1 and microtubules at kinetochores regulates spindle checkpoint signaling. Science, 348(6240), 1264-1267. doi:10.1126/science.aaa4055

Hochegger, H., Takeda, S., & Hunt, T. (2008). Cyclin-dependent kinases and cell-cycle transitions: does one fit all? Nat Rev Mol Cell Biol, 9(11), 910-916. doi:10.1038/nrm2510

Holland, A. J., & Cleveland, D. W. (2009). Boveri revisited: chromosomal instability, aneuploidy and tumorigenesis. Nat Rev Mol Cell Biol, 10(7), 478-487. doi:10.1038/nrm2718

Hooke, R. (1987). Micrographia (London, 1665), preface. *For more details, see the discussion by Nick Wilding in*.

Howell, B. J., McEwen, B. F., Canman, J. C., Hoffman, D. B., Farrar, E. M., Rieder, C. L., & Salmon, E. D. (2001). Cytoplasmic dynein/dynactin drives kinetochore protein transport to the spindle poles and has a role in mitotic spindle checkpoint inactivation. J Cell Biol, 155(7), 1159-1172. doi:10.1083/jcb.200105093

Howell, B. J., Moree, B., Farrar, E. M., Stewart, S., Fang, G., & Salmon, E. D. (2004). Spindle checkpoint protein dynamics at kinetochores in living cells. Curr Biol, 14(11), 953-964. doi:10.1016/j.cub.2004.05.053

Hoyt, M. A., Totis, L., & Roberts, B. T. (1991). S. cerevisiae genes required for cell cycle arrest in response to loss of microtubule function. Cell, 66(3), 507-517.

Ikui, A. E., Furuya, K., Yanagida, M., & Matsumoto, T. (2002). Control of localization of a spindle checkpoint protein, Mad2, in fission yeast. J Cell Sci, 115(Pt 8), 1603-1610.

Ito, D., Saito, Y., & Matsumoto, T. (2012). Centromere-tethered Mps1 pombe homolog (Mph1) kinase is a sufficient marker for recruitment of the spindle checkpoint protein Bub1, but not Mad1. Proceedings of the National Academy of Sciences of the United States of America, 109(1), 209-214. doi:10.1073/pnas.1114647109

Ito, H., Fukuda, Y., Murata, K., & Kimura, A. (1983). Transformation of intact yeast cells treated with alkali cations. J Bacteriol, 153(1), 163-168.

Izawa, D., & Pines, J. (2015). The mitotic checkpoint complex binds a second CDC20 to inhibit active APC/C. Nature, 517(7536), 631-634. doi:10.1038/nature13911

Jakopec, V., Topolski, B., & Fleig, U. (2012). Sos7, an essential component of the conserved Schizosaccharomyces pombe Ndc80-MIND-Spc7 complex, identifies a new family of fungal kinetochore proteins. Mol Cell Biol, 32(16), 3308-3320. doi:10.1128/MCB.00212-12

Jang, J. K., Messina, L., Erdman, M. B., Arbel, T., & Hawley, R. S. (1995). Induction of metaphase arrest in Drosophila oocytes by chiasma-based kinetochore tension. Science, 268(5219), 1917-1919.

Jelluma, N., Dansen, T. B., Sliedrecht, T., Kwiatkowski, N. P., & Kops, G. J. (2010). Release of Mps1 from kinetochores is crucial for timely anaphase onset. J Cell Biol, 191(2), 281-290. doi:10.1083/jcb.201003038

Ji, Z., Gao, H., Jia, L., Li, B., & Yu, H. (2017). A sequential multi-target Mps1 phosphorylation cascade promotes spindle checkpoint signaling. Elife, 6. doi:10.7554/eLife.22513

Jia, L., Li, B., & Yu, H. (2016). The Bub1-Plk1 kinase complex promotes spindle checkpoint signalling through Cdc20 phosphorylation. Nat Commun, 7, 10818. doi:10.1038/ncomms10818

Kaisari, S., Sitry-Shevah, D., Miniowitz-Shemtov, S., Teichner, A., & Hershko, A. (2017). Role of CCT chaperonin in the disassembly of mitotic checkpoint complexes. Proc Natl Acad Sci U S A, 114(5), 956-961. doi:10.1073/pnas.1620451114

Kallio, M. J., Beardmore, V. A., Weinstein, J., & Gorbsky, G. J. (2002). Rapid microtubule-independent dynamics of Cdc20 at kinetochores and centrosomes in mammalian cells. J Cell Biol, 158(5), 841-847. doi:10.1083/jcb.200201135

Kawashima, S. A., Yamagishi, Y., Honda, T., Ishiguro, K., & Watanabe, Y. (2010). Phosphorylation of H2A by Bub1 Prevents Chromosomal Instability Through Localizing Shugoshin. Science, 327(5962), 172-177. doi:10.1126/science.1180189

Kellis, M., Birren, B. W., & Lander, E. S. (2004). Proof and evolutionary analysis of ancient genome duplication in the yeast Saccharomyces cerevisiae. Nature, 428(6983), 617-624. doi:10.1038/nature02424

Khodjakov, A., & Pines, J. (2010). Centromere tension: a divisive issue. Nat Cell Biol, 12(10), 919-923. doi:10.1038/ncb1010-919

Kim, S., Sun, H., Tomchick, D. R., Yu, H., & Luo, X. (2012). Structure of human Mad1 C-terminal domain reveals its involvement in kinetochore targeting. Proc Natl Acad Sci U S A, 109(17), 6549-6554. doi:10.1073/pnas.1118210109

Kim, S., Sun, H., Tomchick, D. R., Yu, H., & Luo, X. (2012). Structure of human Mad1 C-terminal domain reveals its involvement in kinetochore targeting. Proc Natl Acad Sci U S A, 109(17), 6549-6554. doi:10.1073/pnas.1118210109

King, E. M., van der Sar, S. J., & Hardwick, K. G. (2007). Mad3 KEN boxes mediate both Cdc20 and Mad3 turnover, and are critical for the spindle checkpoint. PLoS One, 2(4), e342. doi:10.1371/journal.pone.0000342

Kitajima, T. S., Ohsugi, M., & Ellenberg, J. (2011). Complete kinetochore tracking reveals error-prone homologous chromosome biorientation in mammalian oocytes. Cell, 146(4), 568-581. doi:10.1016/j.cell.2011.07.031

Kiyomitsu, T., Murakami, H., & Yanagida, M. (2011). Protein interaction domain mapping of human kinetochore protein Blinkin reveals a consensus motif for binding of spindle assembly checkpoint proteins Bub1 and BubR1. Mol Cell Biol, 31(5), 998-1011. doi:10.1128/MCB.00815-10

Klebig, C., Korinth, D., & Meraldi, P. (2009). Bub1 regulates chromosome segregation in a kinetochore-independent manner. J Cell Biol, 185(5), 841-858. doi:10.1083/jcb.200902128

Klebig, F., Fischer, C., Petri, S., Gerull, H., Wagener, C., & Tschentscher, P. (2007). Limitations in molecular detection of lymph node micrometastasis from colorectal cancer. Diagn Mol Pathol, 16(2), 91-95. doi:10.1097/PDM.0b013e31803278ee

Kops, G. J., Kim, Y., Weaver, B. A., Mao, Y., McLeod, I., Yates, J. R., 3rd, . . . Cleveland, D. W. (2005). ZW10 links mitotic checkpoint signaling to the structural kinetochore. J Cell Biol, 169(1), 49-60. doi:10.1083/jcb.200411118

Krapp, A., & Simanis, V. (2008). An overview of the fission yeast septation initiation network (SIN). Biochem Soc Trans, 36(Pt 3), 411-415. doi:10.1042/BST0360411

Krenn, V., Overlack, K., Primorac, I., van Gerwen, S., & Musacchio, A. (2014). KI motifs of human Knl1 enhance assembly of comprehensive spindle checkpoint complexes around MELT repeats. Curr Biol, 24(1), 29-39. doi:10.1016/j.cub.2013.11.046

Krenn, V., Wehenkel, A., Li, X., Santaguida, S., & Musacchio, A. (2012). Structural analysis reveals features of the spindle checkpoint kinase Bub1-kinetochore subunit Knl1 interaction. J Cell Biol, 196(4), 451-467. doi:10.1083/jcb.201110013

Kruse, T., Larsen, M. S., Sedgwick, G. G., Sigurdsson, J. O., Streicher, W., Olsen, J. V., & Nilsson, J. (2014). A direct role of Mad1 in the spindle assembly checkpoint beyond Mad2 kinetochore recruitment. EMBO Rep, 15(3), 282-290. doi:10.1002/embr.201338101

Kuijt, T. E., Omerzu, M., Saurin, A. T., & Kops, G. J. (2014). Conditional targeting of MAD1 to kinetochores is sufficient to reactivate the spindle assembly checkpoint in metaphase. Chromosoma, 123(5), 471-480. doi:10.1007/s00412-014-0458-9

Kulukian, A., Han, J. S., & Cleveland, D. W. (2009). Unattached kinetochores catalyze production of an anaphase inhibitor that requires a Mad2 template to prime Cdc20 for BubR1 binding. Dev Cell, 16(1), 105-117. doi:10.1016/j.devcel.2008.11.005

Lampson, M. A., & Cheeseman, I. M. (2011). Sensing centromere tension: Aurora B and the regulation of kinetochore function. Trends Cell Biol, 21(3), 133-140. doi:10.1016/j.tcb.2010.10.007

Lara-Gonzalez, P., Scott, M. I., Diez, M., Sen, O., & Taylor, S. S. (2011). BubR1 blocks substrate recruitment to the APC/C in a KEN-box-dependent manner. J Cell Sci, 124(Pt 24), 4332-4345. doi:10.1242/jcs.094763

Lara-Gonzalez, P., Westhorpe, F. G., & Taylor, S. S. (2012). The spindle assembly checkpoint. Curr Biol, 22(22), R966-980. doi:10.1016/j.cub.2012.10.006

Larsen, N. A., Al-Bassam, J., Wei, R. R., & Harrison, S. C. (2007). Structural analysis of Bub3 interactions in the mitotic spindle checkpoint. Proc Natl Acad Sci U S A, 104(4), 1201-1206. doi:10.1073/pnas.0610358104

Lee, I. J., Coffman, V. C., & Wu, J. Q. (2012). Contractile-ring assembly in fission yeast cytokinesis: Recent advances and new perspectives. Cytoskeleton (Hoboken), 69(10), 751-763. doi:10.1002/cm.21052

Lee, M. G., & Nurse, P. (1987). Cell cycle genes of the fission yeast. Sci Prog, 71(281 Pt 1), 1-14.

Li, R., & Murray, A. W. (1991). Feedback control of mitosis in budding yeast. Cell, 66(3), 519-531.

Li, X., & Nicklas, R. B. (1995). Mitotic forces control a cell-cycle checkpoint. Nature, 373(6515), 630-632. doi:10.1038/373630a0

Liang, F. S., Ho, W. Q., & Crabtree, G. R. (2011). Engineering the ABA plant stress pathway for regulation of induced proximity. Sci Signal, 4(164), rs2. doi:10.1126/scisignal.2001449

Liu, D., Vleugel, M., Backer, C. B., Hori, T., Fukagawa, T., Cheeseman, I. M., & Lampson, M. A. (2010). Regulated targeting of protein phosphatase 1 to the outer kinetochore by KNL1 opposes Aurora B kinase. J Cell Biol, 188(6), 809-820. doi:10.1083/jcb.201001006

Liu, X., McLeod, I., Anderson, S., Yates, J. R., 3rd, & He, X. (2005). Molecular analysis of kinetochore architecture in fission yeast. EMBO J, 24(16), 2919-2930. doi:10.1038/sj.emboj.7600762

London, N., & Biggins, S. (2014). Mad1 kinetochore recruitment by Mps1-mediated phosphorylation of Bub1 signals the spindle checkpoint. Genes Dev, 28(2), 140-152. doi:10.1101/gad.233700.113

London, N., & Biggins, S. (2014). Signalling dynamics in the spindle checkpoint response. Nat Rev Mol Cell Biol, 15(11), 736-747. doi:10.1038/nrm3888

London, N., Ceto, S., Ranish, J. A., & Biggins, S. (2012). Phosphoregulation of Spc105 by Mps1 and PP1 regulates Bub1 localization to kinetochores. Curr Biol, 22(10), 900-906. doi:10.1016/j.cub.2012.03.052

Looke, M., Kristjuhan, K., & Kristjuhan, A. (2011). Extraction of genomic DNA from yeasts for PCR-based applications. Biotechniques, 50(5), 325-328. doi:10.2144/000113672

Luo, X., Fang, G., Coldiron, M., Lin, Y., Yu, H., Kirschner, M. W., & Wagner, G. (2000). Structure of the Mad2 spindle assembly checkpoint protein and its interaction with Cdc20. Nat Struct Biol, 7(3), 224-229. doi: 10.1038/73338

Luo, X., Tang, Z., Rizo, J., & Yu, H. (2002). The Mad2 spindle checkpoint protein undergoes similar major conformational changes upon binding to either Mad1 or Cdc20. Mol Cell, 9(1), 59-71.

Luo, X., Tang, Z., Xia, G., Wassmann, K., Matsumoto, T., Rizo, J., & Yu, H. (2004). The Mad2 spindle checkpoint protein has two distinct natively folded states. Nat Struct Mol Biol, 11(4), 338-345. doi:10.1038/nsmb748

Maciejowski, J., George, K. A., Terret, M. E., Zhang, C., Shokat, K. M., & Jallepalli, P. V. (2010). Mps1 directs the assembly of Cdc20 inhibitory complexes during interphase and mitosis to control M phase timing and spindle checkpoint signaling. J Cell Biol, 190(1), 89-100. doi:10.1083/jcb.201001050

Magidson, V., O'Connell, C. B., Loncarek, J., Paul, R., Mogilner, A., & Khodjakov, A. (2011). The spatial arrangement of chromosomes during prometaphase facilitates spindle assembly. Cell, 146(4), 555-567. doi: 10.1016/j.cell.2011.07.012

Maiato, H., DeLuca, J., Salmon, E. D., & Earnshaw, W. C. (2004). The dynamic kinetochore-microtubule interface. J Cell Sci, 117(Pt 23), 5461-5477. doi:10.1242/jcs.01536

Maldonado, M., & Kapoor, T. M. (2011). Moving right along: how PP1 helps clear the checkpoint. Dev Cell, 20(6), 733-734. doi:10.1016/j.devcel.2011.05.017

Malumbres, M. (2014). Cyclin-dependent kinases. Genome Biol, 15(6), 122.

Malureanu, L. A., Jeganathan, K. B., Hamada, M., Wasilewski, L., Davenport, J., & van Deursen, J. M. (2009). BubR1 N terminus acts as a soluble inhibitor of cyclin B degradation by APC/C(Cdc20) in interphase. Dev Cell, 16(1), 118-131. doi:10.1016/j.devcel.2008.11.004

Mapelli, M., Filipp, F. V., Rancati, G., Massimiliano, L., Nezi, L., Stier, G., . . . Musacchio, A. (2006). Determinants of conformational dimerization of Mad2 and its inhibition by p31comet. EMBO J, 25(6), 1273-1284. doi:10.1038/sj.emboj.7601033

Mapelli, M., & Musacchio, A. (2007). MAD contortions: conformational dimerization boosts spindle checkpoint signaling. Current Opinion in Structural Biology, 17(6), 716-725. doi:10.1016/j.sbi.2007.08.011

Maresca, T. J., & Salmon, E. D. (2010). Welcome to a new kind of tension: translating kinetochore mechanics into a wait-anaphase signal. J Cell Sci, 123(Pt 6), 825-835. doi:10.1242/jcs.064790

Mariani, L., Chiroli, E., Nezi, L., Muller, H., Piatti, S., Musacchio, A., & Ciliberto, A. (2012). Role of the Mad2 dimerization interface in the spindle assembly checkpoint independent of kinetochores. Curr Biol, 22(20), 1900-1908. doi:10.1016/j.cub.2012.08.028

Martel, R. R., Klicius, J., & Galet, S. (1977). Inhibition of the immune response by rapamycin, a new antifungal antibiotic. Can J Physiol Pharmacol, 55(1), 48-51.

Martinez-Balbas, M. A., Dey, A., Rabindran, S. K., Ozato, K., & Wu, C. (1995). Displacement of sequence-specific transcription factors from mitotic chromatin. Cell, 83(1), 29-38.

May, K. M., Paldi, F., & Hardwick, K. G. (2017). Fission Yeast Apc15 Stabilizes MCC-Cdc20-APC/C Complexes, Ensuring Efficient Cdc20 Ubiquitination and Checkpoint Arrest. Curr Biol, 27(8), 1221-1228. doi: 10.1016/j.cub.2017.03.013

McCollum, D., & Gould, K. L. (2001). Timing is everything: regulation of mitotic exit and cytokinesis by the MEN and SIN. Trends Cell Biol, 11(2), 89-95.

McCully, E. K., & Robinow, C. F. (1971). Mitosis in the fission yeast Schizosaccharomyces pombe: a comparative study with light and electron microscopy. J Cell Sci, 9(2), 475-507.

McIntosh, J. R. (2016). Mitosis. Cold Spring Harb Perspect Biol, 8(9). doi:10.1101/cshperspect.a023218

Meadows, J. C., Shepperd, L. A., Vanoosthuyse, V., Lancaster, T. C., Sochaj, A. M., Buttrick, G. J., . . . Millar, J. B. (2011). Spindle checkpoint silencing requires association of PP1 to both Spc7 and kinesin-8 motors. Dev Cell, 20(6), 739-750. doi:10.1016/j.devcel.2011.05.008

Mellone, B. G., & Allshire, R. C. (2003). Stretching it: putting the CEN(P-A) in centromere. Curr Opin Genet Dev, 13(2), 191-198.

Mendoza, M., Norden, C., Durrer, K., Rauter, H., Uhlmann, F., & Barral, Y. (2009). A mechanism for chromosome segregation sensing by the NoCut checkpoint. Nat Cell Biol, 11(4), 477-483. doi:10.1038/ncb1855

Meraldi, P. (2019). Bub1-the zombie protein that CRISPR cannot kill. EMBO J, 38(7). doi:10.15252/embj.2019101912

Meraldi, P., Honda, R., & Nigg, E. A. (2004). Aurora kinases link chromosome segregation and cell division to cancer susceptibility. Curr Opin Genet Dev, 14(1), 29-36. doi:10.1016/j.gde.2003.11.006

Miniowitz-Shemtov, S., Eytan, E., Ganoth, D., Sitry-Shevah, D., Dumin, E., & Hershko, A. (2012). Role of phosphorylation of Cdc20 in p31(comet)-stimulated disassembly of the mitotic checkpoint complex. Proceedings of the National Academy of Sciences of the United States of America, 109(21), 8056-8060. doi:10.1073/pnas.1204081109

Miyamoto, T., DeRose, R., Suarez, A., Ueno, T., Chen, M., Sun, T. P., . . . Inoue, T. (2012). Rapid and orthogonal logic gating with a gibberellin-induced dimerization system. Nat Chem Biol, 8(5), 465-470. doi:10.1038/nchembio.922

Miyazono, K., Miyakawa, T., Sawano, Y., Kubota, K., Kang, H. J., Asano, A., . . . Tanokura, M. (2009). Structural basis of abscisic acid signalling. Nature, 462(7273), 609-614. doi:10.1038/nature08583

Mora-Santos, M. D., Hervas-Aguilar, A., Sewart, K., Lancaster, T. C., Meadows, J. C., & Millar, J. B. (2016). Bub3-Bub1 Binding to Spc7/KNL1 Toggles the Spindle Checkpoint Switch by Licensing the Interaction of Bub1 with Mad1-Mad2. Curr Biol, 26(19), 2642-2650. doi:10.1016/j.cub.2016.07.040

Moyle, M. W., Kim, T., Hattersley, N., Espeut, J., Cheerambathur, D. K., Oegema, K., & Desai, A. (2014). A Bub1-Mad1 interaction targets the Mad1-Mad2 complex to unattached kinetochores to initiate the spindle checkpoint. J Cell Biol, 204(5), 647-657. doi:10.1083/jcb.201311015

Moyle, M. W., Kim, T., Hattersley, N., Espeut, J., Cheerambathur, D. K., Oegema, K., & Desai, A. (2014). A Bub1-Mad1 interaction targets the Mad1-Mad2 complex to unattached kinetochores to initiate the spindle checkpoint. J Cell Biol, 204(5), 647-657. doi:10.1083/jcb.201311015

Nezi, L., & Musacchio, A. (2009). Sister chromatid tension and the spindle assembly checkpoint. Curr Opin Cell Biol, 21(6), 785-795. doi:10.1016/j.ceb.2009.09.007

Nicklas, R. B., & Koch, C. A. (1969). Chromosome micromanipulation. 3. Spindle fiber tension and the reorientation of mal-oriented chromosomes. J Cell Biol, 43(1), 40-50.

Norden, C., Mendoza, M., Dobbelaere, J., Kotwaliwale, C. V., Biggins, S., & Barral, Y. (2006). The NoCut pathway links completion of cytokinesis to spindle midzone function to prevent chromosome breakage. Cell, 125(1), 85-98. doi:10.1016/j.cell.2006.01.045

Novak, B., Kapuy, O., Domingo-Sananes, M. R., & Tyson, J. J. (2010). Regulated protein kinases and phosphatases in cell cycle decisions. Curr Opin Cell Biol, 22(6), 801-808. doi:10.1016/j.ceb.2010.07.001

Nurse, P., Thuriaux, P., & Nasmyth, K. (1976). Genetic control of the cell division cycle in the fission yeast Schizosaccharomyces pombe. Mol Gen Genet, 146(2), 167-178.

Ohkuma, K., Smith, O. E., Lyon, J. L., & Addicott, F. T. (1963). Abscisin 2, an Abscission-Accelerating Substance from Young Cotton Fruit. Science, 142(359), 1592-&. doi:DOI 10.1126/science.142.3599.1592

Oliveira, R. A., & Nasmyth, K. (2010). Getting through anaphase: splitting the sisters and beyond. Biochemical Society Transactions, 38, 1639-1644. doi:10.1042/Bst0381639

Orth, J. D., Tang, Y., Shi, J., Loy, C. T., Amendt, C., Wilm, C., . . . Mitchison, T. J. (2008). Quantitative live imaging of cancer and normal cells treated with Kinesin-5 inhibitors indicates significant differences in phenotypic responses and cell fate. Mol Cancer Ther, 7(11), 3480-3489. doi:10.1158/1535-7163.MCT-08-0684

Overlack, K., Primorac, I., Vleugel, M., Krenn, V., Maffini, S., Hoffmann, I., . . . Musacchio, A. (2015). A molecular basis for the differential roles of Bub1 and BubR1 in the spindle assembly checkpoint. Elife, 4, e05269. doi:10.7554/eLife.05269

Palmer, D. K., O'Day, K., Wener, M. H., Andrews, B. S., & Margolis, R. L. (1987). A 17-kD centromere protein (CENP-A) copurifies with nucleosome core particles and with histones. J Cell Biol, 104(4), 805-815.

Pan, J., & Chen, R. H. (2004). Spindle checkpoint regulates Cdc20p stability in Saccharomyces cerevisiae. Genes Dev, 18(12), 1439-1451. doi:10.1101/gad.1184204

Paweletz, N. (2001). Walther Flemming: pioneer of mitosis research. Nat Rev Mol Cell Biol, 2(1), 72-75. doi: 10.1038/35048077

Peters, J. M. (2006). The anaphase promoting complex/cyclosome: a machine designed to destroy. Nat Rev Mol Cell Biol, 7(9), 644-656. doi:10.1038/nrm1988

Petrovic, A., Keller, J., Liu, Y., Overlack, K., John, J., Dimitrova, Y. N., . . . Musacchio, A. (2016). Structure of the MIS12 Complex and Molecular Basis of Its Interaction with CENP-C at Human Kinetochores. Cell, 167(4), 1028-1040 e1015. doi:10.1016/j.cell.2016.10.005

Petrovic, A., Mosalaganti, S., Keller, J., Mattiuzzo, M., Overlack, K., Krenn, V., . . . Musacchio, A. (2014). Modular assembly of RWD domains on the Mis12 complex underlies outer kinetochore organization. Mol Cell, 53(4), 591-605. doi:10.1016/j.molcel.2014.01.019

Pidoux, A. L., & Allshire, R. C. (2004). Kinetochore and heterochromatin domains of the fission yeast centromere. Chromosome Res, 12(6), 521-534. doi:10.1023/B:CHRO.0000036586.81775.8b

Pinsky, B. A., & Biggins, S. (2005). The spindle checkpoint: tension versus attachment. Trends Cell Biol, 15(9), 486-493. doi:10.1016/j.tcb.2005.07.005

Pinsky, B. A., Nelson, C. R., & Biggins, S. (2009). Protein phosphatase 1 regulates exit from the spindle checkpoint in budding yeast. Curr Biol, 19(14), 1182-1187. doi:10.1016/j.cub.2009.06.043

Primorac, I., Weir, J. R., Chiroli, E., Gross, F., Hoffmann, I., van Gerwen, S., . . . Musacchio, A. (2013). Bub3 reads phosphorylated MELT repeats to promote spindle assembly checkpoint signaling. Elife, 2, e01030. doi: 10.7554/eLife.01030

Proudfoot, K. G., Anderson, S. J., Dave, S., Bunning, A. R., Sinha Roy, P., Bera, A., & Gupta, M. L., Jr. (2019). Checkpoint Proteins Bub1 and Bub3 Delay Anaphase Onset in Response to Low Tension Independent of Microtubule-Kinetochore Detachment. Cell Rep, 27(2), 416-428 e414. doi:10.1016/j.celrep.2019.03.027

Putyrski, M., & Schultz, C. (2012). Protein translocation as a tool: The current rapamycin story. FEBS Lett, 586(15), 2097-2105. doi:10.1016/j.febslet.2012.04.061

Raaijmakers, J. A., van Heesbeen, R., Blomen, V. A., Janssen, L. M. E., van Diemen, F., Brummelkamp, T. R., & Medema, R. H. (2018). BUB1 Is Essential for the Viability of Human Cells in which the Spindle Assembly Checkpoint Is Compromised. Cell Rep, 22(6), 1424-1438. doi:10.1016/j.celrep.2018.01.034

Rachfall, N., Johnson, A. E., Mehta, S., Chen, J. S., & Gould, K. L. (2014). Cdk1 promotes cytokinesis in fission yeast through activation of the septation initiation network. Mol Biol Cell, 25(15), 2250-2259. doi:10.1091/mbc.E14-04-0936

Rahmani, Z., Gagou, M. E., Lefebvre, C., Emre, D., & Karess, R. E. (2009). Separating the spindle, checkpoint, and timer functions of BubR1. J Cell Biol, 187(5), 597-605. doi:10.1083/jcb.200905026

Rappsilber, J., Ishihama, Y., & Mann, M. (2003). Stop and go extraction tips for matrix-assisted laser desorption/ionization, nanoelectrospray, and LC/MS sample pretreatment in proteomics. Anal Chem, 75(3), 663-670.

Reddy, S. K., Rape, M., Margansky, W. A., & Kirschner, M. W. (2007). Ubiquitination by the anaphase-promoting complex drives spindle checkpoint inactivation. Nature, 446(7138), 921-925. doi:10.1038/nature05734

Riedel, C. G., Katis, V. L., Katou, Y., Mori, S., Itoh, T., Helmhart, W., . . . Nasmyth, K. (2006). Protein phosphatase 2A protects centromeric sister chromatid cohesion during meiosis I. Nature, 441(7089), 53-61. doi: 10.1038/nature04664

Rieder, C. L., Cole, R. W., Khodjakov, A., & Sluder, G. (1995). The Checkpoint Delaying Anaphase in Response to Chromosome Monoorientation Is Mediated by an Inhibitory Signal Produced by Unattached Kinetochores. Journal of Cell Biology, 130(4), 941-948. doi:DOI 10.1083/jcb.130.4.941

Rieder, C. L., & Maiato, H. (2004). Stuck in division or passing through: What happens when cells cannot satisfy the spindle assembly checkpoint. Developmental Cell, 7(5), 637-651. doi:DOI 10.1016/j.devcel.2004.09.002

Rivera, V. M., Clackson, T., Natesan, S., Pollock, R., Amara, J. F., Keenan, T., . . . Gilman, M. (1996). A humanized system for pharmacologic control of gene expression. Nat Med, 2(9), 1028-1032.

Rodriguez-Bravo, V., Maciejowski, J., Corona, J., Buch, H. K., Collin, P., Kanemaki, M. T., . . . Jallepalli, P. V. (2014). Nuclear pores protect genome integrity by assembling a premitotic and Mad1-dependent anaphase inhibitor. Cell, 156(5), 1017-1031. doi:10.1016/j.cell.2014.01.010

Rodriguez-Rodriguez, J. A., Lewis, C., McKinley, K. L., Sikirzhytski, V., Corona, J., Maciejowski, J., . . . Jallepalli, P. V. (2018). Distinct Roles of RZZ and Bub1-KNL1 in Mitotic Checkpoint Signaling and Kinetochore Expansion. Curr Biol, 28(21), 3422-3429 e3425. doi:10.1016/j.cub.2018.10.006

Rosenberg, J. S., Cross, F. R., & Funabiki, H. (2011). KNL1/Spc105 recruits PP1 to silence the spindle assembly checkpoint. Curr Biol, 21(11), 942-947. doi:10.1016/j.cub.2011.04.011

Samejima, I., Matsumoto, T., Nakaseko, Y., Beach, D., & Yanagida, M. (1993). Identification of seven new cut genes involved in Schizosaccharomyces pombe mitosis. J Cell Sci, 105 (Pt 1), 135-143.

San-Segundo, P. A., & Roeder, G. S. (1999). Pch2 links chromatin silencing to meiotic checkpoint control. Cell, 97(3), 313-324.

Santaguida, S., & Musacchio, A. (2009). The life and miracles of kinetochores. EMBO J, 28(17), 2511-2531. doi: 10.1038/emboj.2009.173

Santaguida, S., Tighe, A., D'Alise, A. M., Taylor, S. S., & Musacchio, A. (2010). Dissecting the role of MPS1 in chromosome biorientation and the spindle checkpoint through the small molecule inhibitor reversine. J Cell Biol, 190(1), 73-87. doi:10.1083/jcb.201001036

Schafer, K. A. (1998). The cell cycle: a review. Vet Pathol, 35(6), 461-478. doi:10.1177/030098589803500601

Schleiden, M. J. Beiträge zur Phytogenesis. Müller´s Arch. Anat. Physiol. Wiss. Med. 136–176 (1838). 4.

Schmitz, M. H., Held, M., Janssens, V., Hutchins, J. R., Hudecz, O., Ivanova, E., . . . Gerlich, D. W. (2010). Live-cell imaging RNAi screen identifies PP2A-B55alpha and importin-beta1 as key mitotic exit regulators in human cells. Nat Cell Biol, 12(9), 886-893. doi:10.1038/ncb2092

Schwann, T. Mikroskopische Untersuchungen über die Übereinstimmung in der Struktur und dem Wachsthum der Thiere und Pflanzen (Verlag der Sander´schen Buchhandlung, Berlin, 1839).

Sczaniecka, M., Feoktistova, A., May, K. M., Chen, J. S., Blyth, J., Gould, K. L., & Hardwick, K. G. (2008). The spindle checkpoint functions of Mad3 and Mad2 depend on a Mad3 KEN box-mediated interaction with Cdc20-anaphase-promoting complex (APC/C). J Biol Chem, 283(34), 23039-23047. doi:10.1074/jbc.M803594200

Sewart, K., & Hauf, S. (2017). Different Functionality of Cdc20 Binding Sites within the Mitotic Checkpoint Complex. Curr Biol, 27(8), 1213-1220. doi:10.1016/j.cub.2017.03.007

Shah, J. V., Botvinick, E., Bonday, Z., Furnari, F., Berns, M., & Cleveland, D. W. (2004). Dynamics of centromere and kinetochore proteins; implications for checkpoint signaling and silencing. Curr Biol, 14(11), 942-952. doi:10.1016/j.cub.2004.05.046

Shepperd, L. A., Meadows, J. C., Sochaj, A. M., Lancaster, T. C., Zou, J., Buttrick, G. J., . . . Millar, J. B. (2012). Phosphodependent recruitment of Bub1 and Bub3 to Spc7/KNL1 by Mph1 kinase maintains the spindle checkpoint. Curr Biol, 22(10), 891-899. doi:10.1016/j.cub.2012.03.051

Shi, J., Orth, J. D., & Mitchison, T. (2008). Cell type variation in responses to antimitotic drugs that target microtubules and kinesin-5. Cancer Res, 68(9), 3269-3276. doi:10.1158/0008-5472.CAN-07-6699

Shi, T. Q., Peng, H., Zeng, S. Y., Ji, R. Y., Shi, K., Huang, H., & Ji, X. J. (2017). Microbial production of plant hormones: Opportunities and challenges. Bioengineered, 8(2), 124-128. doi:10.1080/21655979.2016.1212138

Silio, V., McAinsh, A. D., & Millar, J. B. (2015). KNL1-Bubs and RZZ Provide Two Separable Pathways for Checkpoint Activation at Human Kinetochores. Dev Cell, 35(5), 600-613. doi:10.1016/j.devcel.2015.11.012

Silva, P. M., Reis, R. M., Bolanos-Garcia, V. M., Florindo, C., Tavares, A. A., & Bousbaa, H. (2014). Dynein-dependent transport of spindle assembly checkpoint proteins off kinetochores toward spindle poles. FEBS Lett, 588(17), 3265-3273. doi:10.1016/j.febslet.2014.07.011

Sironi, L., Mapelli, M., Knapp, S., De Antoni, A., Jeang, K. T., & Musacchio, A. (2002). Crystal structure of the tetrameric Mad1-Mad2 core complex: implications of a 'safety belt' binding mechanism for the spindle checkpoint. EMBO J, 21(10), 2496-2506. doi:10.1093/emboj/21.10.2496

Sliedrecht, T., Zhang, C., Shokat, K. M., & Kops, G. J. (2010). Chemical genetic inhibition of Mps1 in stable human cell lines reveals novel aspects of Mps1 function in mitosis. PLoS One, 5(4), e10251. doi:10.1371/journal.pone.0010251

Spencer, D. M., Wandless, T. J., Schreiber, S. L., & Crabtree, G. R. (1993). Controlling signal transduction with synthetic ligands. Science, 262(5136), 1019-1024.

Stachowiak, M. R., Laplante, C., Chin, H. F., Guirao, B., Karatekin, E., Pollard, T. D., & O'Shaughnessy, B. (2014). Mechanism of cytokinetic contractile ring constriction in fission yeast. Dev Cell, 29(5), 547-561. doi: 10.1016/j.devcel.2014.04.021

Stern, B., & Nurse, P. (1996). A quantitative model for the cdc2 control of S phase and mitosis in fission yeast. Trends Genet, 12(9), 345-350.

Stern, B. M., & Murray, A. W. (2001). Lack of tension at kinetochores activates the spindle checkpoint in budding yeast. Curr Biol, 11(18), 1462-1467.

Sudakin, V., Chan, G. K., & Yen, T. J. (2001). Checkpoint inhibition of the APC/C in HeLa cells is mediated by a complex of BUBR1, BUB3, CDC20, and MAD2. J Cell Biol, 154(5), 925-936. doi:10.1083/jcb.200102093

Suijkerbuijk, S. J., Vleugel, M., Teixeira, A., & Kops, G. J. (2012). Integration of kinase and phosphatase activities by BUBR1 ensures formation of stable kinetochore-microtubule attachments. Dev Cell, 23(4), 745-755. doi:10.1016/j.devcel.2012.09.005

Tanaka, K., Chang, H. L., Kagami, A., & Watanabe, Y. (2009). CENP-C functions as a scaffold for effectors with essential kinetochore functions in mitosis and meiosis. Dev Cell, 17(3), 334-343. doi:10.1016/j.devcel.2009.08.004

Tang, Z., Shu, H., Oncel, D., Chen, S., & Yu, H. (2004). Phosphorylation of Cdc20 by Bub1 provides a catalytic mechanism for APC/C inhibition by the spindle checkpoint. Mol Cell, 16(3), 387-397. doi:10.1016/j.molcel.2004.09.031

Tange, Y., & Niwa, O. (2008). Schizosaccharomyces pombe Bub3 is dispensable for mitotic arrest following perturbed spindle formation. Genetics, 179(2), 785-792. doi:10.1534/genetics.107.081695

Terrano, D. T., Upreti, M., & Chambers, T. C. (2010). Cyclin-dependent kinase 1-mediated Bcl-xL/Bcl-2 phosphorylation acts as a functional link coupling mitotic arrest and apoptosis. Mol Cell Biol, 30(3), 640-656. doi:10.1128/MCB.00882-09

Thornton, B. R., & Toczyski, D. P. (2003). Securin and B-cyclin/CDK are the only essential targets of the APC. Nature Cell Biology, 5(12), 1090-1094. doi:10.1038/ncb1066

Uemura, T., & Yanagida, M. (1984). Isolation of type I and II DNA topoisomerase mutants from fission yeast: single and double mutants show different phenotypes in cell growth and chromatin organization. EMBO J, 3(8), 1737-1744.

Uzawa, S., & Yanagida, M. (1992). Visualization of centromeric and nucleolar DNA in fission yeast by fluorescence in situ hybridization. J Cell Sci, 101 (Pt 2), 267-275.

Vader, G. (2015). Pch2(TRIP13): controlling cell division through regulation of HORMA domains. Chromosoma, 124(3), 333-339. doi:10.1007/s00412-015-0516-y

Van Leeuwenhoek, A. Letter no. 35, March 3, 1682.

Vanoosthuyse, V., & Hardwick, K. G. (2009). A novel protein phosphatase 1-dependent spindle checkpoint silencing mechanism. Curr Biol, 19(14), 1176-1181. doi:10.1016/j.cub.2009.05.060

Varma, D., & Salmon, E. D. (2012). The KMN protein network--chief conductors of the kinetochore orchestra. J Cell Sci, 125(Pt 24), 5927-5936. doi:10.1242/jcs.093724

Varma, D., Wan, X., Cheerambathur, D., Gassmann, R., Suzuki, A., Lawrimore, J., . . . Salmon, E. D. (2013). Spindle assembly checkpoint proteins are positioned close to core microtubule attachment sites at kinetochores. J Cell Biol, 202(5), 735-746. doi:10.1083/jcb.201304197

Vezina, C., Kudelski, A., & Sehgal, S. N. (1975). Rapamycin (AY-22,989), a new antifungal antibiotic. I. Taxonomy of the producing streptomycete and isolation of the active principle. J Antibiot (Tokyo), 28(10), 721-726.

Vigneron, S., Prieto, S., Bernis, C., Labbe, J. C., Castro, A., & Lorca, T. (2004). Kinetochore localization of spindle checkpoint proteins: who controls whom? Mol Biol Cell, 15(10), 4584-4596. doi:10.1091/mbc.e04-01-0051

Visintin, R., Craig, K., Hwang, E. S., Prinz, S., Tyers, M., & Amon, A. (1998). The phosphatase Cdc14 triggers mitotic exit by reversal of Cdk-dependent phosphorylation. Mol Cell, 2(6), 709-718.

Vleugel, M., Hoogendoorn, E., Snel, B., & Kops, G. J. (2012). Evolution and function of the mitotic checkpoint. Dev Cell, 23(2), 239-250. doi:10.1016/j.devcel.2012.06.013

Vleugel, M., Tromer, E., Omerzu, M., Groenewold, V., Nijenhuis, W., Snel, B., & Kops, G. J. (2013). Arrayed BUB recruitment modules in the kinetochore scaffold KNL1 promote accurate chromosome segregation. J Cell Biol, 203(6), 943-955. doi:10.1083/jcb.201307016

Wang, X., Babu, J. R., Harden, J. M., Jablonski, S. A., Gazi, M. H., Lingle, W. L., . . . van Deursen, J. M. (2001). The mitotic checkpoint protein hBUB3 and the mRNA export factor hRAE1 interact with GLE2p-binding sequence (GLEBS)-containing proteins. J Biol Chem, 276(28), 26559-26567. doi:10.1074/jbc.M101083200

Watanabe, Y. (2006). A one-sided view of kinetochore attachment in meiosis. Cell, 126(6), 1030-1032. doi: 10.1016/j.cell.2006.09.005

Watanabe, Y. (2010). Temporal and spatial regulation of targeting aurora B to the inner centromere. Cold Spring Harb Symp Quant Biol, 75, 419-423. doi:10.1101/sqb.2010.75.035

Weaver, B. A. A., Bonday, Z. Q., Putkey, F. R., Kops, G. J. P. L., Silk, A. D., & Cleveland, D. W. (2003). Centromere-associated protein-E is essential for the mammalian mitotic checkpoint to prevent aneuploidy due to single chromosome loss. Journal of Cell Biology, 162(4), 551-563. doi:10.1083/jcb.200303167

Weinert, T. A., & Hartwell, L. H. (1988). The RAD9 gene controls the cell cycle response to DNA damage in Saccharomyces cerevisiae. Science, 241(4863), 317-322.

Weisman, R., & Choder, M. (2001). The fission yeast TOR homolog, tor1+, is required for the response to starvation and other stresses via a conserved serine. J Biol Chem, 276(10), 7027-7032. doi:10.1074/jbc.M010446200

Weiss, E., & Winey, M. (1996). The Saccharomyces cerevisiae spindle pole body duplication gene MPS1 is part of a mitotic checkpoint. Journal of Cell Biology, 132(1-2), 111-123. doi:DOI 10.1083/jcb.132.1.111

Welburn, J. P., Vleugel, M., Liu, D., Yates, J. R., 3rd, Lampson, M. A., Fukagawa, T., & Cheeseman, I. M. (2010). Aurora B phosphorylates spatially distinct targets to differentially regulate the kinetochore-microtubule interface. Mol Cell, 38(3), 383-392. doi:10.1016/j.molcel.2010.02.034

Westhorpe, F. G., Tighe, A., Lara-Gonzalez, P., & Taylor, S. S. (2011). p31comet-mediated extraction of Mad2 from the MCC promotes efficient mitotic exit. J Cell Sci, 124(Pt 22), 3905-3916. doi:10.1242/jcs.093286

Windecker, H., Langegger, M., Heinrich, S., & Hauf, S. (2009). Bub1 and Bub3 promote the conversion from monopolar to bipolar chromosome attachment independently of shugoshin. EMBO Rep, 10(9), 1022-1028. doi: 10.1038/embor.2009.183

Wolpert, L. (1996). The evolution of 'the cell theory'. Curr Biol, 6(3), 225-228.

Yamada, H. Y., Matsumoto, S., & Matsumoto, T. (2000). High dosage expression of a zinc finger protein, Grt1, suppresses a mutant of fission yeast slp1(+), a homolog of CDC20/p55CDC/Fizzy. J Cell Sci, 113 (Pt 22), 3989-3999.

Yamagishi, Y., Yang, C. H., Tanno, Y., & Watanabe, Y. (2012). MPS1/Mph1 phosphorylates the kinetochore protein KNL1/Spc7 to recruit SAC components. Nat Cell Biol, 14(7), 746-752. doi:10.1038/ncb2515

Yamaguchi, M., VanderLinden, R., Weissmann, F., Qiao, R., Dube, P., Brown, N. G., . . . Schulman, B. A. (2016). Cryo-EM of Mitotic Checkpoint Complex-Bound APC/C Reveals Reciprocal and Conformational Regulation of Ubiquitin Ligation. Mol Cell, 63(4), 593-607. doi:10.1016/j.molcel.2016.07.003

Yamamoto, A., & Hiraoka, Y. (2003). Monopolar spindle attachment of sister chromatids is ensured by two distinct mechanisms at the first meiotic division in fission yeast. EMBO J, 22(9), 2284-2296. doi:10.1093/emboj/cdg222

Yamano, H., Gannon, J., & Hunt, T. (1996). The role of proteolysis in cell cycle progression in Schizosaccharomyces pombe. EMBO J, 15(19), 5268-5279.

Yamano, H., Gannon, J., & Hunt, T. (1996). The role of proteolysis in cell cycle progression in Schizosaccharomyces pombe. EMBO J, 15(19), 5268-5279.

Yamashita, Y. M., Nakaseko, Y., Samejima, I., Kumada, K., Yamada, H., Michaelson, D., & Yanagida, M. (1996). 20S cyclosome complex formation and proteolytic activity inhibited by the cAMP/PKA pathway. Nature, 384(6606), 276-279. doi:10.1038/384276a0

Yanagida, M. (1998). Fission yeast cut mutations revisited: control of anaphase. Trends Cell Biol, 8(4), 144-149.

Ye, Q., Rosenberg, S. C., Moeller, A., Speir, J. A., Su, T. Y., & Corbett, K. D. (2015). TRIP13 is a protein-remodeling AAA+ ATPase that catalyzes MAD2 conformation switching. Elife, 4. doi:10.7554/eLife.07367

Yuan, I., Leontiou, I., Amin, P., May, K. M., Soper Ni Chafraidh, S., Zlamalova, E., & Hardwick, K. G. (2017). Generation of a Spindle Checkpoint Arrest from Synthetic Signaling Assemblies. Curr Biol, 27(1), 137-143. doi: 10.1016/j.cub.2016.11.014

Zhang, G., Kruse, T., Guasch Boldu, C., Garvanska, D. H., Coscia, F., Mann, M., . . . Nilsson, J. (2019). Efficient mitotic checkpoint signaling depends on integrated activities of Bub1 and the RZZ complex. EMBO J, 38(7). doi: 10.15252/embj.2018100977

Zhang, G., Kruse, T., Lopez-Mendez, B., Sylvestersen, K. B., Garvanska, D. H., Schopper, S., . . . Nilsson, J. (2017). Bub1 positions Mad1 close to KNL1 MELT repeats to promote checkpoint signalling. Nat Commun, 8, 15822. doi:10.1038/ncomms15822

Zhang, G., Lischetti, T., Hayward, D. G., & Nilsson, J. (2015). Distinct domains in Bub1 localize RZZ and BubR1 to kinetochores to regulate the checkpoint. Nat Commun, 6, 7162. doi:10.1038/ncomms8162

Zich, J., & Hardwick, K. G. (2010). Getting down to the phosphorylated 'nuts and bolts' of spindle checkpoint signalling. Trends Biochem Sci, 35(1), 18-27. doi:10.1016/j.tibs.2009.09.002

Zich, J., May, K., Paraskevopoulos, K., Sen, O., Syred, H. M., van der Sar, S., . . . Hardwick, K. G. (2016). Mps1Mph1 Kinase Phosphorylates Mad3 to Inhibit Cdc20Slp1-APC/C and Maintain Spindle Checkpoint Arrests. PLoS Genet, 12(2), e1005834. doi:10.1371/journal.pgen.1005834

Zich, J., Sochaj, A. M., Syred, H. M., Milne, L., Cook, A. G., Ohkura, H., . . . Hardwick, K. G. (2012). Kinase activity of fission yeast Mph1 is required for Mad2 and Mad3 to stably bind the anaphase promoting complex. Curr Biol, 22(4), 296-301. doi:10.1016/j.cub.2011.12.049